VOLUME 37 JULY 1959 NUMBER 7

Canadian Journal of Physics

Editor: H. E. DUCKWORTH

Associate Editors:

L. G. ELLIOTT, *Atomic Energy of Canada, Ltd., Chalk River*
J. S. FOSTER, *McGill University*
G. HERZBERG, *National Research Council of Canada*
L. LEPRINCE-RINGUET, *Ecole Polytechnique, Paris*
B. W. SARGENT, *Queen's University*
G. M. VOLKOFF, *University of British Columbia*
W. H. WATSON, *University of Toronto*
G. A. WOONTON, *McGill University*

Published by THE NATIONAL RESEARCH COUNCIL

OTTAWA CANADA

CANADIAN JOURNAL OF PHYSICS

Under the authority of the Chairman of the Committee of the Privy Council on Scientific and Industrial Research, the National Research Council issues THE CANADIAN JOURNAL OF PHYSICS and five other journals devoted to the publication, in English or French, of the results of original scientific research. Matters of general policy concerning these journals are the responsibility of a joint Editorial Board consisting of: members representing the National Research Council of Canada; the Editors of the Journals; and members representing the Royal Society of Canada and four other scientific societies.

EDITORIAL BOARD

Representatives of the National Research Council

I. McT. Cowan, *University of British Columbia*
A. Gauthier, *University of Montreal*
H. G. Thode (Chairman), *McMaster University*
D. L. Thomson, *McGill University*

Editors of the Journals

D. L. Bailey, *University of Toronto*
T. W. M. Cameron, *Macdonald College*
H. E. Duckworth, *McMaster University*
K. A. C. Elliott, *Montreal Neurological Institute*
Léo Marion, *National Research Council*
R. G. E. Murray, *University of Western Ontario*

Representatives of Societies

D. L. Bailey, *University of Toronto*
Royal Society of Canada
T. W. M. Cameron, *Macdonald College*
Royal Society of Canada
H. E. Duckworth, *McMaster University*
Royal Society of Canada
Canadian Association of Physicists
K. A. C. Elliott, *Montreal Neurological Institute*
Canadian Physiological Society
P. R. Gendron, *University of Ottawa*
Chemical Institute of Canada
R. G. E. Murray, *University of Western Ontario*
Canadian Society of Microbiologists
T. Thorvaldson, *University of Saskatchewan*
Royal Society of Canada

Ex officio

Léo Marion (Editor-in-Chief), *National Research Council*
J. B. Marshall (Administration and Awards), *National Research Council*

Manuscripts for publication should be submitted to Dr. H. E. Duckworth, Editor, Canadian Journal of Physics, Hamilton College, McMaster University, Hamilton, Ontario.
For instructions on preparation of copy, see **NOTES TO CONTRIBUTORS** (back cover).

Proof, correspondence concerning proof, and orders for reprints should be sent to the Manager, Editorial Office (Research Journals), Division of Administration and Awards, National Research Council, Ottawa 2, Canada.

Subscriptions, renewals, requests for single or back numbers, and all remittances should be sent to Division of Administration and Awards, National Research Council, Ottawa 2, Canada. Remittances should be made payable to the Receiver General of Canada, credit National Research Council.

The journals published, frequency of publication, and prices are:

Canadian Journal of Biochemistry and Physiology	Monthly	$9.00 a year
Canadian Journal of Botany	Bimonthly	$6.00 a year
Canadian Journal of Chemistry	Monthly	$12.00 a year
Canadian Journal of Microbiology	Bimonthly	$6.00 a year
Canadian Journal of Physics	Monthly	$9.00 a year
Canadian Journal of Zoology	Bimonthly	$5.00 a year

The price of regular single numbers of all journals is $2.00.

Canadian Journal of Physics

Issued by THE NATIONAL RESEARCH COUNCIL OF CANADA

VOLUME 37 JULY 1959 NUMBER 7

THE SCATTERING OF ELECTROMAGNETIC WAVES BY A CORRUGATED SHEET[1]

T. B. A. SENIOR

ABSTRACT

The physical optics method is used to determine the scattering of a plane wave by a perfectly conducting sheet having sinusoidal corrugations. The only approximation concerns the current distribution on the sheet and the scattered field then appears as a spectrum of plane waves whose amplitudes are given by a simple integral expression.

1. INTRODUCTION

The problem of scattering by a corrugated sheet is one which is easy to formulate in mathematical terms but extremely difficult to solve, and in spite of its importance in many applications (for example, the reflection of low-frequency radio waves from an idealized sea) an exact solution has yet to be found. Indeed, very little progress has been made since the original treatment by Lord Rayleigh (1878) and the approximations which he proposed have been the basis for much of the later work.

A direct attack upon the problem starts by assuming an expression for the scattered field as an angular spectrum of plane waves, the amplitudes of which have to be chosen to satisfy the boundary conditions. This leads to a single equation, valid at all points of the sheet, from which to determine the unknown amplitudes. It is here that approximations come in and some of those which have been suggested are referred to in Section 2.

To avoid the difficulties associated with the series formulation several theories have been suggested which do not use the above equation as their starting point. Two of these will be mentioned because of their affinity to the physical optics approach, and both have been considered by LaCasce and Tamarkin (1956) in connection with the reflection of sound waves at an air–water interface.

The first is due to Eckart (1953) and is a scalar theory. The source of radiation is at a finite distance with the field confined to a narrow two-dimensional beam, and the scattered field ϕ^s is then expressed as a Helmholtz integral involving ϕ^s and its normal derivative on the sheet. Although these

[1]Manuscript received February 6, 1959.
Contribution from the Radiation Laboratory, The University of Michigan, Ann Arbor, Michigan.

are not independent and cannot be specified independently of one another, the crux of the method is to replace both ϕ^s and $\partial\phi^s/\partial n$ by the values appropriate to the incident field alone. A further assumption is to regard the reflection as taking place at an equivalent flat surface and the scattered field then appears as a spectrum of waves whose amplitudes have a simple Bessel function form.

The second theory (Brekhovskikh 1952) is also based on the Helmholtz integral. Here again the crucial step is the determination of one boundary condition having specified the other, and Brekhovskikh estimates $\partial\phi^s/\partial n$ by assuming that the incident field is scattered by each element of the corrugated sheet as though undergoing ordinary specular reflection. As such the method is similar to physical optics, but the advantages which should accrue are sacrificed by an ill-advised use of approximate techniques in evaluating the resulting integrals.

The physical optics method itself is described in Section 3. The essential approximation is to replace the current distribution on the sheet by twice the tangential component of the incident magnetic field and the scattered field is then given by a double integral over the surface of the sheet. By a careful use of a steepest descent technique, the integrals can be evaluated in such a way as to preserve all the features of an exact solution, and some of the consequences are examined in Section 4.

2. SERIES FORMULATION

The sheet is assumed to be perfectly conducting and to have the equation

$$y = a \cos Kx \tag{1}$$

where a is the amplitude of the corrugations and $2\pi/K$ is the period. It is infinite in both the x and z directions and can be visualized as a tin roof whose corrugations are parallel to the z axis of the co-ordinate system. At any point (x, y, z) on the sheet the unit vector normal is

$$\mathbf{n} = (aK \sin Kx, 1, 0) \frac{1}{\sqrt{\{1+(aK \sin Kx)^2\}}}. \tag{2}$$

The simplest case to consider is that in which the plane wave is incident normally, corresponding to propagation in the negative y direction. For ease of comparison with results obtained for the analogous problem in the theory of sound, it is convenient to take the magnetic vector entirely in the z direction and hence along the corrugations. The incident field is then*

$$\mathbf{E}^i = (E_x^i, 0, 0), \qquad \mathbf{H}^i = (0, 0, H_z^i) \tag{3}$$

with

$$E_x^i = \exp(-iky) \qquad \text{and} \qquad H_z^i = Y \exp(-iky) \tag{4}$$

where Y is the intrinsic admittance of free space and k is the propagation constant.

*Throughout this paper, m.k.s. units are employed and a time factor $\exp(-i\omega t)$ suppressed throughout.

Concerning the scattered field, the symmetry of the problem requires that its magnetic vector also lie in the z direction. If this is written as an angular spectrum of plane waves each of which is propagated at some angle θ_m to the positive y axis, we have

$$H_z^s = Y \sum_m A_m \exp\{ik(x \sin \theta_m + y \cos \theta_m)\}$$

which can be inserted into the boundary condition

$$\frac{\partial H_z^s}{\partial n} = -\frac{\partial H_z^i}{\partial n}$$

at the surface $y = a \cos Kx$ to give

$$(5) \quad \sum_m A_m(aK \sin Kx \sin \theta_m + \cos \theta_m) \exp[ik\{x \sin \theta_m + (1+\cos \theta_m)\, a \cos Kx\}] = 1.$$

Because of the nature of the sheet, however, equation (5) must be periodic in x with period $2\pi/K$, and this implies that

$$k \sin \theta_m = mK$$

where m can take all integer values, positive, negative, or zero. Hence

$$k \cos \theta_m = \pm\sqrt{\{k^2 - (mK)^2\}}$$

and since the positive sign must be chosen in order to comply with the condition of outgoing radiation at infinity, the equation from which to determine the A_m is

$$(6) \quad \sum_{m=-\infty}^{\infty} A_m[amK^2 \sin Kx + \sqrt{\{k^2 - (mK)^2\}}] \exp(imKx + i\mu_m \cos Kx) = k$$

where $\mu_m = a[k + \sqrt{\{k^2 - (mK)^2\}}]$. This is valid for all x, and, in theory at least, is sufficient to enable the A_m to be calculated.

Once the A_m have been found, H_z^s is given by

$$(7) \quad H_z^s = Y \sum_{m=-\infty}^{\infty} A_m \exp[imKx + i\sqrt{\{k^2 - (mK)^2\}}y]$$

and the components of the electric vector can then be obtained from Maxwell's equations. For an incident field of the above polarization the entire problem can be expressed in terms of the single component H_z and this is directly analogous to the velocity potential in the theory of sound. If **E** and **H** are interchanged it is still true that one component suffices (indeed, the equation for the A_m is somewhat simpler in this case), but the solution no longer applies to the scattering of sound by a rigid surface.

Although the exact solution of equation (6) is still unknown, a certain amount of information about the scattered field can be obtained without a knowledge of the A_m. If, in equation (6), m is replaced by $-m$ and x by $-x$, the equation is unaltered except for the fact that A_{-m} appears instead of A_m. Hence $A_{-m} = A_m$ and, from equation (7), the scattered field is seen to consist of a fundamental wave propagated in the direction of the y axis

(specular reflection by the equivalent flat sheet), together with an infinity of pairs of higher-order modes. Each pair is composed of two waves of equal amplitude and phase whose directions of propagation are at angles $\pm\theta_m$ to the y axis, where

$$\theta_m = \tan^{-1} \frac{mK}{\sqrt{\{k^2-(mK)^2\}}}, \qquad m = 1, 2, 3, \ldots$$

As m increases these directions become more nearly horizontal until, finally, the value of m is such that $k^2 < (mK)^2$. The corresponding mode and all those of higher order now travel horizontally and, being attenuated in the y direction, are surface waves whose influence is confined to the immediate vicinity of the sheet. Similarly, if attention is concentrated on a particular mode, the mth say, and if k is slowly decreased, a frequency will be reached at which propagation in the y direction ceases. The appropriate frequency has $k = mK$ and is often referred to as the 'cutoff' for that mode. All except the fundamental exhibit this behavior.

Unfortunately, only a limited amount of information can be obtained in this manner and sooner or later it becomes necessary to determine the amplitudes A_m. The main difficulty with equation (6) is due to the form of the functions which multiply the individual terms. If these functions were orthogonal the equation could be inverted and though the presence of the exponentials prevents this from being done, the exponentials themselves can be expanded in terms of an orthogonal set of functions. The most direct way of doing this was proposed by Lord Rayleigh (1878). Since the functions $\exp(ipKx)$, $p = 0, \pm1, \pm2, \ldots$ are orthogonal over any $2\pi/K$ range of x, the expansion

$$\exp(i\mu_m \cos Kx) = \sum_{p=-\infty}^{\infty} i^p J_p(\mu_m) \exp(ipKx)$$

can be used to generate an infinite set of equations from which to calculate the modal amplitudes. To proceed any further, however, approximations have to be introduced and a typical one is to assume K/k is small, with ak of order unity. This leads to an expansion of A_m in ascending powers of K/k. Similar results have been derived by LaCasce and Tamarkin (1956).

Once the need to approximate has been admitted, a more direct approach is to modify the exponentials in the original equation (6). If, for example, it is assumed that K is sufficiently small for $(mK)^2$ to be neglected in comparison with k^2 for all values of m, equation (6) can be inverted to give a recurrence relation for the A_m. Whilst it is clear that the assumption on which this is based will ultimately fail no matter how small K is, the solution is in good agreement with the results of other approximate methods.

All the methods described above impose similar restrictions on the magnitudes of K/k and ak, and in essence the requirements are $K \ll k$, $ak = 0(1)$. These conditions are aimed at minimizing the influence of the cutoff modes and reducing the effect of any one mode on those of lower order. In some cases it is actually assumed that all cutoff modes can be omitted from equation (6), and since the sum then contains only a finite number of terms, the equation

can be solved 'exactly'. The assumption, however, is quite invalid. Just because a mode does not carry energy away from the sheet its amplitude need not be zero, and cannot be neglected in an equation which refers to the very place where such a mode may predominate.

3. PHYSICAL OPTICS

The only approximation inherent in this method is one which is implied by an assumption about the current distribution excited on the surface of the sheet. The exact current is determined by the total field, and this is unknown, but according to physical optics a reasonable approximation can be found by reference to the incident field alone and is

$$\mathbf{J} = 2(\mathbf{n} \wedge \mathbf{H}^i).$$

In other words, the distribution at every point of the surface is the same as if the reflection were taking place at an infinite tangent plane.

For the plane wave whose components are given by equations (3) and (4), the postulated current distribution is

$$\mathbf{J} = (1, -aK \sin Kx, 0) \frac{2Y \exp(-iak \cos Kx)}{\sqrt{\{1+(aK \sin Kx)^2\}}}.$$

This generates a scattered field

$$\mathbf{H}^s = -\frac{1}{4\pi} \int J \wedge \nabla P \, dS$$

where $P = \{\exp(ikR)\}/R$, R being the distance of the receiver from a variable point on the surface. If the co-ordinates of the receiver are $(x_0, y_0, 0)$, then

$$R = \sqrt{\{(x_0-x)^2+(y_0-a \cos Kx)^2+z^2\}}$$

and since

$$\nabla P = \left(\frac{x_0-x}{R}, \frac{y_0-a \cos Kx}{R}, 0\right) \frac{\partial P}{\partial R},$$

it follows that

$$\mathbf{H}^s = (0, 0, H_z^s)$$

where

$$(8) \quad H_z^s = \frac{Y}{2\pi} \int_{-\infty}^{\infty} \int_{-\infty}^{\infty} \frac{(a \cos Kx-y_0)+(x-x_0)aK \sin Kx}{R\sqrt{\{1+(aK \sin Kx)^2\}}} \times \frac{\partial P}{\partial R} \exp(-iak \cos Kx) \, dx \, dz$$

with

$$\frac{\partial P}{\partial R} = \left(ik-\frac{1}{R}\right) \frac{\exp(ikR)}{R}.$$

There are two features of this result which should be noticed. If x_0 is increased by $2m\pi/K$, where m is an integer, the integral can be reduced to

its original form by writing $x' = x - 2m\pi/K$. The expression for H_z^s is therefore periodic in x_0 with period $2\pi/K$, a property which is essential in view of the corrugated nature of the sheet. Secondly, when $a = 0$,

$$H_z^s = -\frac{Yy_0}{2\pi}\int_{-\infty}^{\infty}\int_{-\infty}^{\infty}\frac{1}{R}\frac{\partial P}{\partial R}\,dx\,dz$$

and by introducing polar co-ordinates the integrals can be evaluated exactly to give

$$H_z^s = Y\exp(iky_0),$$

as required for reflection from a flat sheet.

When a is not zero, however, the integrals can only be evaluated by approximate techniques. The one parameter at our disposal is y_0 and since our main interest is in the field at large distances, y_0 can be assumed large compared with everything except the lateral dimensions of the sheet.

Equation (8) can be written as

$$H_z^s = Y\int_{-\infty}^{\infty}\frac{(a\cos Kx - y_0) + (x_0 - x)\,aK\sin Kx}{\sqrt{\{1+(aK\sin Kx)^2\}}}\exp(-iak\cos Kx)\;I(x)\,dx$$

where

$$I(x) = \frac{1}{2\pi}\int_{-\infty}^{\infty}\frac{1}{R}\frac{\partial P}{\partial R}\,dz$$

with

$$R = \sqrt{(z^2+b^2)} \qquad \text{and} \qquad b = \sqrt{\{(x_0-x)^2+(y_0-a\cos Kx)^2\}}.$$

The z integration will be carried out first. Since b is a constant in this integration, the substitution $z = b\sinh\alpha$ reduces $I(x)$ to the form

$$I(x) = \frac{1}{\pi}\int_0^{\infty}\left(ik - \frac{1}{b\cosh\alpha}\right)\frac{\exp(ibk\cosh\alpha)}{b\cosh\alpha}\,d\alpha.$$

But

$$b \geqslant |y_0 - a\cos Kx|,$$

and the right-hand side can be made as large as we please by choosing y_0 appropriately. This makes possible an asymptotic evaluation of $I(x)$ by the method of steepest descents. The saddle point is $\alpha = 0$ and hence

$$I(x) \sim -\frac{1}{b}\sqrt{\frac{k}{2\pi b}}\exp\{i(bk - \pi/4)\},$$

which is accurate to the first order in y_0. By insertion into equation (8), we now have

$$(9)\quad H_z^s = -Y\frac{k}{2\pi}\exp(-i\pi/4)\int_{-\infty}^{\infty}\frac{(a\cos Kx - y_0) + (x - x_0)aK\sin Kx}{\sqrt{\{1+(aK\sin Kx)^2\}}} \times \frac{\exp\{ik(b - a\cos Kx)\}}{b\sqrt{b}}\,dx.$$

Rather than attempt to carry out the x integration immediately, it is more convenient to find the Fourier transform with respect to x_0. The transform is defined as

$$\bar{H} = \int_{-\infty}^{\infty} \exp(i\nu x_0) H_z^s \, dx_0$$

and consequently, from equation (9),

$$\bar{H} = Y \int_{-\infty}^{\infty} \frac{L(x)}{\sqrt{\{1+(aK \sin Kx)^2\}}} \exp(-iak \cos Kx) \, dx \tag{10}$$

where

$$L(x) = -\sqrt{\frac{k}{2\pi}} \exp(-i\pi/4) \int_{-\infty}^{\infty} \{(a \cos Kx - y_0) + (x - x_0) \, aK \sin Kx\} \times \frac{\exp(i\nu x_0 + ibk)}{b\sqrt{b}} \, dx_0. \tag{11}$$

This last integration can be performed by making the substitution

$$x_0 = x + c \sinh \beta$$

where $c = |y_0 - a \cos Kx|$. Since $b = c \cosh \beta$, the exponential factor in the integrand becomes

$$\exp i \{\nu x + d \cosh(\beta + \gamma)\}$$

with $d \cosh \gamma = kc$, $d \sinh \gamma = \nu c$, and $d = c\sqrt{(k^2 - \nu^2)}$. Here again c, and therefore d, can be made as large as we please providing $\nu \neq k$, and if this particular value of ν is excluded for the time being, the integral can be treated by the steepest descents method. The saddle point is $\beta = -\gamma$ and to the first order in y_0,

$$L(x) \sim \exp\{i(\nu x + d)\} \left\{1 - \frac{\nu}{\sqrt{(k^2 - \nu^2)}} aK \sin Kx\right\},$$

which can be substituted into equation (10) to give

$$\bar{H} = Y \exp\{iy_0 \sqrt{(k^2 - \nu^2)}\} \int_{-\infty}^{\infty} \frac{1 - \{\nu / \sqrt{(k^2 - \nu^2)}\} \, aK \sin Kx}{\sqrt{\{1 + (aK \sin Kx)^2\}}} \times \exp[i\nu x - ia\{k + \sqrt{(k^2 - \nu^2)}\} \cos Kx] \, dx. \tag{12}$$

Having reached this stage, it is a simple matter to express H_z^s in a form which brings forth the dependence on the co-ordinates x_0 and y_0. For this purpose equation (12) is written as

$$\bar{H} = Y \exp\{iy_0 \sqrt{(k^2 - \nu^2)}\} \int_{-\infty}^{\infty} F(Kx) \exp(i\nu x) \, dx \tag{13}$$

where

$$F(Kx) = \frac{1 - \{\nu / \sqrt{(k^2 - \nu^2)}\} aK \sin Kx}{\sqrt{\{1 + (aK \sin Kx)^2\}}} \exp[-ia\{k + \sqrt{(k^2 - \nu^2)}\} \cos Kx]. \tag{14}$$

Since $F(Kx)$ is a periodic function of x of period $2\pi/K$, it can be expanded as a Fourier series

$$F(Kx) = \sum_{m=-\infty}^{\infty} A_m(\nu) \exp(imKx)$$

with amplitudes $A_m(\nu)$ given by

$$A_m(\nu) = \frac{K}{2\pi} \int_{-\pi/K}^{\pi/K} F(Kx) \exp(-imKx)\, dx. \tag{15}$$

If this expansion is inserted into equation (13), we have

$$\bar{H} = Y \exp\{iy_0 \sqrt{(k^2-\nu^2)}\} \sum_{m=-\infty}^{\infty} A_m(\nu) \int_{-\infty}^{\infty} \exp\{i(\nu+mK)x\}\, dx$$

and the integral is simply a delta function having unit area when $\nu = -mK$ but zero otherwise. Hence

$$\bar{H} = Y \exp\{iy_0 \sqrt{(k^2-\nu^2)}\} \sum_{m=-\infty}^{\infty} A_m(\nu)\delta(\nu+mK)$$

and application of the inverse transform now gives

$$H_z^s = Y \sum_{m=-\infty}^{\infty} A_m(-mK) \exp[imKx_0 + i\sqrt{\{k^2-(mK)^2\}}y_0] \tag{16}$$

(cf. equation (7)). This is a representation of the scattered field as an angular spectrum of plane waves. The form is precisely that which would be expected of an exact solution and, from equations (14) and (15), the amplitude of the mth mode is

$$A_m = \frac{1}{2\pi} \int_{-\pi}^{\pi} \frac{1+[mK/\sqrt{\{k^2-(mK)^2\}}]\, aK \sin x}{\sqrt{\{1+(aK \sin x)^2\}}} \exp(-imx - i\mu_m \cos x)\, dx. \tag{17}$$

It will be observed that for $a = 0$

$$A_m = \frac{1}{2\pi} \int_{-\pi}^{\pi} \exp(imx)\, dx,$$

which reduces to unity when $m = 0$ and to zero otherwise.

4. DISCUSSION

In evaluating the above integrals the only approximation which has been made is to take ky_0 large compared with unity. The expression for H_z^s then appears as a spectrum of plane waves propagating in the directions θ_m, $|m| \leqslant k/K$, together with an infinity of waves which are attenuated in the direction normal to the sheet. For large y_0, however, the amplitudes must be the same as would be obtained by rigorous evaluation of the integrals in (8) and the fact that the entire dependence on y_0 is through the complex exponentials representing the plane waves now shows that the solution is valid for all y_0. In other words, since the 'error' terms are inverse powers of y_0 which cannot be expressed as exponentials (so as to produce a modification to the A_m), the solution must correspond to an exact evaluation of the original integrals.

Let us consider the behavior of the spectrum as a function of k. From equation (16) the number of modes carrying energy from the sheet depends upon the values of K and k. If attention is concentrated on the mth mode, where $m > 0$, then for $k > mK$ the mode propagates in the direction specified by the angle θ_m and as k decreases, θ_m increases towards $\pi/2$. The amplitude A_m also increases due to the presence of the factor $\sqrt{\{k^2-(mK)^2\}}$ in the denominator and since equation (17) is certainly valid for all $k \neq mK$, the increase must continue until, ultimately, A_m becomes infinite. This occurs when $k = mK$, the cutoff value for the mth mode. The wave is now travelling horizontally and any further decrease in k introduces an attenuation in the y direction which confines the wave to the immediate vicinity of the corrugated sheet. In effect we have a surface wave whose amplitude decreases with k but is not necessarily small.

In a formal sense the behavior when $k = mK$ is still unknown because of the assumption $\nu \neq k$ in evaluating the expression for $L(x)$. Continuity, however, obviously requires that A_m be infinite there and this can be confirmed by putting $\nu = k$ in equation (11). The substitution $x_0 = x+c \sinh \beta$ then gives

$$L(x) = \sqrt{\frac{kc}{2\pi}} \exp\{i(kx-\pi/4)\} \int_{-\infty}^{\infty} (1+aK \sin Kx \sinh \beta) \frac{d\beta}{\sqrt{\cosh \beta}}$$

and since $\sinh \beta$ is an odd function of β,

$$L(x) = \sqrt{\frac{kc}{2\pi}} \exp\{i(kx-\pi/4)\} \int_{-\infty}^{\infty} \frac{d\beta}{\sqrt{\cosh \beta}} \sim \sqrt{\frac{ky_0}{2\pi}} \exp\{i(kx-\pi/4)\} \left\{\Gamma\left(\frac{1}{4}\right)\right\}^2$$

for large y_0, where Γ denotes the gamma function. The rest of the analysis is as before with the result that, at cutoff,

$$A_m = \frac{\exp(-i\pi/4)}{4\pi^2} \sqrt{ky_0} \left\{\Gamma\left(\frac{1}{4}\right)\right\}^2 \int_{-\pi}^{\pi} \frac{\exp(-imx - iak \cos x)}{\sqrt{\{1+(aK \sin x)^2\}}} dx. \tag{18}$$

The dependence on y_0 through a positive power is the only means by which A_m can become infinite when $k = mK$, since y_0 is the one variable (and large) parameter appearing in equation (11) and $L(x)$ cannot be infinite per se. As cutoff is approached, y_0 must be taken larger and larger in order to fulfill the condition $y_0\sqrt{(k^2-\nu^2)} \gg 1$ in the evaluation of $L(x)$ and hence, in (18), y_0 must be treated as infinite.

These conclusions only apply to the amplitude factor A_m and for other field components the cutoff behavior may differ from the above. With the incident field of Section 2, the non-zero components in the scattered field are H_z^s, E_x^s, and E_y^s. From equation (16), we have

$$E_x^s = -\sum_{m=-\infty}^{\infty} \frac{\sqrt{\{k^2-(mK)^2\}}}{k} A_m \exp[imKx_0+i\sqrt{\{k^2-(mK)^2\}}\, y_0],$$

$$E_y^s = \sum_{m=-\infty}^{\infty} \frac{mK}{k} A_m \exp[imKx_0+i\sqrt{\{k^2-(mK)^2\}}\, y_0],$$

and whereas E_y^s is similar to H_z^s in that its mth mode becomes infinite at the cutoff frequency, the corresponding mode in the expansion for E_z^s remains finite when k approaches mK and its amplitude has the limiting value

$$(19) \qquad \frac{iaK}{\pi}\int_0^\pi \frac{\sin x \sin mx}{\sqrt{\{1+(aK\sin x)^2\}}}\exp(-imaK\cos x)\,dx.$$

This difference is a direct consequence of the boundary conditions and provides an explanation for the discrepancy between the formulae of Eckart and Brekhovskikh near to cutoff (see LaCasce and Tamarkin 1956). In both theories conditions are imposed on the function and its derivative at the conducting sheet, and since the subsequent analysis is approximate, the amplitude factors will depend on the relative weights attached to these conditions in the derivation of the solution.

All the field components are determined by the amplitudes A_m and an expression for A_m as a finite integral is given in equation (17). Unfortunately, no method for evaluating this has been found. The integral is a function of the three parameters a, K, and k, and the case which would be the most interesting to study is that in which aK is not small compared with unity. The theories referred to in Sections 1 and 2 then fail and though it is difficult to justify the use of an optics current if aK is as large as k/K, the integral has been evaluated numerically for a few values of the parameters satisfying this condition. The results are in good agreement with the experimental measurements of LaCasce and Tamarkin.

If $aK < 1$ it is relatively easy to obtain an approximation to the integral. The denominator in the integrand can then be expanded in ascending powers of aK to give

$$A_m = \frac{1}{2\pi}\int_{-\pi}^{\pi}\left\{1+\frac{maK^2\sin x}{\sqrt{\{k^2-(mK)^2\}}}-\frac{1}{2}(aK\sin x)^2+0(aK^3)\right\} \times \exp(-imx-i\mu_m\cos x)\,dx$$

and since

$$\frac{1}{2\pi}\int_{-\pi}^{\pi}\exp(-imx-i\mu_m\cos x)\,dx = (-i)^m J_m(\mu_m),$$

it follows that

$$(20) \quad A_m = (-i)^m\left[\frac{k}{\sqrt{\{k^2-(mK)^2\}}}J_m(\mu_m)-\frac{(aK)^2}{4\mu_m} \times\{(m-1)\,J_{m-1}(\mu_m)+(m+1)\,J_{m+1}(\mu_m)\}\right]$$

where terms of order $(aK)^3$ have been omitted. Of particular interest are the amplitudes of the fundamental and first harmonic, and these are

$$A_0 = J_0(2ak)-\frac{aK^2}{4k}J_1(2ak),$$

$$A_1 = -i\left\{\frac{k}{\sqrt{(k^2-K^2)}}J_1(\mu_1)-\frac{(aK)^2}{2\mu_1}J_2(\mu_1)\right\}$$

which are similar to the results of Lord Rayleigh (1878). However, the case $aK < 1$ is not a good one for demonstrating the advantages of the present solution. In the absence of an exact evaluation of the integral for A_m, it would be most desirable to have an expansion corresponding to (20) but appropriate to large aK. This would permit a more complete comparison with the experimental data, but no way of adequately treating the case $aK > 1$ has yet been found.*

5. CONCLUSIONS

Physical optics is known to be an effective method for treating scattering by bodies whose dimensions (including radii of curvature) are large compared with the wavelength, and this is particularly true when the entire surface is illuminated by the incident field. The problem of a corrugated sheet satisfies these requirements.

The optics method as such is, of course, not new, but in the past there has been a tendency to squander some of the advantages by a lack of care in the evaluation of the resulting integrals. Inaccuracies which then appear may arise as a consequence of the evaluation and should not be automatically ascribed to a failure in the approximation to the current.

The main feature of the present paper is the evaluation of the optics integral. Although a steepest descents technique is used on two separate occasions, these are such that the only condition is upon the distance of the receiver from the sheet ($ky_0 \gg 1$), and since the solution is a spectrum of plane waves, this must be equivalent to an exact evaluation of the integral. It is interesting to note that even the cutoff modes, which would not be expected to contribute to the field at infinity, do appear in the final solution.

The amplitudes of the plane waves are given by a simple integral over a finite range, but no method for evaluating this has been found. For $aK < 1$, however, the integrand can be expanded to give a series expression for the amplitude, and this is in good agreement with the available experimental data. For certain larger values of aK the integral has been evaluated numerically for different ak, and the fact that these results also agree with experiment suggests that the solution has a wide range of applicability.

REFERENCES

Brekhovskikh, L. M. 1952. J. Exptl. Theoret. Phys. U.S.S.R. **23**, 305.
Eckart, C. 1953. J. Acoust. Soc. Am. **25**, 566.
LaCasce, E. O. and Tamarkin, P. 1956. J. Appl. Phys. **27**, 138.
Lord Rayleigh. 1878. The theory of sound, Vol. II (Macmillan & Co., Ltd., London).

*Since this was written a series evaluation has been obtained which is convergent (and useful) for all values of aK. This will be described in a future paper.

THERMAL CONDUCTIVITY OF POWDERS[1]

M. J. LAUBITZ

ABSTRACT

The effective thermal conductivity of several powders of reasonably uniform particle size, and one powder of graded particle size, was measured in the temperature range of 100° C to 1000° C. Most of the results can be very satisfactorily explained by assuming that the effective conductivity of the powder is composed of two parts, the first part being a two-phase gas–solid conductivity, and the second an equivalent radiation conductivity.

INTRODUCTION

There has been in the past a continuous interest in the effective conductivity of multiphase media, particularly of the two-phase gas–solid medium. The conductivity of such a two-phase medium depends on which of the two is the continuous phase, and which is what may conveniently be called an obstacle. The case of dense ceramics, where the ceramic may be considered as the continuous phase, has been studied in detail by Francl and Kingery (1954). They compared their results with several of the available theoretical formulae, and found reasonably good agreement. Powdered ceramics, however, where air or another gas is the continuous phase, have not yielded particularly consistent results, and the agreement with the theoretical expressions derived from various models has not been spectacular. The chief shortcomings of the theoretical expression are due to the necessary simplicity and artificiality of the models for which they have been calculated. The difficulty here lies in two directions: primarily, the construction of a model that represents reasonably well the two-phase system under consideration, and secondarily, the calculation of the effective conductivity of that model. The first part is difficult, particularly if irregular particles of varying size are considered. The second is impossible except for very simple geometry, or under some simplifying though highly unreasonable assumptions. So far, only one accurate expression for the effective thermal conductivity has been obtained. This was calculated by Lord Rayleigh (1892) for a cubical array of uniform spheres, and his result can be put into the following form:

$$\frac{K}{K_m} = \frac{(2+\nu)/(1-\nu)-2p}{(2+\nu)/(1-\nu)+p} \tag{1}$$

where K = the effective conductivity of the two-phase medium,
K_m = the conductivity of the continuous phase,
$\nu = K_o/K_m$,
K_o = the conductivity of the obstacles,
p = the fractional volume of obstacles.

This expression was later generalized by Burgers (1919) to include arrays of arbitrary ellipsoids in a cubical arrangement.

[1]Manuscript received March 31, 1959.
Contribution from the Division of Applied Physics, National Research Council, Ottawa, Canada.
Issued as N.R.C. No. 5227.

Fairly recently the cubical array of spheres has been considered again, with certain simplifying assumptions. Deissler and Eian (1952) envisaged such an array of spheres with the heat flow lines being parallel straight lines. This is equivalent to assuming that the conductivity of the components of the medium is vanishingly small in directions perpendicular to the heat flow. Their calculation is done for a closely packed structure, i.e. $p = \pi/6$. It can, however, be easily generalized for arbitrary $p \leqslant \pi/6$, and has then the form

$$\frac{K}{K_m} = \frac{\pi}{2}\frac{\{(1/\nu-1)R-\ln[1+(1/\nu-1)R]\}}{(1/\nu-1)^2} + 1 - \frac{\pi R^2}{4} \tag{2}$$

where $R = (6p/\pi)^{1/3}$ is the radius of the spherical obstacles. Woodside (1958), on the other hand, takes the cubical array of spheres and assumes that the isotherms are planes perpendicular to the direction of heat flow (equivalent to assuming an infinite lateral conductivity). He obtains the following expression:

$$\left(\frac{K}{K_m}\right)^{-1} = 1-R\left[1-\left(\frac{\alpha^2-1}{2\alpha}\right)\ln\left(\frac{\alpha+1}{\alpha-1}\right)\right] \tag{3}$$

where

$$\alpha = \left[1+\frac{4}{\pi(\nu-1)R^2}\right]^{1/2}.$$

There is one further model to consider, proposed by Russell (1935). He calculated the conductivity of cubes in a cubical array, assuming again that isotherms are planes perpendicular to the direction of heat flow. For this model he obtains

$$\frac{K}{K_m} = \frac{\nu p^{2/3}+(1-p^{2/3})}{\nu(p^{2/3}-p)+(1-p^{2/3}+p)}. \tag{4}$$

It is worth noting that for large ν Russell's equation reduces to

$$\frac{K}{K_m} = \frac{1}{1-p^{1/3}} \tag{5}$$

and this is identical with the form obtained for large ν if one treats the cubical array of cubes in the straight flow-line approximation.

It may well be asked why one should consider any but Lord Rayleigh's equation, which is the only exact one. The answer to that lies in the dual difficulty of the theoretical calculations mentioned before. Lord Rayleigh provides an exact mathematical calculation, but his model is so rigid and artificial, permitting the spheres to be located only in the center of their unit cubical spaces, that it radically departs from powders encountered in practice. The plane isotherm models, on the other hand, though their mathematical treatment is unrigorous, permit an arbitrarily irregular location of obstacles in their unit cubical spaces, and hence are more realistic. Furthermore, Lord Rayleigh's model (and the other models using spheres) limits the value of p to less than $\pi/6$, while Russell's model permits the whole range of p from zero to unity.

Figures 1 and 2 show some of the values of K/K_m obtained from the equations (1), (2), (3), and (4). The conductivities K(L.R), K(D and E),

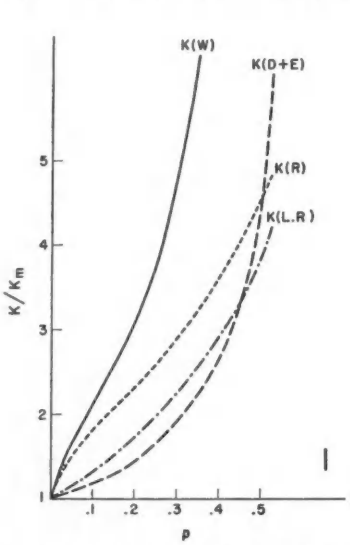

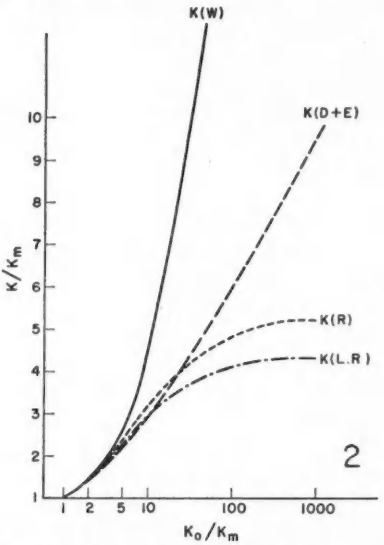

FIG. 1. Variation of effective conductivity with obstacle volume fraction, for a fixed value of solid-to-gas conductivities, $K_o/K_m = 100$.

FIG. 2. Variation of effective conductivity with ratio of solid-to-gas conductivity for fixed obstacle volume fraction, $p = \pi/6$.

K(W), and K(R) refer to the conductivities calculated from equations (1) to (4) respectively. It is seen from these two figures that K(L.R) and K(R) do not differ very much from each other. This is true for all values of p and K_o/K_m. On the other hand, K(W) and K(D and E) deviate considerably from K(L.R), particularly for large p and K_o/K_m. This deviation may condemn these models from the mathematical point of view. From the practical point of view they may still be useful, however, as the final selection of the model is in this case a purely empirical matter.

To determine which of these models, if any, best represents the actual powders, a set of experiments was undertaken with powders of various materials, various porosities, and various grain sizes. The effective thermal conductivity of these powders was measured in the range of 100° C to 1000° C, and the results compared with those predicted by the theoretical equations.

EXPERIMENTAL PROCEDURE AND RESULTS

The experimental arrangement is illustrated in Fig. 3. Essentially the apparatus consists of a long cylindrical furnace, inside which there is a centrally located heater 4 mm in diameter and 30 cm long. Two Pt/(Pt–10% Rh) thermocouples are held rigidly at radial distances of 5.6 mm and 10.1 mm, the tip of the outside thermocouple being about 1 cm above the tip of the inside one. The furnace was filled with the required powder, tapped, and filled

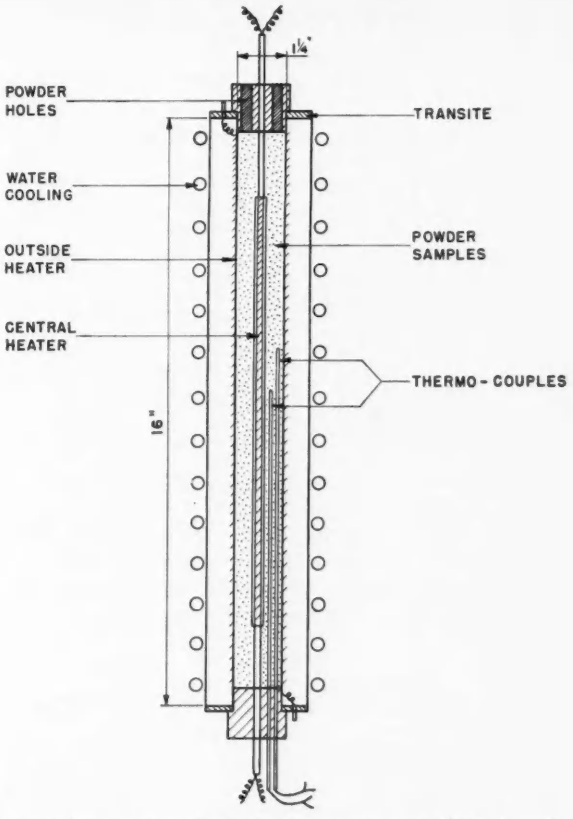

FIG. 3. The experimental arrangement for the measurement of the thermal conductivity of powders.

again. This was continued until the powder no longer subsided on reasonable tapping. From the weight of the powder put in, and the known volume of the furnace, the porosity of the powder under experimental conditions was calculated.

The following procedure was employed to measure the thermal conductivity. With no power through the central heater, the input into the furnace was adjusted until the outside thermocouple registered a required temperature T_0. At equilibrium, the radial gradient $\Delta T(0)$ was measured. Then the power through the central heater was switched on, and again the furnace adjusted until the outside thermocouple read approximately T_0. At equilibrium, the gradient $\Delta T(P)$, corresponding to the central heater power input of P watts was measured. The effective conductivity of the powder at the temperature $T_0+[\Delta T(P)]/2$ was then calculated from the formula

$$K\left(T_0+\frac{\Delta T(P)}{2}\right)=\frac{\ln r_2/r_1}{2\pi l}\cdot\frac{P}{\Delta T(P)-\Delta T(0)}$$

where l is the length of the central heater in centimeters, r_2 and r_1 are the radial distances of the outer and inner thermocouples respectively, and $K(T)$ is the thermal conductivity of the powder at temperature T in watt/cm °C.

The powders studied are listed in Table I, together with their pertinent properties. The powders marked "D" were composed of dense crystalline

TABLE I

Properties of the powders

Powder	Nature of particles	Particle diam., cm	Powder density, g/cc	Volume fraction of particles, P
MgO D(10–20)	Dense crystals	0.140±0.060	1.60	0.469
MgO D(35–50)	Dense crystals	0.040±0.010	1.70	0.475
MgO D(100–200)	Dense crystals	0.011±0.004	1.54	0.430
Al_2O_3 D(35–50)	Dense crystals	0.040±0.010	1.82	0.475
Al_2O_3 B(35–50)	Porous bubbles	0.040±0.010	1.15	0.29
ZrO_2 B(35–50)	Porous bubbles	0.040±0.010	2.02	0.33
Al_2O_3 R	Graded size		1.00	0.25

particles of porosity no larger than 4%, and of irregular shape. The powders marked "B" were in the form of bubbles, with the ceramic shells surrounding air. Their shape was nearly spherical, and surfaces smooth. The numbers in parentheses behind the powder material indicate the mesh of the sieves limiting the particle size. The Al_2O_3 R powder was a reagent grade alumina with a wide range of particle size (Table II). Its low density indicates that

TABLE II

Particle distribution of Al_2O_3 R

Mesh	Powder retained on sieve, %
50	0
100	13.1
200	58.2
325	19.9
Through 325	8.8
	100.0

the particles were highly porous. The experimentally obtained conductivities for these powders are shown in Figs. 4 to 8.

The absolute accuracy of the measurements is not very high. The maximum deviation from the average observed in the measured conductivity for four separate fillings of the furnace with one and the same powder was ±12%. The inaccuracy due to thermocouple positioning and possibly lack of concentricity of central heater and furnace tube is estimated at ±10%. Thus one has to put an uncertainty of ±20% on the absolute value of the measurements. The relative accuracy, that is the relative values of thermal conductivity of the different materials is much better, of the order of ±10%. This is also the accuracy one would expect for the relative values of the conductivity of one and the same powder at various temperatures.

ANALYSIS AND DISCUSSION

The analysis of the dense particle powders being more straightforward, it is undertaken here first. In Figs. 4 to 6 are shown the results for the four

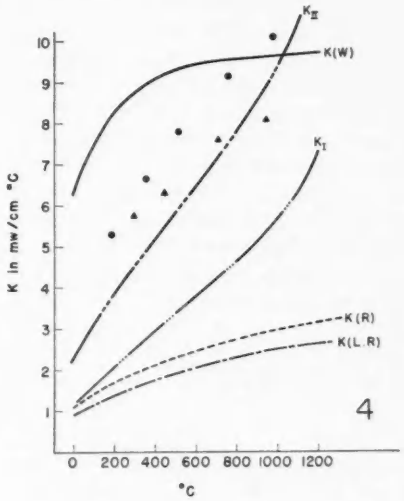

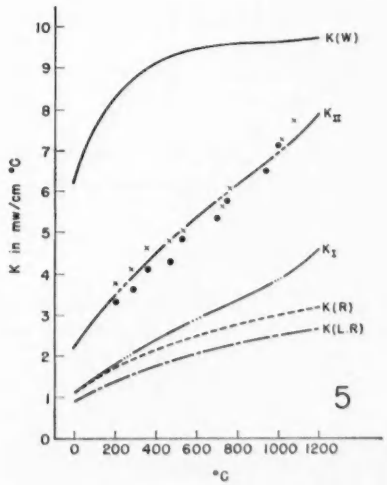

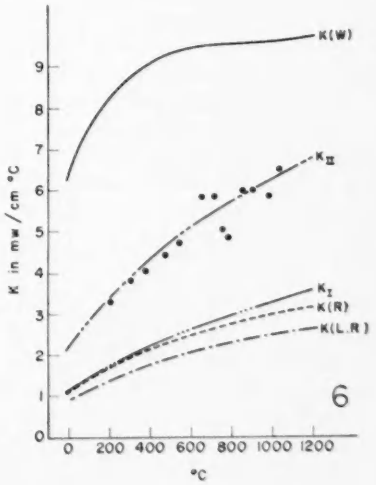

FIG. 4. Thermal conductivity of MgO D(10–20). ●●● Experimental points for central heater power input of 4 watts/cm. ▲▲▲ Experimental points for central heater power input of 2 watts/cm.

FIG. 5. Thermal conductivity of MgO D(35–50) cm and Al_2O_3 D(35–50). ××× Experimental points for Al_2O_3. ●●● Experimental points for MgO.

FIG. 6. Thermal conductivity of MgO D(100–200). ●●● Experimental points.

dense particle powders, together with the calculated effective conductivities $K(\mathrm{L.R})$, $K(\mathrm{R})$, and $K(\mathrm{W})$. In these calculations the values for dense ceramics were taken from Kingery *et al.* (1954) and for air from Russell (1935). The calculated conductivities do not correspond to the experimental ones, either in absolute value or in their temperature variation. All the experimental conductivities increase more rapidly with temperature than any of the models predict. This points to the omission of some temperature-dependent factor in the theoretical analysis. Such a factor is, of course, radiation.

The inclusion of radiation into any of the previously mentioned models is impossible without some structural changes. For, as these models stand now, continuous paths are open to the radiant energy. To obtain finite radiation path particles must be randomly positioned in their respective unit cells—this is possible only in the models of Woodside and Russell. As Woodside's conductivities are already larger than the experimental ones, Russell's model alone is left for modification to include radiation. Using that model, an expression for the contribution of radiation is derived in the appendix. The final formula for the effective conductivity is then

$$K_{\mathrm{I}} = K(\mathrm{R}) + 4\sigma T^3 \epsilon \frac{a}{p} (1 - p^{2/3} + p^{4/3}) \tag{6}$$

where

$$K(\mathrm{R}) = K_{\mathrm{m}} \frac{\nu p^{2/3} + (1 - p^{2/3})}{\nu(p^{2/3} - p) + (1 - p^{2/3} + p)}$$

is the conductivity calculated by Russell.

ϵ is the emissivity of the ceramic (given in High Temperature Technology (1956)),

a is the linear dimension of the particles,

p is the fractional volume of the particles,

σ is the Stefan–Boltzmann constant.

The conductivity K_{I} accounts well for the shape of the temperature curve, but not for its absolute value. One can get a very good agreement with the experimental data, however, if one uses the formula

$$K_{\mathrm{II}} = 2K(\mathrm{R}) + 4\sigma T^3 \epsilon \frac{a}{p} (1 - p^{2/3} + p^{4/3}). \tag{7}$$

The reason why $K(\mathrm{R})$ has to be doubled can be seen qualitatively as follows. In actual powders there are densely packed regions where particles touch each other, and empty air pockets. The densely packed regions contribute chiefly by conduction while the air pockets contribute by radiation. As shown in the appendix, the air pockets have roughly a length of a/p_0, where a is the linear dimension of the particles, and p_0 the average particle volume fraction for the aggregate. But then the p value for the densely packed region is not p_0 but $p_0^{1/3}$, and the equivalent conductivity of the powder becomes $K(\mathrm{R}, p_0^{1/3}) . p_0^{2/3}$, where $K(\mathrm{R}, p_0^{1/3})$ is the Russell's conductivity calculated for $p = p_0^{1/3}$. For the powders used in these experiments

$$K(\mathrm{R}, p^{1/3}) . p^{2/3} \approx 2K(\mathrm{R}, p),$$

which gives a rough reason for the factor of two used in equation (7).

One can now determine whether equation (7) applies to the other powders tested. The blown powders can be considered in the following way. The radiation contribution will depend primarily on the size of the particles and their packing, and not on the true porosity. Thus the radiation contribution has to be evaluated on the basis of $p = p_1$, where p_1 corresponds to the packing of the particles, and equals approximately 0.5. The conductivity, on the other hand, has to be evaluated for the true porosity, $p \sim 0.3$. Thus

$$K_{II} = 2K(R, p) + 4\sigma T^3 \epsilon \frac{a}{p_1} (1 - p_1^{2/3} + p_1^{4/3})$$

where $p_1 \sim 0.5$,
$p \sim 0.3$.

Figure 7 shows that K_{II} accounts quite well for the experimental results. It can be pointed out here that for alumina and magnesia, the conductivities of

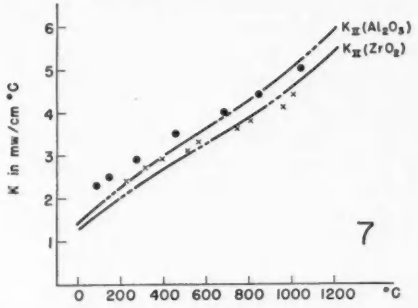

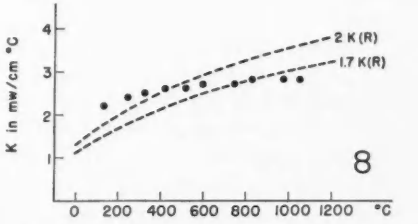

FIG. 7. Thermal conductivity for Al_2O_3 B(35–50) and ZrO_2 B(35–50). ●●● Experimental points for Al_2O_3. ××× Experimental points for ZrO_2.
FIG. 8. Thermal conductivity for Al_2O_3 R. ●●● Experimental points.

the solids are so high that equation (5), independent of K_0, can be used to an accuracy of 2 to 4%. This is not the case for zirconia, whose conductivity is relatively small. Thus, for a given particle size, the conductivities calculated for alumina and magnesia are the same, but different from that for zirconia.

There remain the results for the graded alumina. Because of its very small average particle size one expects to have no significant contribution from radiation, and equation (7) reduces to

(8) $$K_{II} = 2K(R).$$

However, this does not explain the experimental results obtained (Fig. 8). In fact, the temperature variation of $K(R)$, or of any other of the previously considered conductivities, is such that it cannot account for the graded powder. It may well be that such powder will require the construction of completely new models, but there is not as yet sufficient experimental information available to confirm that. Furthermore, some of the experimental work is rather confusing. For instance, Deissler and Eian published results on graded magnesia in argon, air, and helium for a p value of 0.58 in 1952 and 0.64 in 1953. Their 1952 results for air and argon but not helium can be described quite well by equation (8), while their 1953 results are completely different from what is predicted by that equation. Particularly confusing is the curvature they obtained in 1953 for the magnesia in helium.

Another interesting thing may here be mentioned. Figure 4 shows the results for the MgO D(10–20). The experimental points lie on two curves which meet at the lower and diverge at the higher temperatures. These two sets of points correspond to two different power inputs for the central heater, the higher conductivity being obtained from the large power input. This effect may be due to the transparency of magnesia to infrared, an effect which has been previously observed (see discussion after Russell 1935). Such transparency would increase the effective conductivity of the powder, the increase being a function of both temperature and temperature gradient. However, this contribution would only be significant in coarse powders, where there are relatively few reflecting grain surfaces. This is precisely what has been observed.

SUMMARY

The effective thermal conductivity of several powders of reasonably uniform particle size, and one powder of graded particle size, has been measured in the temperature range 100° C to 1000° C. The results for the powders with uniform particle size can be very well accounted for if the effective conductivity is assumed to be composed of two parts, the two-phase conductivity as calculated by Russell (1935), arbitrarily doubled, and an equivalent radiation conductivity. For a large ratio of obstacle to medium conductivity, the formula for the effective conductivity can be put in the form

$$K = \frac{2K_m}{1-p^{1/3}} + 4\sigma T^3 \epsilon \frac{a}{p}(1-p^{2/3}+p^{4/3}).$$

The conductivity calculated by this formula does not agree with the measurements on graded powders. It is likely that for such powders a new model will have to be devised for the calculation of effective conductivity.

REFERENCES

BURGERS, H. C. 1919. Physik. Z. **20**, 73.
CAMPBELL, I. E. 1956. High temperature technology (John Wiley & Sons), p. 55.
DEISSLER, R. G. and EIAN, C. S. 1952. National Advisory Committee for Aeronautics R.M., E52C05.
——— 1953. National Advisory Committee for Aeronautics, R.M., E53G03.
FRANCL, J. and KINGERY, W. D. 1954. J. Am. Ceram. Soc. **37**, 99.

KINGERY, W. D., FRANCL, J., COBBE, R. L., and VASILOS, T. 1954. J. Am. Ceram. Soc. **37**, 107.
RAYLEIGH, LORD. 1892. Phil. Mag. **34**, 481.
RUSSELL, H. W. 1935. J. Am. Ceram. Soc. **18**, 1.
WOODSIDE, W. 1958. Can. J. Phys. **36**, 815.

APPENDIX

CALCULATION OF THE CONTRIBUTION OF RADIATION TO THE EFFECTIVE CONDUCTIVITY OF POWDERS

The basic model is one given by Russell (1935). The obstacles are assumed to be cubes of length, a, located in cubical volumes of the medium of length, d. It is then assumed that the obstacles are randomly scattered in the cubical volumes, but in such a manner that the faces of the two cubes remain parallel. Such a scattering does not affect the thermal conductivity of the two-phase medium. Let the probability that radiation will pass a cube without hitting an obstacle be r, then

$$r = 1-\frac{a^2}{d^2}.$$

If L is the average length that radiation travels if it has not hit an obstacle in the first cube, then

$$L = d+rd+r^2d+\ldots$$
$$= \frac{d}{1-r} = \frac{d^3}{a^2}.$$

If p is the particle volume fraction, then

$$p = \frac{a^3}{d^3}$$

and

$$L = \frac{a}{p}.$$

The rate of heat transfer by that radiation is

$$\dot{Q} = 4\sigma T^3\epsilon(d^2-a^2)\Delta T$$
$$= 4\sigma T^3\epsilon L\left(1-\frac{a^2}{d^2}\right)\frac{\Delta T d^2}{L}$$

where T is the absolute temperature, ϵ is the emissivity of the obstacles, and $\Delta T/L$ is the gradient in the two-phase medium, assumed small compared to T. Therefore the contribution of that radiation to the effective conductivity is

$$4\sigma T^3\epsilon L\left(1-\frac{a^2}{d^2}\right) = 4\sigma T^3\epsilon\frac{a}{p}(1-p^{2/3}).$$

There will also be a contribution by the radiation that does hit an obstacle in the first cube of the medium. This contribution is difficult to calculate, but one can estimate it by assuming that the radiation that does hit an obstacle in the first cube travels on the average a distance of $(d-a)$. Thus the rate of heat transfer by this process is

$$\dot{Q} = \frac{a^2 dK_r K_o}{aK_r + LK_o} \cdot \frac{\Delta T}{d}$$

where

$$K_r = 4\sigma T^3 \epsilon L$$

and its contribution to the effective conductivity is

$$\frac{a^2 K_r K_o}{d(aK_r + LK_o)} = \frac{p^{1/3} K_r K_o}{K_r + K_o/p}$$

and as usually $K_o/p \gg K_r$, the contribution becomes

$$p^{4/3} K_r = p^{4/3} 4\sigma T^3 \epsilon \frac{a}{p}.$$

The total contribution by radiation is then

$$4\sigma T^3 \epsilon \frac{a}{p} (1 - p^{2/3} + p^{4/3})$$

and the total effective conductivity

$$K = K(\mathrm{R}) + 4\sigma T^3 \epsilon \frac{a}{p} (1 - p^{2/3} + p^{4/3})$$

where $K(\mathrm{R})$ is the two-phase conductivity calculated by Russell.

THE PHOTODISINTEGRATION OF TANTALUM[1]

R. W. PARSONS[2] AND L. KATZ

ABSTRACT

The cross section for the absorption of photons by Ta^{181} has been deduced from measurements of the neutrons emitted when tantalum is irradiated in the X-ray beam of a 22-Mev betatron. The cross section has well-defined peaks at $12.75\pm.25$ and $15.25\pm.25$ Mev, and from this the intrinsic electric quadrupole moment is deduced to be 5.7 ± 1.3 barns.

INTRODUCTION

It has been suggested by Okimoto (1958) and Danos (1958) that the half-width of the photonuclear photon absorption cross section should be related to the nuclear eccentricity and hence to the intrinsic electric quadrupole moment. For sufficiently large eccentricities, the giant resonance is expected to show two distinct maxima at energies E_a and E_b corresponding, on the hydrodynamical model of Goldhaber and Teller (1948) as developed by Danos, to oscillations of the proton and neutron fluids either parallel to the axis of rotational symmetry or normal to it. Danos predicts that, for a spheroidal nucleus with half-axes a and b,

$$E_b/E_a = 0.911\, a/b + 0.089 \tag{1}$$

where a and b are related to the atomic number Z and the intrinsic quadrupole moment Q by the equation

$$Q = \frac{2}{5}Z(a^2-b^2).$$

If the separation E_b-E_a between the resonance energies is smaller than the half-widths of the component resonance curves, the total photon absorption cross section may show a single broad peak instead of two distinct ones.

Nathans and Halpern (1954) found that the giant resonance half-widths for photon absorption by closed shell nuclei, for which $Q = 0$, are abnormally small. Katz and Chidley (1958) confirmed this and, in a study of 17 elements, found that the half-widths agreed reasonably well with those predicted by Okimoto (1958). Their measurements were not sufficiently precise to show evidence of double peaks, but such evidence has been found by Fuller and Weiss (1958), who studied tantalum and terbium, and Spicer *et al.* (1958), who studied tantalum. Both these groups measured the neutron yield when a specimen is irradiated with X rays and deduced the photon absorption cross section from a knowledge of the X-ray bremsstrahlung curves and the neutron multiplicity. Both found two peaks in the giant resonance of tantalum, and from their separation the intrinsic quadrupole moment was estimated to

[1]Manuscript received April 13, 1959.
Contribution from the Physics Department, University of Saskatchewan, Saskatoon, Saskatchewan.
[2]National Research Council Postdoctorate Fellow.

be 5.7±0.3 barns (Fuller and Weiss 1958) and 6.1±0.6 barns (Spicer 1958). Fuller and Hayward (1958) have recently reported measurements of the elastic scattering cross section for photons by tantalum, but although the results are suggestive the statistics are not good enough to provide convincing evidence for two peaks.

The above results, however, are not confirmed by the recent work of Carver and Turchinetz (1959). They found the cross section σ_1 for the reaction $Ta^{181}(\gamma, n)Ta^{180}$ by irradiating tantalum with X rays and measuring the residual activity of the 8.15-hour isomeric state of Ta^{180}. The ratio of the $Ta^{181}(\gamma, 2n)Ta^{179}$ cross section, σ_2, to σ_1 had previously been deduced from residual activity and total neutron measurements by Carver, Edge, and Lokan (1957), and so the photon absorption cross section $\sigma_1+\sigma_2$ was found. This showed a giant resonance of half-width 6.3 Mev, in reasonable agreement with the calculations of Okimoto (1958), but there was no evidence for two peaks.

The present work gives an account of further measurements which provide additional evidence for the existence of two peaks.

EXPERIMENTAL PROCEDURE

A stack of tantalum foils, of total thickness 4.98 g cm^{-2}, was irradiated in the X-ray beam from the University of Saskatchewan betatron, and the photoneutrons were detected by BF_3 counters; details of the method have been described previously (Montalbetti, Katz, and Goldemberg 1953). The room in which the detection system is housed was maintained between 19° and 20° C throughout the experiments, and the detection efficiency was monitored regularly with a Ra–Be neutron source; the variation during a period of several weeks was $\pm\frac{1}{2}\%$. Except near threshold, the counting rate was kept near 60 per second, corresponding to a maximum rate at the instant of opening the gate of 2500 per second, and observed counts were corrected for both counting losses and small variations in the neutron detection efficiency.

Measurements were made at intervals of 0.2 Mev between 7.6 and 22 Mev, the energy scale being monitored regularly by irradiating oxygen samples at 17.26 Mev and measuring the induced 2.1-minute β^+ activity. The dose was measured with an aluminum wall, transmission ionization chamber, and this was subsequently calibrated against a Victoreen thimble in an 8-cm lucite cube. The yield curve was normalized by comparing the yields from copper and tantalum at 22 Mev and assuming the former to be 2.71×10^8 neutrons/mole 100 r.

RESULTS AND DISCUSSION

In Fig. 1, the photoneutron yield per mole per 100 r, A, is plotted against the maximum photon energy E_m in the X-ray spectrum; except near the γ, n threshold, between 40,000 and 100,000 counts were taken for each point. The (γ, n) threshold was found to be 7.63±0.05 Mev, in good agreement with earlier measurements (Chidley, Katz, and Kowalski 1958).

The yield curve was smoothed before being analyzed. It was fitted roughly

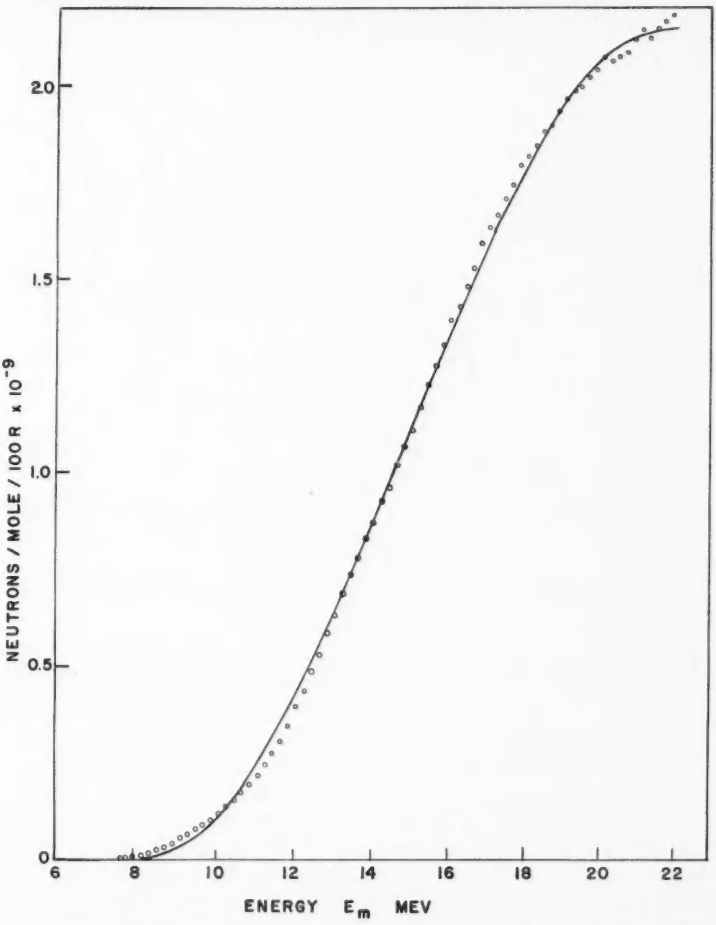

FIG. 1. Photoneutron yield from tantalum. The full curve is the sine approximation.

by the function $A' = \alpha\{1+\sin(\beta E_m - \delta)\}$, the constants α, β, and δ being determined by trial and error. The deviations $A - A'$ of the experimental points from the sine curve are shown in Fig. 2; a smooth curve was drawn through the points by inspection. It was then assumed that the true yield curve is the sum of the sine curve A' and the smooth deviation curve. Excluding the points near threshold, the r.m.s. percentage deviation of the experimental points from the smoothed yield curve was 0.49%, and a rough check showed that the distribution was consistent with a normal error curve; this suggests that no significant features were removed from the yield curve by the smoothing process.

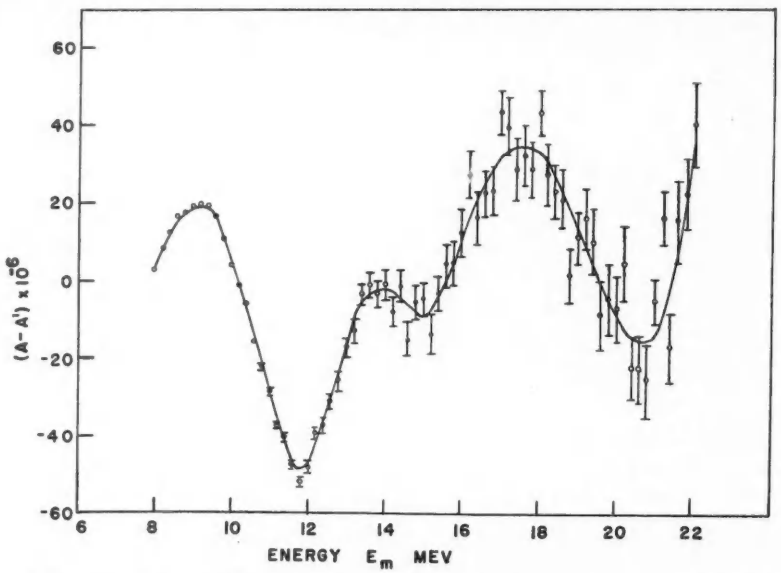

FIG. 2. Deviations of the experimental points from the sine curve. Where the standard deviation is not shown it is smaller than the radius of the circles.

The yield curve was analyzed by the inverted matrix method of Penfold and Leiss (1958) using a bin width of 0.5 Mev; the resulting values of $\sigma_1+2\sigma_2$ are shown in Fig. 3. These values were then corrected for neutron multiplicity using (*a*) the data of Carver and Turchinetz (1959) and (*b*) calculations based on the statistical model described by Blatt and Weisskopf (1952), to give the photon absorption cross section $\sigma_1+\sigma_2$. Multiplicities derived from the data of Whalin and Hanson (1953) are between those used above. The cross section, which is very similar to that found by Fuller and Weiss (1958), has two distinct peaks at 12.75 ± 0.25 and 15.25 ± 0.25 Mev, and so, assuming that equation (1) is valid, the intrinsic quadrupole moment is 5.7 ± 1.3 barns. This is in good agreement with the results of other observers which have already been quoted.

The sudden increase that occurs above 21 Mev is almost certainly spurious; the calculated cross section is very sensitive to changes of slope of the yield curve in this region and if the observed yields for the last three points are reduced by approximately $\frac{2}{3}\%$ the abnormality is removed. The cross section deduced by Fuller and Weiss also shows large fluctuations in this energy region.

Several attempts were made to fit theoretical curves to the experimentally measured cross section; either a Lorentz curve, as used by Fuller and Weiss, or an optical dispersion curve can be made to fit the data reasonably well. The curve shown in Fig. 3 is of the latter type, viz.

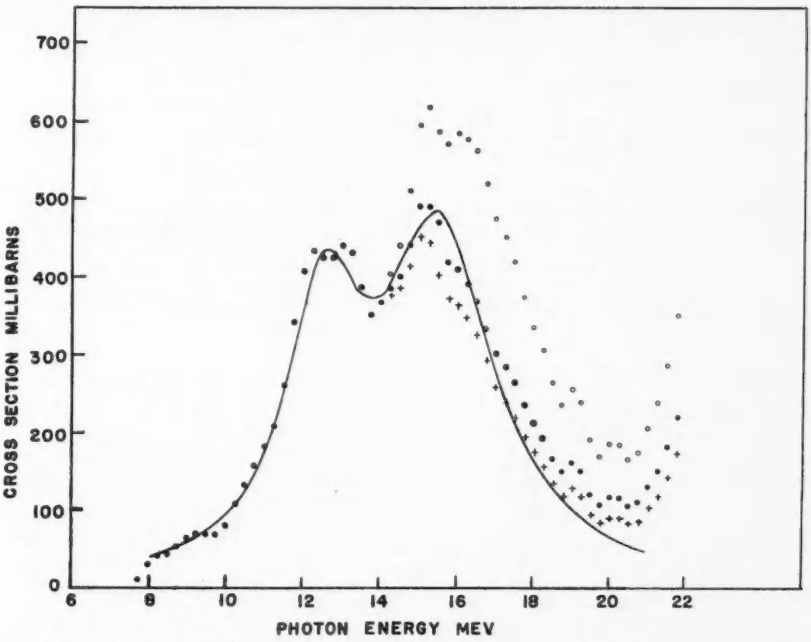

FIG. 3. The cross section for neutron production $\sigma_1+2\sigma_2$ and photon absorption $\sigma_1+\sigma_2$. The full curve is compounded of two resonance curves whose parameters are given in the text. ○ $\sigma_1+2\sigma_2$; ● $\sigma_1+\sigma_2$ (*a*); + $\sigma_1+\sigma_2$ (*b*).

$$\sigma = \frac{\sigma_1}{1+\{(E-E_1)/\Gamma_1/2\}^2} + \frac{\sigma_2}{1+\{(E-E_2)/\Gamma_2/2\}^2},$$

where $\sigma_1 = 317$ mb, $\sigma_2 = 444$ mb, $E_1 = 12.5$ Mev, $E_2 = 15.5$ Mev, $\Gamma_1 = 2.3$ Mev, and $\Gamma_2 = 3.6$ Mev. Using these values of the parameters the over-all agreement with the experimental points is reasonable, although the separation between the peaks of the composite curve is rather too large. The ratio of the areas under the peaks of the component resonance curves is $\sigma_1\Gamma_1/\sigma_2\Gamma_2 = 0.46$, the predicted value being 0.5. Not such a good fit, however, was obtained with the standard Breit–Wigner formula in which σ_1 and σ_2 above are replaced by $\sigma_1(E_1/E)^2$ and $\sigma_2(E_2/E)^2$.

ACKNOWLEDGMENT

One of the authors (R. W. P.) is indebted to the National Research Council for a Postdoctoral Fellowship.

REFERENCES

BLATT, J. M. and WEISSKOPF, V. F. 1952. Theoretical nuclear physics (John Wiley & Sons, Inc., New York), p. 379.
CARVER, J. H., EDGE, R. D., and LOKAN, K. H. 1957. Proc. Phys. Soc. A, **70**, 415.
CARVER, J. H. and TURCHINETZ, W. 1959. Proc. Phys. Soc. **73**, 69.

CHIDLEY, B. G., KATZ, L., and KOWALSKI, S. 1958. Can. J. Phys. **36**, 407.
DANOS, M. 1958. Nuclear Phys. **5**, 23.
FULLER, E. G. and WEISS, M. S. 1958. National Bureau of Standards Report 5687.
FULLER, E. G. and HAYWARD, E. 1958. Phys. Rev. Letters, **1**, 465.
GOLDHABER, M. and TELLER, E. 1948. Phys. Rev. **74**, 1046.
KATZ, L. and CHIDLEY, G. B. 1958. Nuclear reactions at low and medium energies (Academy of Sciences of the U.S.S.R.), p. 371.
PENFOLD, A. S. and LEISS, J. E. 1958. Analysis of photo cross-sections (Physics Research Laboratory, University of Illinois, Chicago).
MONTALBETTI, R., KATZ, L., and GOLDEMBERG, J. 1953. Phys. Rev. **91**, 659.
NATHANS, R. and HALPERN, J. 1954. Phys. Rev. **93**, 437.
OKIMOTO, K. 1958. Phys. Rev. **110**, 143.
SPICER, B. M., THIES, H. H., BAGLIN, J. E., and ALLUM, F. R. 1958. Australian J. Phys. **11**, 298.
WHALIN, E. A. and HANSON, A. O. 1953. Phys. Rev. **89**, 324.

THE OCCURRENCE OF $(n, 3n)$ REACTIONS IN A NUCLEAR REACTOR[1]

T. A. Eastwood and J. C. Roy

ABSTRACT

The reactions $Bi^{209}(n, 3n)Bi^{207}$ and $Au^{197}(n, 3n)Au^{195}$ have been observed to occur in NRX, a thermal neutron reactor. Competing reactions leading from Bi^{209} or Au^{197} to the same products have been shown to be negligible. Within the uncertainties of the methods used the yields of Bi^{207} and Au^{195} are about those expected on the basis of neutron evaporation from the compound nucleus formed by the amalgamation of the incoming neutron and the target nucleus.

INTRODUCTION

The complete exploration of the neutron spectrum in a nuclear reactor using activation detectors requires reactions with thresholds in a region above those in current use. The $(n, 3n)$ reactions have suitable thresholds (14–25 Mev) for this purpose but their occurrence in a nuclear reactor has not been reported. There is, of course, no reason why such reactions should not occur if the excitation of the nucleus is sufficiently high. Marquez (1952) states that Cu^{61} is produced during the irradiation of natural copper with neutrons of mean energy of about 370 Mev and this is probably the product of a $(n, 3n)$ reaction. However, this energy region is much above that encountered in nuclear reactors. Watt (1952) has observed neutrons with energies up to 17.2 Mev in the spectrum of neutrons from U^{235} fission and it is thought that the neutron energy spectrum extends to 20 Mev (Hughes 1953).

The detection of the $(n, 3n)$ reaction is difficult because the product is an isotope of the target element and chemical methods cannot be employed to separate it from the products of the more probable (n, γ) and $(n, 2n)$ reactions. Nevertheless, the decay characteristics of the neutron deficient nuclei are now sufficiently well known to permit the choice of a few elements in which the $(n, 3n)$ reaction might be observed. A consideration of the properties of the nuclides indicates that the most likely elements with which to detect the $(n, 3n)$ reaction are those in which the product of the $(n, 3n)$ reaction is radioactive and has a reasonably long half-life. The half-life of the product should differ by several orders of magnitude from the half-lives of the products of the (n, γ) or $(n, 2n)$ reactions. Then a long irradiation followed by suitable decay period facilitates the detection of the $(n, 3n)$ reaction product. This approach requires rigorous chemical purification following the irradiation because even trace impurities can yield large amounts of radioactive products on long irradiations.

The nuclear properties of bismuth and gold isotopes shown in Table I are

[1]Manuscript received March 16, 1959.
Contribution from the Research Chemistry Branch, Atomic Energy of Canada Limited, Chalk River, Ontario.
Issued as A.E.C.L. No. 816.

TABLE I

Nuclear properties of bismuth and gold isotopes involved in neutron-induced reactions

Bi^{207}	Bi^{208}	Bi^{209}	Bi^{210}
28 years	3×10^{4} years	Stable	2.6×10^{6} years
K and L electron capture	K electron capture	100% abundance	α—4.94
γ—0.57, 0.89, 1.06, 1.43, 1.77	γ—2.615		

Au^{195}	Au^{196}	Au^{197}	Au^{198}	Au^{199}
180 days	5.6 days	Stable	2.70 days	3.15 days
K and L electron capture	Electron capture	100% abundance	β^{-}—0.96, 0.29, 1.37	β^{-}—0.30, 0.25, 0.46
γ—0.031, 0.098, 0.13	β^{-}—0.27 γ—0.331, 0.354		γ—0.4118, 0.68, 1.09	γ—0.05, 0.158, 0.208

NOTE: Short-lived isomeric states are omitted. Energies are in Mev.

such that these elements are suitable targets. The $(n, 3n)$ reaction thresholds are 14.3 Mev for $Bi^{209}(n, 3n)Bi^{207}$ and 13.2 Mev for $Au^{197}(n, 3n)Au^{195}$ (Wapstra 1958). In addition they are obtainable in pure form and their chemistry is relatively well understood.

EXPERIMENTAL METHODS

Irradiations

With the exception of one bismuth irradiation all irradiations were made in empty fuel rod positions in the NRX reactor. This is a D_2O-moderated, natural-uranium-fueled reactor, the physical characteristics of which have been described by Hurst (1955). The sample position was in the center of a hexagonal array of fuel rods and was separated from the fuel rods by 17.3 cm of D_2O. The thermal neutron flux in the positions used was about 6×10^{13} n/cm^2-sec.

Four bismuth irradiations were made. In the first a 160-mg sample of bismuth metal was irradiated to an integrated thermal neutron flux of 2.7×10^{21} n/cm^2. It was allowed to decay for about 2 years before it was used for the measurements reported here. For identification this is called sample A. Two other samples of bismuth (called B and C) weighing about 3 g each were irradiated near each other in the reactor. The integrated thermal neutron flux was 2.8×10^{20} n/cm^2. In order to separate thermal neutrons from fast neutron effects, one sample (C) was placed inside a cadmium box with 0.064-cm thick walls. Measurements with these bismuth samples began 5 months after the irradiations. The fourth irradiation was the exception mentioned previously. It was made in the center of a hollow natural-uranium cylinder, 3.5 cm in external diameter and with walls 0.023 cm thick. This "neutron transformer" was placed in an empty fuel rod position in the NRX reactor. The sample (D) weighed about 800 mg and was irradiated for 33 days. A period of 10 months elapsed before the measurements reported here were made.

One irradiation of 250 mg of metallic gold was made. The integrated neutron flux was 1.7×10^{20} n/cm^2. Measurements with this sample were begun 5 months after the irradiation.

Chemical Purification

(*a*) *Bismuth.*—As pointed out earlier, extensive purification of the target is required to detect a small amount of Bi^{207} produced. It was found that the main radiochemical contaminants were Po, Zn, Hg, Sn, Sb, and Cd. The chemical treatment used to remove these contaminants from sample A has been described previously (Roy *et al.* 1958). This method was not suitable for the purification of samples B, C, and D owing to the large amount of bismuth involved. The samples were dissolved and the polonium was removed as described for sample A. The following preliminary steps were then made before the purification treatment described for sample A was applied. Mercury carrier as Hg^{++} was added to the solution and Hg_2Cl_2 plus some Hg was precipitated by the addition of $SnCl_2$. The precipitate was removed by centrifugation and discarded. After the addition of cadmium carrier to the solution, Bi and Sn in metallic form were precipitated by the addition of finely powdered Zn in dilute HCl; Cd remained dissolved under these conditions. The precipitated metal was treated with hot concentrated HCl, which dissolved the tin, and the precipitate was removed by centrifugation. The Bi was dissolved upon treatment with HNO_3. This procedure was repeated several times. Finally, the Bi was further purified by the chemical treatment described for sample A.

(*b*) *Gold.*—The irradiated gold sample was dissolved in aqua regia and, because a measurement of the amount of 48-day Hg^{203} produced in the irradiation was required for reasons presented in the Discussion, a known amount of mercury carrier was added. The solution was adjusted to be 3 *N* in HCl and the gold was extracted with ethyl acetate. The organic phase was washed several times with 3 *N* HCl containing platinum carrier. The ethyl acetate was removed by evaporation and the residue was dissolved in 2 *N* HNO_3. Metallic gold was precipitated by the addition of stannous chloride. The gold was redissolved in aqua regia and the extraction was repeated. Finally the metallic gold was mounted on an aluminum tray for examination of its γ-ray spectrum.

Counting Techniques

The decay of both Bi^{207} and Au^{195} gives rise to well-known γ-rays. Therefore, the γ-ray spectra of the purified Bi and Au were examined with a scintillation γ-ray spectrometer which consisted of a 1 in. $\times$ 1½ in. NaI(Tl) crystal coupled to an RCA 5819 photomultiplier tube, conventional electronics, and a 24-channel pulse height analyzer. The energy scale of the spectrometer was determined using γ-rays from the decay of Am^{241}, Na^{22}, Cs^{137}, Co^{60}, and Na^{24}. The efficiency was determined using sources of Na^{22}, Na^{24}, Au^{198}, and Cs^{137} prepared from solutions standardized by 4π β-counting techniques.

RESULTS

(*a*) *Bismuth*

The γ-ray spectra of the four samples of irradiated, purified bismuth in the region of 0.3 to 1.3 Mev are shown in Fig. 1. The two well-known gamma

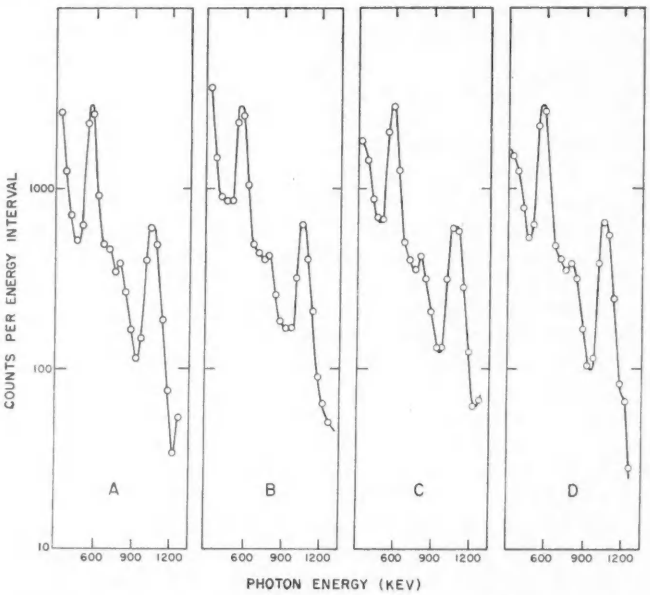

FIG. 1. Portions of the gamma-ray spectra of four samples of irradiated purified bismuth.
Sample A was irradiated in a predominantly thermal neutron spectrum, integrated thermal neutron flux 2.7×10^{21} n/cm^2.
Sample B was irradiated in a predominantly thermal neutron spectrum, integrated thermal neutron flux 2.8×10^{20} n/cm^2.
Sample C was irradiated with epi-cadmium neutrons near sample B.
Sample D was irradiated for 1 month in a "neutron transformer".

rays of Bi^{207} at 0.569 and 1.063 Mev (Alburger and Sunyar 1955) are clearly resolved in all four spectra. The other γ-rays of Bi^{207} are in low abundance and were not detected. It was therefore concluded that Bi^{207} was present in the sources.

The complete γ-ray spectra of each of the four samples also show peaks at 0.270, 2.1, and 2.6 Mev. These are not associated with the decay of Bi^{207}. The 2.1- and 2.6-Mev peaks are due to Bi^{208} as described previously (Roy *et al.* 1958). The γ-ray spectrum of sample A in the energy range 1.8 to 3.5 Mev was given there. The 270-kev peak is certainly due to bismuth since its peak height relative to the peaks of Bi^{207} and Bi^{208} does not depend on the degree of chemical purification. It seems to be associated with the product of an (n, γ) reaction since it is much more predominant in samples A and B which were irradiated in a thermal neutron flux than in samples C and D which

were irradiated with epi-thermal or fast neutrons. This point is illustrated by the spectra in Fig. 2. It is suggested that the 270-kev γ-ray arises from the

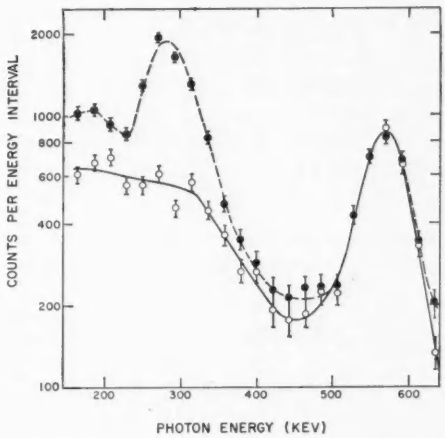

FIG. 2. Gamma-ray spectra of irradiated, purified bismuth samples.
The two samples were irradiated near each other in the reactor. Sample C (open circles) was enclosed in cadmium and sample B (full circles) was uncovered. The low abundance of the 270-kev γ-ray in the spectrum of the covered bismuth indicates that the 270-kev γ-ray is associated with a thermal neutron induced activity.

decay of 2.6×10^6-year Bi^{210}, a hypothesis which is supported by preliminary α–γ coincidence experiments.* Further work on the source of this γ-ray is in progress and the results will be reported separately.

The yield of Bi^{207} was estimated from the observed counting rate of the 1.063-Mev γ-ray peak, the efficiency of the γ-ray spectrometer (1.6%), the known decay scheme of Bi^{207}, and the weight of the bismuth sample used for counting. The half-life of Bi^{207} was taken to be 28 years (Sosniak and Bell 1959). The results are given in Table II. For reasons to be discussed later it

TABLE II

Results of bismuth irradiations

Sample	Irradiation position in NRX	Integrated thermal neutron flux, n/cm²	Weight of purified sample, g	Observed Bi^{207} disintegration rate, dis/sec	Effective $(n, 3n)$ reaction cross section, cm
A	Empty fuel rod	2.7×10^{21}	0.054	73	2.2×10^{-31}
B	Empty fuel rod	2.8×10^{20}	0.308	47	2.4×10^{-31}
C	Empty fuel rod (Cd-covered sample)	2.8×10^{20}	0.654	94	2.2×10^{-31}
D	"Neutron transformer"	1.9×10^{20}*	0.150	50	7.8×10^{-31}

*Estimated integrated thermal neutron flux in this position in the absence of the "neutron transformer".

*NOTE ADDED IN PROOF.—This hypothesis is substantiated by the work of S. V. Golenetskii, L. I. Rusinov, and Iu. I. Filimonov, Zhur. Eksptl. i Teoret. Fiz. **35**, 1313 (1958); JETP, **8**, 917 (1959).

is convenient to deduce an effective cross section for the $Bi^{209}(n, 3n)Bi^{207}$ reaction which, when multiplied by the thermal neutron flux, gives the observed reaction rate. The effective cross sections so obtained are also given in Table II.

(*b*) *Gold*

The γ-ray spectrum of the purified gold sample is shown in Fig. 3. The γ-ray spectrum was measured 5 months after the end of the irradiation so

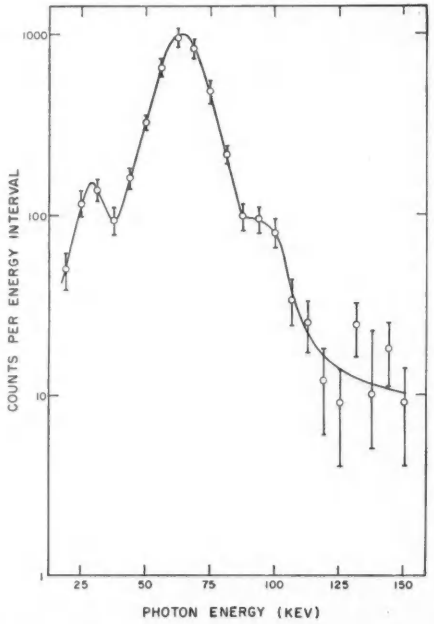

FIG. 3. X- and γ-ray spectrum of irradiated, purified gold.

that the Au^{198}, Au^{199}, and Au^{196} activity had essentially all decayed. Cressman and Wilkinson (1958) have found that Au^{195} decays entirely by electron capture and that the electromagnetic spectrum consists of a strong K X-ray peak at 67 kev, less intense peaks at 31 and 98 kev, and a very low intensity peak at 129 kev. All but the lowest intensity peak are present in the spectrum in Fig. 3. No γ-rays above 98 kev were observed in the γ-ray spectrum and no electrons with energy sufficient to penetrate 3 mg/cm^2 of aluminum were detected from the sample of gold, thus attesting to the radiochemical purity of the sample. The activity, observed for a period of 200 days, decayed with a half-life of about 190 days, in agreement with the average of published half-lives of 183 days for Au^{195} (Strominger 1958). It was therefore concluded that Au^{195} was present in the irradiated gold samples.

It is difficult to estimate the yield of Au^{195} from this irradiation because

the amount of internal conversion of the γ-rays is not accurately known. However, approximately 1000 disintegrations per second of Au^{195} were observed in 230 mg of gold corresponding to an effective cross section of 3×10^{-31} cm^2.

DISCUSSION

The experimental results presented in the preceding section show that Bi^{207} and Au^{195} are present in samples of bismuth and gold irradiated in the NRX reactor. The isotopes might be produced by a number of mechanisms but it will be shown that the most probable is the $(n, 3n)$ reaction.

(*a*) *Bismuth*

Let us first consider the possibility of two successive $(n, 2n)$ reactions. The disintegration rate of the product of two successive $(n, 2n)$ reactions is given by a relationship of the type:

$$(1) \qquad \frac{dN_B}{dt} = \frac{N_S\sigma_S\sigma_A\phi^2T_A}{0.693(T_A-T_B)}\left[T_A(1-e^{-\lambda_A t})-T_B(1-e^{-\lambda_B t})\right]$$

where the subscripts S, A, and B refer to the target nuclide, and the product of the first- and second-order neutron capture reactions respectively; N_S is the number of atoms of target nuclide; σ is the effective cross section of the individual $(n, 2n)$ reactions; ϕ is the neutron flux; T is the half-life; λ is the disintegration constant; and t is the duration of the irradiation.

All factors in equation 1 are known except the cross-section values. Ideally these would be measured but there are technical difficulties. Therefore we have made an estimate of the appropriate cross sections based on the cross sections observed for other $(n, 2n)$ reactions under similar irradiation conditions. The results of these auxiliary measurements are given in Table III.

TABLE III

Relation between the effective $(n, 2n)$ cross section and E_{eff}

Target nuclide	Effective cross section,* millibarns	$\sigma/A^{2/3}$	E_{eff}, Mev
Th^{232}	2.7 ± 0.7	7.2×10^{-2}	7.5 ± 0.2†
Pb^{204}	0.094 ± 0.02	2.8×10^{-3}	10.2 ± 0.5
Tl^{203}	$0.13 \pm^{0.06}_{0.02}$	3.6×10^{-3}	10.8 ± 0.6
I^{127}	0.052 ± 0.01	2.1×10^{-3}	11.0 ± 0.7
As^{75}	0.009 ± 0.002	5.1×10^{-4}	12.5 ± 0.2
Y^{89}	0.005 ± 0.002	2.5×10^{-4}	14.3 ± 0.4
Fe^{54}	$(1.0\pm0.2)\times10^{-4}$‡	7.2×10^{-6}	16.7 ± 0.3

*The effective cross section is used only because it is convenient. It has no significance except that it gives the observed reaction rate in the particular neutron spectrum used in this investigation when multiplied by the thermal neutron flux.

†The errors given in this column are due to the uncertainties in the masses of the nuclei involved (Duckworth 1958) plus an uncertainty of about ±0.2 Mev in the estimation of E_{eff}.

‡Betts and Dahlinger (1957).

It should be emphasized that the tabulations are effective cross sections. The only significance of the effective cross section is that when multiplied by the thermal neutron flux it gives the observed reaction rate. Effective cross

sections are used as a matter of convenience only. Clearly they apply to this particular neutron spectrum only and cannot be used directly to give the rate of reaction in a different neutron spectrum.

In order to form the best estimate of the bismuth cross sections required it is desirable to interrelate the cross sections observed for the other $(n, 2n)$ reaction on some theoretical basis. At bombarding energies below about 20 Mev, according to current theories, fast-neutron-induced reactions in which neutrons are emitted proceed predominantly by the amalgamation of the incident neutron with the target nucleus to form a compound nucleus with all the available energy as excitation energy. This excitation energy is then carried off by one or more nucleons ("evaporation"). For heavy elements charged particle emission is hindered by the coulomb barrier and neutron emission predominates. The general feature of $(n, 2n)$ reactions in this energy range are reasonably well understood (see for example Blatt and Weisskopf 1952). The cross section σ is related to the excitation energy E by the relation

$$\sigma = \sigma_c [1-(1+y)e^{-y}] \tag{2}$$

where

$$y = \frac{E-E_T}{T},$$

E_T is the threshold energy, T is the nuclear temperature, and σ_c is the cross section for the formation of the compound nucleus.

Equation 2 would give the desired relation for monoenergetic neutrons, but, of course, the reactions occurred in a spectrum of neutron energies from the reactor. It is therefore convenient to define an effective neutron energy, E_{eff}, following Hughes (1953). The effective energy is chosen in such a way that the correct reaction rate is obtained on the assumption that neutrons below E_{eff} produce no reaction while all those above it are equally effective in producing the reaction. Then

$$\sigma = \sigma_c[1-(1+y)\, e^{-y}]\left[\int_{E_{eff}}^{\infty} N(E)dE\right] \Big/ \left[\int_0^{\infty} N(E)dE\right] \tag{3}$$

where

$$\left[\int_{E_{eff}}^{\infty} N(E)dE\right] \Big/ \left[\int_0^{\infty} N(E)dE\right]$$

is the fraction of neutrons with energy greater than E_{eff}.

For the present purpose this relation can be simplified by assuming (1) σ_c is equal to the geometric cross sections $\pi\ 2.3\times10^{-26}\ A^{2/3}$ cm^2, (2) the factor $1-(1+y)e^{-y}$ is constant (in fact it varies from 0.30 to 0.44 for the reactions involved here), and (3) the fraction

$$\left[\int_{E_{eff}}^{\infty} N(E)dE\right] \Big/ \left[\int_0^{\infty} N(E)dE\right]$$

is proportional to $e^{-E_{eff}}$ (a very good approximation for the fission neutron spectrum at energies above 6 Mev). Thus equation 3 reduces to

$$\sigma = k A^{2/3} e^{-E_{eff}} \tag{4}$$

or

$$\frac{\sigma}{A^{2/3}} = k e^{-E_{eff}} . \tag{5}$$

The validity of equation 5 has been tested by plotting log $\sigma/A^{2/3}$ against E_{eff} in Fig. 4. The experimental results are shown by the points with their

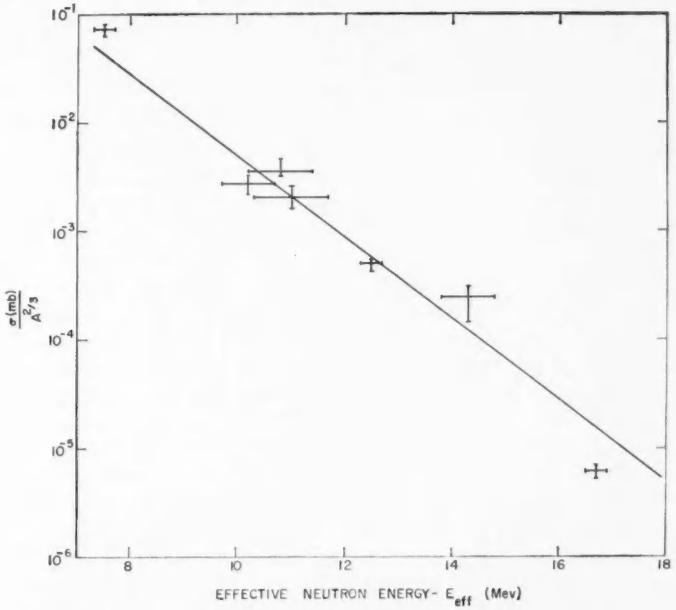

FIG. 4. The relationship between the observed effective $(n, 2n)$ cross sections and the effective neutron energy. The effective cross section has no significance except that it gives the observed reaction rate in the particular neutron spectrum used in this investigation when multiplied by the *thermal* neutron flux. The points are the experimental results with an estimate of the errors. The line has the slope expected from theory.

associated errors. The line in Fig. 4 has the slope predicted by evaporation theory. Since the points lie on a line of approximately the predicted slope, estimates of the cross section of other $(n, 2n)$ reactions can be made with some confidence. On this basis the maximum cross sections for the bismuth and gold reactions were deduced and are given in Table IV.

The effective cross sections in Table IV were used to predict the yield of Bi^{207} from two successive $(n, 2n)$ reactions starting with Bi^{209}. It was found to be 2×10^{-2} disintegrations per second for sample B. This is about 1/3000 of the observed yield and shows that successive $(n, 2n)$ reactions are negligible.

Inspection of the properties of nuclides in the neighborhood of Bi^{207} shows that

TABLE IV

Expected effective $(n, 2n)$ cross sections

Target nuclide	E_{eff}, Mev	Maximum expected effective cross section, millibarns
Bi^{209}	8.8±0.2	1.3
Bi^{208}	8.0±0.2	2.9
Au^{197}	9.5±1.1	0.89
Au^{196}	7.0±1.1	19.0
Hg^{196}	9.3±1.1	1.1

the only other means, apart from the $(n, 3n)$ reaction, by which Bi^{207} could be formed during a neutron irradiation of bismuth is by the series of reactions $Bi^{209}(n,\gamma)Bi^{210} \xrightarrow{\beta\text{-decay}} Po^{210}(n,\gamma)Po^{211} \xrightarrow{\beta\text{-decay}} At^{211} \xrightarrow{\alpha\text{-decay}} Bi^{207}$. All of these reactions are known to occur except the β-decay of Po^{211}. Two

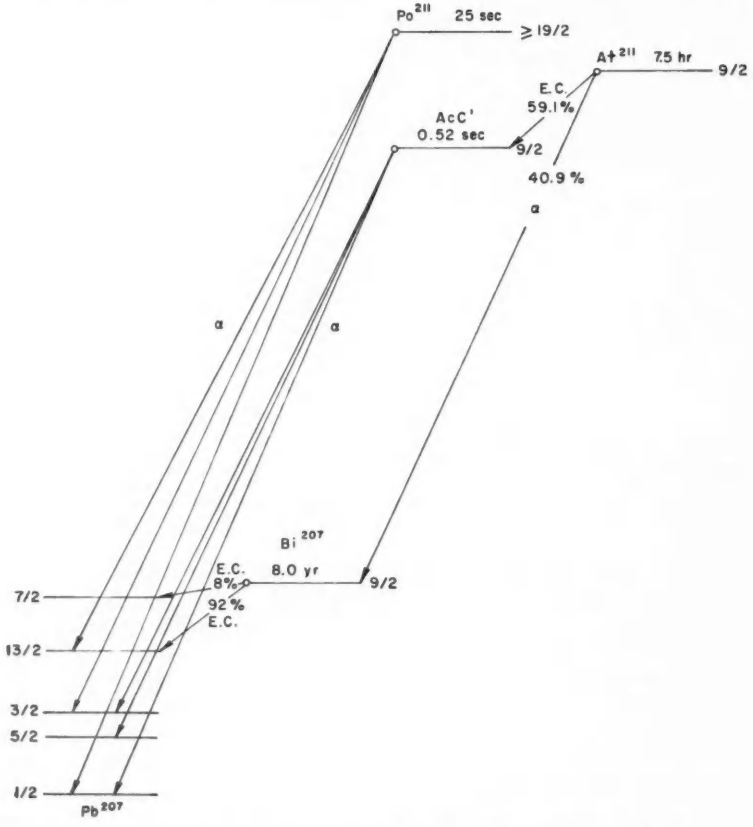

FIG. 5. Decay schemes of nuclei in the Bi^{207} region (Strominger *et al.* 1958).

isomeric states of Po^{211} have been observed and both decay by the emission of an α-particle. No β-decay has been found. It is clear from Fig. 5 that β-decay from the 25-second state of Po^{211} to At^{211} is energetically possible although highly forbidden if the spin assignments are correct. Therefore this mechanism for Bi^{207} formation cannot be neglected. The proposed chain of reactions involves two (n, γ) reactions which would be expected to be more probable in a thermal neutron flux than in a fast neutron flux. The yield of Bi^{207} would therefore be expected to be smaller in the cadmium-covered sample C than in the uncovered sample B. This is contrary to the experimental observations and thus this possibility is eliminated.

It is therefore concluded that Bi^{207} found in neutron-irradiated bismuth was produced by the $Bi^{209}(n, 3n)Bi^{207}$ reaction.

(b) Gold

In order to estimate the importance of two successive $(n, 2n)$ reactions in the production of Au^{195} from Au^{197} the cross sections of the reactions involved were estimated by the method outlined for bismuth and the results are given in Table IV. Using these cross sections the expected yield of Au^{195} by this route was found to be 2 disintegrations per second or 1/500 of the observed yield. Here again it was concluded that successive $(n, 2n)$ reactions make an insignificant contribution to the observed yield of Au^{195}.

A possible source of Au^{195} in the present experiments is from mercury impurity in the gold sample which was irradiated. The $Hg^{196}(n, 2n)$ reaction leads to Hg^{195} which in turn decays to Au^{195} by electron capture. The amount of mercury in the gold sample was determined by activation analysis. A known amount of mercury carrier was added during the gold purification procedure outlined in a previous section. From the chemical yield and the disintegration rate of the recovered 48-day Hg^{203}, determined by counting the 0.28-Mev γ-ray, the amount of mercury was found to be 7×10^{-9} g. If the $Hg^{196}(n, 2n)Hg^{195}$ cross section is taken to be 1.1 millibarns (Table IV) the expected disintegration rate of Au^{195} from this source is 2×10^{-4} per second. Clearly this reaction is an unimportant source of Au^{195}.

On the basis of these results it is concluded that the reaction $Au^{197}(n, 3n)Au^{195}$ with a threshold energy of 13.2 Mev has occurred in reactor irradiations.

The emission of three neutrons from the compound nucleus at low excitation energy is predominantly an evaporation process and it should be possible to predict the cross section on the same basis as the $(n, 2n)$ cross sections were predicted. When this is done the observed cross section for $Bi^{209}(n, 3n)Bi^{207}$ is found to be one-quarter of that expected. This is probably a satisfactory agreement in view of the approximations involved. The agreement for the $Au^{197}(n, 3n)Au^{195}$ reaction cross section is not as satisfactory; the observed cross section is one-sixth of that calculated. However, as pointed out earlier there is insufficient information about the decay of Au^{195} to permit an accurate measurement of the effective cross section.

The occurrence of $(n, 3n)$ reactions indicates that neutrons of high energy exist in the sample irradiation positions of a well-moderated thermal neutron

reactor such as NRX and it would be of interest to search for neutrons of still higher energies using suitable threshold detectors. One promising reaction is the $C^{12}(n, 2n)C^{11}$ reaction which has a threshold energy of 20.3 Mev (E_{ett} = 24.5 Mev). Extrapolation of the relationship in Fig. 4 indicates that the yield of C^{11} should be sufficient to permit its detection by the 510-kev annihilation radiation. The results of such an investigation are reported in the paper which follows.

REFERENCES

ALBURGER, D. E. and SUNYAR, A. W. 1955. Phys. Rev. **99**, 695.
BETTS, R. H. and DAHLINGER, O. 1957. Private communication.
BLATT, J. M. and WEISSKOPF, V. F. 1952. Theoretical nuclear physics (John Wiley & Sons, Inc., New York).
CRESSMAN, P. J. and WILKINSON, R. G. 1958. Phys. Rev. **109**, 872.
DUCKWORTH, H. E. 1958. Mass spectroscopy (Cambridge University Press, Cambridge, England).
HUGHES, D. J. 1953. Pile neutron research (Addison-Wesley Publishing Co., Inc., Cambridge, Mass.).
HURST, D. G. 1955. Proceedings of the International Conference on the Peaceful Uses of Atomic Energy, Vol. 5, 111.
MARQUEZ, L. 1952. Phys. Rev. **88**, 225.
ROY, J. C., EASTWOOD, T. A., and HAWKINGS, R. C. 1958. Can. J. Phys. **36**, 18.
SOSNIAK, J. and BELL, R. E. 1959. Can. J. Phys. **37**, 1.
STROMINGER, D., HOLLANDER, J. M., and SEABORG, G. T. 1958. Revs. Modern Phys. **30**, 585.
WAPSTRA, A. H. 1958. Atomic masses of nuclides, *in* Encyclopedia of Physics, Vol. 38/1 (Springer-Verlag, Berlin).
WATT, B. E. 1952. Phys. Rev. **87**, 1037.

EVIDENCE FOR NEUTRONS WITH AN ENERGY OF 20.3 MEV IN THE NRX REACTOR[1]

J. C. Roy

ABSTRACT

Experimental evidence is presented on the occurrence of the $C^{12}(n, 2n)C^{11}$ reaction in the NRX reactor. The probability of occurrence of the competing processes $C^{12}(\gamma, n)C^{11}$ and $C^{12}(p, pn)C^{11}$ is discussed. A comparison is made of the observed reaction rate with the one predicted by the formula representing the energy distribution of the prompt neutrons from the thermal fission of U^{235}. Since the threshold of the $C^{12}(n, 2n)C^{11}$ reaction is 20.3 Mev, observation of the reaction in the NRX reactor means that there are neutrons with an energy of at least 20.3 Mev produced in fission.

INTRODUCTION

It seems to be accepted that the fission neutron spectrum extends to about 20 Mev (Hughes 1957). However, experimentally the fission neutron spectrum has been determined only up to 17.2 Mev (Watt 1952). Watt measured the ranges of knock-on protons by a telescope of proportional counters. The preceding paper on the observation of $(n, 3n)$ reaction in the NRX reactor and the comparative studies of $(n, 2n)$ and $(n, 3n)$ effective cross sections supports the belief of Hughes that the fission neutron spectrum extends to 20 Mev or more. Eastwood and Roy (1959) also suggested that the studies of some high-energy threshold reactions of the types $(n, 2n)$ and $(n, 3n)$ could be used to examine the fission neutron spectrum in the 20-Mev range. One such reaction is $C^{12}(n, 2n)C^{11}$ which has a Q value of 18.72 ± 0.02 Mev (Wapstra 1955) and a threshold of 20.3 Mev. Experimental evidence on the observation of the $C^{12}(n, 2n)C^{11}$ reaction in the NRX reactor is reported here.

EXPERIMENTAL

Samples of 0.2 g of anthracene were irradiated in a vacant fuel rod position near the center of the NRX reactor for 30 minutes at a thermal neutron flux of about 6.0×10^{13} n/cm^2-sec. Immediately after the irradiation the anthracene was transformed to carbon dioxide and water by combustion in a Parr oxygen bomb. After the combustion the gases were passed through concentrated sulphuric acid and "Anhydrone"; finally the carbon dioxide was absorbed in "Ascarite". The "Ascarite" was pressed onto an aluminum tray (3 cm in diameter) to form a cake about $\frac{1}{4}$ cm thick. This cake constituted the source which was counted as such. The time necessary to complete these operations was about 20 minutes.

Carbon-11 is a 0.96-Mev positron emitter with a half-life of 20.5 minutes (Strominger *et al.* 1958). Its radioactivity therefore can be detected easily by measuring its annihilation radiation or its positrons. In this work, the gamma

[1]Manuscript received March 16, 1959.
Contribution from the Research Chemistry Branch, Atomic Energy of Canada Limited, Chalk River, Ontario.
Issued as A.E.C.L. No. 815.

spectrum was examined with a NaI (Tl) ($1\frac{1}{4}$ in. $\times$ 1 in.) scintillation spectrometer. The positrons were measured with a low background beta-anthracene counter.

RESULTS AND DISCUSSION

In these experiments the only gamma radiation found in the source had an energy of 0.511 Mev as determined by comparison with the annihilation radiation from positrons from Na^{22}. The pulse height spectrum is shown on the right side of Fig. 1. The gamma ray decayed with a half-life of 21 minutes as seen in Fig. 1. It was therefore ascribed to the annihilation of the 0.96-Mev

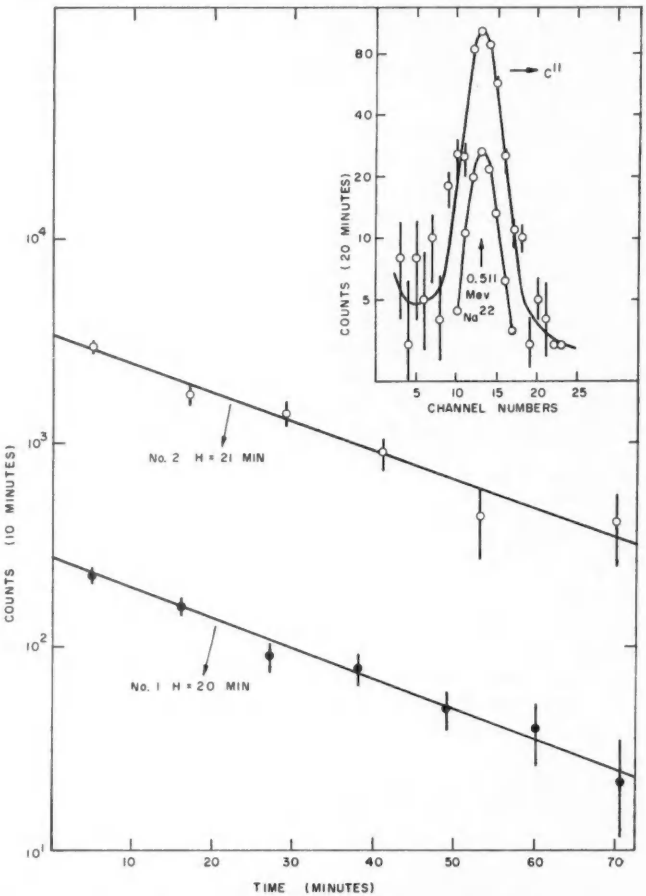

FIG. 1. Line 1 is the decay curve of the positrons; line 2 is the decay curve of the gamma radiations and the points represent 10 times the observed counting rate. The gamma-ray spectrum of C^{11} is shown on the right side of the figure.

positron of C^{11}. Similarly the beta radiations detected on the anthracene crystal decayed with a half-life of 20 minutes as shown in Fig. 1. They were attributed to the positrons from C^{11}. The radiochemical purity of the carbon dioxide obtained by the combustion of anthracene was excellent; no activity other than C^{11} could be detected either with the gamma-scintillation spectrometer or the beta detector. The measured half-lives of the annihilation and positron radiations were obtained by subtracting from the observed counting rate the background of the detectors. For the anthracene counter, the background was 10.0 ± 0.3 counts/minute; for the gamma-scintillation spectrometer it was 15 counts/minute under the energy range covering the annihilation radiation. The results of the measurements are summarized in Table I. The

TABLE I

Measurements leading to the identification of C^{11}

Experiment No.	Method of detection	Radiations detected	Half-life, minutes	Method of irradiations
1	Anthracene	β^+	19.0	Nylon capsule
2	Anthracene	β^+	20.7	Nylon capsule
3	NaI(Tl)	Annihilation	21.0	Nylon capsule
4	NaI(Tl)	Annihilation	21.5	Nylon capsule
5	NaI(Tl)	Annihilation	21.0	Iron capsule
6	NaI(Tl)	Annihilation	22.0	Iron capsule

half-lives listed in the last column have been calculated from the experimental points by the method of least squares, each point being weighted according to the equations developed by Behrens (1951). In terms of Behrens' definitions the case under study was treated as a single exponential decay plus a background of known mean strength. In each determination the calculated half-life is in agreement with the accepted value of 20.5 minutes for that of C^{11}.

In principle the nuclear reactions capable of yielding the C^{11} activity produced under the experimental conditions of the irradiations are the following: the $C^{12}(\gamma, n)C^{11}$ reaction which has a threshold of 18.73 Mev (Bromley and Rutledge 1958), the $C^{12}(p, d)$ or $(p, pn)C^{11}$ reactions caused by recoil protons and which have thresholds at 18.0 and 20.3 Mev respectively (Bromley and Rutledge 1958), and finally, the $C^{12}(n, 2n)C^{11}$ reaction which has been discussed in the introduction. The probability of occurrence of each process will be now examined.

The maximum energy of the gamma rays detected in fission is about 8 Mev (Fraser 1956). The gamma rays arising from (n, γ) reactions in the structural materials of the reactor have energies of no more than about 8 Mev while those arising from the decay of fission products have energies ranging from a few kev to a few Mev. Thus the gamma rays present in the reactor cannot account for the (γ, n) process since its threshold is 18.73 Mev.

Cowan and O'Brien (1955) conclude that the (p, pn) reaction does not yield a significant amount of C^{11} when anthracene is used as a fast-neutron detector based on the $C^{12}(n, 2n)C^{11}$ reaction. However, their conclusion is open to criticism because it was reached on the assumption that the cross

section of the (p, pn) reaction is one-sixth that of the $(n, 2n)$ reaction. In fact the measured cross sections of the two reactions (p, d) and (p, pn) (Aamodt *et al.* 1952) are about seven times greater than the $(n, 2n)$ cross section (Brolley *et al.* 1952) from threshold up to 40 Mev.

In order to determine the relative importance of the (p, d) or (p, pn) and $(n, 2n)$ reactions in the experiments described here, the following method was used. In one group of irradiations (experiments 1 to 4, Table I) the anthracene samples were irradiated in a nylon capsule so that the concentration of protons per square centimeter surrounding the anthracene was 10 times greater than in the anthracene sample itself; in another group (experiments 5 and 6, Table I) the anthracene samples were irradiated in iron capsules. In both groups of irradiations the reaction rates were essentially the same, thus showing that the C^{11} was produced mainly by a $(n, 2n)$ reaction. Moreover this experiment demonstrated that the (p, pn) or the (p, d) processes do not cause appreciable error in the measurement of fast-neutron fluxes using the $C^{12}(n, 2n)C^{11}$ reaction in anthracene.

The measured reaction rate, R, for the reaction $C^{12}(n, 2n)C^{11}$ may be expressed as the product of an effective cross section, σ, and the conventional neutron flux, ϕ, as measured with a cobalt monitor

$$R = \sigma\phi. \tag{1}$$

R was found to be equal to $(6\pm2)\times10^{-21}$ disintegrations per second per atom of carbon. This value divided by the neutron flux, 6×10^{13} n/cm^2-sec, gives an effective cross section of 10^{-34} cm^2.

It would be interesting to compare this observed reaction rate with the one predicted by the usual formula representing the energy distribution of the prompt neutrons from the thermal fission of U^{235} (Watt 1952)

$$f(E) = \sinh\sqrt{2E}\exp(-E) \tag{2}$$

where E is the neutron energy in Mev. The integrated neutron spectrum, $F(E)$, that is the fraction of neutrons having an energy greater than E is given by

$$F(E) = \left[\int_E^\infty f(E)dE\right] \Big/ \left[\int_0^\infty f(E)dE\right]. \tag{3}$$

In an empty fuel rod position of the NRX reactor the ratio fast flux/thermal flux is about 0.07. This value has been obtained from the ratio of the Ni^{58} $(n, p)Co^{58}$ cross sections measured respectively in an empty fuel rod and in a uranium receptacle slug (Hughes 1953; Mellish *et al.* 1958). The fast-neutron flux is therefore 4×10^{12} n/cm^2-sec. Thus the product $F(E)\times4\times10^{12}$ n/cm^2-sec gives the neutron flux, ϕ_E, having an energy greater than E. The cross section for the reaction $C^{12}(n, 2n)C^{11}$ is known from threshold up to 340 Mev (Brolley *et al.* 1952; Hughes 1958). Now a reaction rate, R_1, can be evaluated by graphical integration from the values of ϕ_E and σ as follows:

$$R_1 = \sum_{20}^{\infty} \Delta R = \sum_{20}^{\infty} \bar{\sigma}\phi\Delta E$$

where $\bar{\sigma}$ is the mean cross section over the energy interval ΔE.

The summation gives a value for R_1 equal to 2.5×10^{-21} disintegrations per second per atom of carbon which is about two times lower than R, the observed reaction rate. Considering the uncertainties associated with the values chosen to calculate R_1 and the error in the determination of R, the agreement between the observed and calculated reaction rates is good. It means that the relation, given in equation 2, can still represent at least qualitatively the energy distribution of the prompt neutrons from the thermal fission of U^{235} in the range 17.3–25 Mev.

Since the threshold of the $C^{12}(n, 2n)C^{11}$ reaction is 20.3 Mev, observation of the reaction in the NRX reactor means that there are neutrons with an energy of at least 20.3 Mev produced in the fission of fissile material present in the NRX reactor. Although the fuel in the NRX reactor is U^{235}, a significant fraction of fissions occur in the plutonium in irradiated fuel rods and in the Pu–Al booster rods; also about 6% of the fissions are due to fast-neutron fissions of U^{238}. At this point it is interesting to consider what is the upper limit of the fission neutron spectrum. At the present time this question cannot be answered without further information on the fission process. However, one probably could still extend the limit to a higher energy than 20.3 Mev by the studies of fast-neutron reaction of the type $(n, 3n)$ having thresholds in the 20–25 Mev range (Eastwood and Roy 1959).

ACKNOWLEDGMENTS

I would like to thank Dr. R. W. Attree for useful discussions and R. L. Cushing for the use of his combustion apparatus. I am also indebted to Dr. D. G. Hurst for his critical reviews of the manuscript.

REFERENCES

Aamodt, R. L., Peterson, V., and Phillips, R. 1952. Phys. Rev. **88**, 739.
Behrens, D. J. 1951. Atomic Energy Research Establishment, Harwell, A.E.R.E. T/R 629.
Brolley, J. E., Jr., Fowler, J. L., and Schlacks, L. K. 1952. Phys. Rev. **88**, 618.
Bromley, D. A. and Rutledge, A. R. 1958. Atomic Energy of Canada Limited Report CRP-789.
Cowan, F. P. and O'Brien, J. F. 1955. Proceedings of the International Conference on the Peaceful Uses of Atomic Energy, Geneva, Vol. 14 (United Nations, New York), p. 213.
Eastwood, T. A. and Roy, J. C. 1959. Can. J. Phys. **37**, 815.
Fraser, J. S. 1956. Proceedings of the Symposium on the Physics of Fission, held at Chalk River, Ontario, pp. 239–262.
Hughes, D. J. 1953. Pile neutron research (Addison-Wesley Publishing Co., Inc., Cambridge, Mass.).
——— 1957. Neutron cross sections (The Pergamon Press, Ltd., London).
Hughes, D. J. and Schwartz, R. B. 1958. Brookhaven National Laboratory Report BNL-325 (2nd edition).
Mellish, C. E., Payne, J. A., and Otlet, R. L. 1958. Atomic Energy Research Establishment, Harwell, A.E.R.E. I/R 2630.
Strominger, D., Hollander, J. M., and Seaborg, G. T. 1958. Revs. Modern Phys. **30**, 385.
Wapstra, A. H. 1955. Physica, **21**, 378.
Watt, B. E. 1952. Phys. Rev. **87**, 1037.

Kr 86 AND Hg 198 WAVELENGTH STANDARDS[1]

K. M. Baird and D. S. Smith

ABSTRACT

New values are given for the vacuum wavelengths of six lines of Kr 86 and five lines of Hg 198 in the visible spectrum. The wavelengths were referred to the Kr 86 primary standard line, 6057.80211, by a series of very careful measurements over a period of several years. The accuracy with which wavelengths can be compared by present methods is discussed at some length.

INTRODUCTION

In order to present new values of wavelength standards in proper perspective it is important to consider rather carefully the accuracy to which such standards can be determined at present. Recent work in connection with the redefinition of the international metre in terms of optical wavelengths has thrown considerable light on this question and indicates that the accuracy is much less than has been generally realized. A few years ago the impression was widely held that an accuracy of .0001 Å in the visible region, i.e. about two parts in 10^8, was not out of the ordinary for wavelength values (Candler 1951; Tolansky 1955). In reality errors 10 times this amount existed in published values of secondary wavelength standards and even in recent determinations of the wavelengths of new isotope sources, which were expected to be much more precise than the earlier standards, it has been difficult to find agreement to ±.0001 Å. This is illustrated in Table I, which lists values for the orange

TABLE I

Recent published values of wavelength standards

No.	Laboratory	Kr 86	Hg 198	References
1	N.B.S. (U.S.A.)		5462.2707*	Meggers 1947
2	N.P.L. (England)		.2707*	Barrell 1947
3	B.I.P.M. (France)		.2707*	Perard 1950
4	N.B.S. (U.S.A.)		.2707*	Meggers 1950
5	N.P.L. (England)		.2702*	Barrell 1951
6	N.B.S. (U.S.A.)		.2702$_4$	Kessler 1955
7	N.P.L. (England)	6057.8014	.2702	Comité intern. pds. mes. 1956
8	B.I.P.M. (France)	.8021	.2707*	Comité intern. pds. mes. 1958*a*
9	P.T.B. (Germany)	.8023	.2707*†	
10	N.P.L. (England)	.8021	.2707	
11	C.I.I.W.M. (Japan)	.8021	.2708*	
12	N.R.C. (Canada)	.8021	.2704	
13	N.R.C. (Canada)		.2706†	
14	N.S.L. (Australia)		.2707*	
15	B.I.P.M.(France)		.2708†	Terrien 1958*c*

*Uncorrected for effect of argon pressure (+.0001 to +0.0003 Å).
†Referred directly to Kr 86 = 6057.8021, others referred to Cd = 6440.2491.

[1]Manuscript received April 3, 1959.
Contribution from the Division of Applied Physics, National Research Council, Ottawa, Canada.
Issued as N.R.C. No. 5232.

line of Kr 86 and the green line of Hg 198 which have been obtained at various standards laboratories during the last 10 years. All the values of this table have either been measured in vacuum or reduced to vacuum by the Edlen formula; in the former case where the Cd red line was used as a reference its value in vacuum was obtained by the same formula. The Kr 86 wavelengths were all measured for a hot cathode lamp of the form described by Engelhard (1951) in all cases at the triple point of N_2 except No. 11, which was at the boiling point of N_2. Otherwise the lamps were used in various ways—viewed from the side, cathode end, or anode end, and at currents, whose exact value was not always specified, up to 6 ma/mm².

The Hg 198 wavelengths were measured for electrodeless lamps of the type due to Meggers (1950*a*) having argon as the carrier gas at an original pressure (at the time of filling) of from $\frac{1}{4}$ to 5 mm Torr. The lamps were cooled by water at from about 0° C to 15° C without always accurate specification of the water temperature.

The table illustrates well the present uncertainty in practice in the determination to the fourth decimal in angstroms of even very good wavelength standards.

REASONS FOR SPREAD IN MEASURED VALUES OF WAVELENGTHS

Although the quite large uncertainty in the fourth decimal of angstroms may be disappointing, it can quite reasonably be accounted for as indicated in Table II.

TABLE II

Various uncertainties contributing to scatter in wavelength comparisons

Source	Uncertainty due to conditions of excitation		Errors of observation (systematic and random-pointing error plus instrumental error)	
Cd	±1.5	(±<1.0)	±1.5	$\times 10^{-4}$ Å
Hg 198	$^{+3.}_{-0.}$	(±0.2)	±1.1	$\times 10^{-4}$ Å
Kr 86	$^{+1.5}_{-0.2}$	(±0.2)	±0.8	$\times 10^{-4}$ Å

The magnitude of the uncertainties given in Table II which are ascribed to *conditions of excitation* are now known from actual measurements of the effects of current, temperature, carrier gas pressure, etc., on the emitted wavelengths. These uncertainties, which apply to many of the determinations of Table I, could be reduced by suitable control of the conditions of excitation to the values shown in parentheses.

One important cause of shift of the Hg 198 green line results from foreign gas broadening which has been found for argon to be .00006 Å to the red per millimetre pressure, i.e. .0003 Å for 5 mm pressure (Baird and Smith 1957). After some use it is likely that the pressure in the lamp becomes reduced

through cleanup but, on the other hand, electrodeless lamps are sometimes reactivated by heating and this procedure may well raise the internal pressure to above the original pressure. Another important cause of shift results from self-absorption if the lamp is not sufficiently cooled; the self-absorption is about 40% at 18° C and will affect the fourth decimal place in angstroms (Terrien 1958*a*). The effect of the nature and intensity of excitation on the Hg 198 lines has not been measured exactly; however, tests at this laboratory have not indicated any significant effect provided the power is not so great that the lamp becomes unduly heated. For most of the values for the mercury line given in Table I one cannot say exactly what total correction should be applied although the fact that the likely shifts are known to be toward the red would make one tend to favor the shorter values. It can be said, however, that if the Hg 198 lamp is excited at low power (so as not to have high-temperature gradients through the walls of the lamp) with cooling water at less than 10° C and having the argon carrier gas pressure less than 0.3 mm then the wavelength of the green line can be assumed with a reasonable degree of certainty to be reproduced to about ±.00002 Å. The best form of lamp is that with a large ballast volume operated at about 300 megacycles. Earlier observations that the line width was reduced by the use of very high frequency excitation have not been substantiated and are likely due to the fact that the large power used caused a doublet effect due to reversal which caused an apparent sharpening of fringes at certain path differences.

The shifts which affect the Kr 86 orange line result from interatomic Stark effect and from Doppler effect due to ion drift in the cases where the lamp is viewed end on. The magnitudes of these effects were measured by Engelhard (1958) and by the present authors (see below). The uncertainties arising from these causes in the determinations listed in Table I would account for a total scatter of about .00015 Å as indicated in Table II. On the other hand, if the Kösters–Engelhard Kr 86 lamp is operated at the triple point of N_2, at a current density of less than 4.0 ma/mm^2, and has the appropriate corrections applied for current and direction of viewing (where this applies), then the wavelengths of the orange line will also be reproduced to about ±.00002 Å.

Although the large scatter of earlier measurements of wavelengths has sometimes been largely attributed to the Cd red line, which was used for reference, independent measurements by Baird (1958) and by Masui, Terrien, and Hamon (1958) showed no reason to expect a variation of much over ±.0001 Å as long as the conditions of excitation were reasonably close to any of the various specifications which have been officially adopted; this tends to be confirmed by the measurements of the Kr 86 orange line relative to the Cd line which are shown in Table I. More rigorous specifications could reasonably be applied which would reduce the uncertainty due to conditions of excitation to less than ±.0001 Å. Thus the Cd red line compares unfavorably with the other two lines discussed above, as they have been used in the past, only insofar as its width is two to two and a half times as great and consequently individual pointings are less precise by about this factor. The Michelson lamp is very inconvenient and no longer useful but

the electrodeless Cd 114 lamp is simple to make and to operate and would make an excellent source for secondary standards.

The estimated error limits due to *observation* cannot be stated other than by an intelligent guess. However, a quantitative consideration of the many possible sources of error shows that the estimates indicated are certainly not too large and they are in fact consistent with the accuracy generally quoted by the authors of the values of Table I.

As indicated in the table these errors can be ascribed to statistical fluctuations in the average of many pointings, systematic errors of pointing and errors due to the interferometer and atmosphere. They have been discussed in detail elsewhere (Terrien 1958*b*; Baird 1958*a*) and will not be repeated here, beyond saying, as an example, that those who have had a great deal of experience in pointing on lines by the use of the most precise conventional methods and equipment have found that the loss of accuracy from this source alone is at least 1% of the line width (i.e. about .0001 Å), however reproducible the pointing may seem under some given conditions. New methods of pointing on fringes are now being developed which appear to make possible a great improvement in precision. On the other hand there is no real assurance that a corresponding elimination of systematic errors of pointing has been attained as yet.

It is quite clear that any reasonable convention for combining the errors of Table II will easily account for the scatter in values, shown in Table I, for the intercomparison of any two of the wavelength standards. Indeed the good agreement of the last six values for the Kr 86 orange line appears even better than one might expect.

In summing up the foregoing, one conclusion is that an uncertainty of greater than $\pm .0001$ Å must be ascribed even to the best determinations of wavelength values up to the present. It may be argued that some of the previous determinations are better than others but there is really no positive basis on which to assess them. For example No. 6 of Table I is called a preliminary value although it is known that it was made in vacuum, that the lamp condition was well known and controlled, and that the result was quoted to $\pm .000008$ Å; the main source of uncertainty is probably in the Cd red line to which it was referred but this is very unlikely to have contributed an error greater than .0002 Å as mentioned above. On the other hand some of the later values in the table which are presumed to be definitive are known to have been made by the use of old lamps without application of accurate corrections; or they were made by new untried methods; or the lamp was at too high a temperature; and so on.

A second conclusion is that as far as the sources themselves are concerned it ought to be possible to obtain approximate agreement in the fifth place of decimals in the case of lines emitted by Hg 198 and Kr 86, provided conditions of excitation are properly controlled. (Although only the green and orange lines have been considered, the conclusions as to reproducibility apply to many other lines from these sources.) Errors of observation can also be reduced by care even without a change from conventional methods, e.g. by

measurement always in vacuum or by reference to vacuum and by adequate statistical evidence in the observations.

The wavelength determinations described below were made with the aim of obtaining the best possible values by the use of methods which are quite standard at present.

The isotope lamps were made in the laboratory so that their characteristics were accurately known and perturbing effects due to the excitation conditions were taken into account. Measurements were made by the use of three independent methods over a long period of time, and by different observers with completely re-set-up equipment, in order to ensure good statistical reduction of systematic errors that may have been associated with any one method, set of interferometer plates, etc.

It may be remarked that new techniques have been under development during the past few years in this laboratory and elsewhere which promise to yield an improvement in accuracy by a factor of 10 to 100. The attainable precision for the new methods, which is limited by quantum effects, has been discussed theoretically by Hanes (1959).

However, before wavelengths can be reported to such accuracy a great deal of work remains to be done, first to give assurance that systematic errors of observation are eliminated to an extent consistent with the improved precision of pointing and secondly to determine and control to the same degree of certainty the small shifts of wavelength due to variations in the conditions of excitation.

EXPERIMENTAL PROCEDURE

The vacuum wavelengths given in Table III for Kr 86 and Hg 198 were measured by reference to the Kr 86 line corresponding to the Paschen designated transition $2p_{10}$–$5d_5$; the wavelength of this line was taken as 6057.80211 $\times 10^{-10}$ metres following the recommendation of the Comité International des Poids et Mesures (1958) and Commission 14 of the International Astronomical Union (1958).

TABLE III

Vacuum wavelengths referred to Kr 86 6057.8021 Å

6458.0719±2	5792.2683±3
5651.1285 1	5771.1982 3
4503.6159 1	5462.2705 1
4464.9414 1	4359.5621 2
4455.1664 2	4047.7144 2
4377.3500 1	

The measurements were made principally by the use of a Fabry–Perot interferometer which was mounted in a vacuum chamber whose temperature was controlled by a water bath. Photographs of the Haidinger fringes were made in the usual way by the use of a Hilger D260 prism spectrograph; they were made in symmetrical sets, such as Hg 198–Kr 86–Kr 86–Hg 198, on any given plate. The control of temperature and the vacuum were sufficient to

assure the introduction of no errors not completely negligible in the fourth decimal of angstroms. The usual precautions were taken regarding the parallelism of the optical flats, proper flooding of the apertures, the use of a lens system with negligible distortion and chromatic aberration, etc. The etalon plates were coated with aluminum of such density that the transmission was about 15%. The etalon length for most exposures was 67. 5 mm. Photographs were also made with 150-mm and 5-mm etalons respectively; the results with the former showed no evidence of asymmetry in the lines; the 5-mm etalon was used to eliminate the effect of dispersion of phase change on reflection.

Measurements of each of the photographic plates were made by at least two observers who used visual setting with an accurate Zeiss Abbé comparator; some measurements were also made by means of a photoelectric comparator.

These measurements were made over a period of several years with different setups and different etalon plates. Most of the values used for Table III are the average of 50 observations on 18 plates.

In order to check for systematic errors some of the lines, listed in Table IV, were measured visually by the use of two other interferometers which were

TABLE IV

Comparison of wavelengths obtained by two different methods

λ (Å), whole part	Fabry–Perot	Michelson
6458	0719_5	0718_5
5651	1285	1284_4
5792	2684	2682
5771	1982_5	1980
5462	2704_5	2705_5

basically of the Michelson type. One of these (Baird 1958*b*) made use of the half-shade technique and by using only highly collimated light with parallel mirrors and the *same* optical surface at the two end points of the reference distance; it avoids many of the systematic errors which are possible in other methods. The other determinations were made by the observation of Fizeau fringes by a method which was basically that of Kösters in which fringe matching is used and in which the refractive index of the air is automatically eliminated. Both of these methods had a precision about the same as that of the Fabry–Perot, viz., about ± .0003 Å standard deviation in single determinations.

These measurements were completely independent of those made by the Fabry–Perot and were made by a different observer, using a different monochromator, lamps, etc.

SOURCES

The Hg 198 lamps were of the Meggers "reservoir" type containing Hg 198 of 99% isotopic purity and argon carrier gas at a pressure of 0.25 mm. The

discharge region of the lamp was cooled to about 4° C and viewed from the side through the water jacket. It was excited gently by an oscillator of the type described by Smith (1957) operating at roughly 250 Mc/sec.

Under these conditions the correction for pressure shift of the Hg 198 lines was .00002 Å to the red for the lines reported; that for self-absorption is known to be negligible in the fourth decimal in angstroms (Terrien 1958*a*); the wavelength shift which may be associated with the excitation current was considered negligible in the present measurements on the basis of previous observations of the effect of excitation of much greater intensity than that used in the wavelength determinations. The effect of isotopic impurity can also be shown to be negligible in the fourth decimal in angstroms (Terrien 1959).

The Kr 86 lamps were similar to the hot cathode type developed at the German P.T.B. and contained only Kr 86 of 99.9% purity. They were cooled by immersion in a bath of N_2 at its triple point and excited by a current density of 2 ma/sq. mm in the thin-walled capillary in which the discharge was observed. The discharge was viewed from the side in the case of the Fabry–Perot measurements and from the end in the direction cathode to anode for the Michelson measurements.

The magnitudes of the wavelength shifts for this source were found by Engelhard (1958) to be as follows: the values for the Doppler shift when the discharge is viewed in the direction cathode to anode is independent of the current density and has the values:

$$\Delta\lambda\ 6057 = 87\times10^{-6}\ \text{Å to the red}$$

and

$$\Delta\lambda\ 5651 = 74\times10^{-6}\ \text{Å to the red.}$$

The magnitude of the Stark shift, which is to the red, follows the law $\Delta\lambda = \text{const.}\ (p.j)^{2/3}$ where p is the pressure of the Kr and j the current density. The pressure is calculated from the Meihuizen formula for the vapor tension of Kr at the temperature of the coldest part of the lamp. The value reported for the shift under the conditions of Engelhard's determination correspond to values for the constant as follows:

$$\Delta\lambda_{6057} = 240\ (p.j)^{2/3}\ (j \text{ in ma/sq. mm; } p \text{ in mm Torr}),$$

$$\Delta\lambda_{5651} = 160\ (p.j)^{2/3}.$$

These shifts were measured by the authors for the 6057 line by a pressure-scanning technique described previously (Baird and Smith 1957) and also by means of observations with the Michelson-type interferometers. The results are as follows:

$$\text{Doppler shift}\quad \Delta\lambda\ 6057 = 48\pm9\times10^{-6}\ \text{Å},$$

$$\text{Stark shift}\quad \Delta\lambda\ 6057 = 200\pm30\ (p.j)^{2/3}.$$

The values obtained by the two methods agreed to within the experimental error indicated above. The Stark shift for the lamp as operated for the wave-

length determinations amounts to 32×10^{-6} Å according to our results as compared with 38×10^{-6} Å as found by Engelhard. The differences between our values and those of Engelhard are not very significant for the measurements reported here; however, it is hoped to determine these corrections considerably more accurately in the near future by the methods referred to earlier. This measurement is made difficult by the fact that the intensity and sharpness of both the 6057 and 5651 lines decrease at higher $p.j$ and the intensity decreases at lower $p.j$ thereby limiting the range over which $\Delta\lambda$ may be measured precisely. It is useful to note that if the lamp is observed in the direction anode to cathode the Doppler shift and Stark shift tend to compensate each other, the compensation being exact at about 4.0 ma/sq. mm.

RESULTS AND ACCURACY

The best vacuum wavelength values derived from all the observations are given in Table III for unperturbed conditions. The values include the observations made by means of the Michelson interferometers in the cases where such observations were made. The results obtained by the two methods (Fabry–Perot and Michelson) are shown separately in Table IV; in combining them they were weighted according to their respective statistical accuracies (which were approximately the same). The differences between the results obtained by the two different methods are not considered significant.

The stated error limits in Table III are the calculated 99% confidence limits, i.e. about three times the calculated root-mean-square error for the average of all the observations on a given wavelength.

Insofar as systematic errors are concerned the following is relevant: the 6057-Å reference line with the corrections which were applied can be considered to have been accurate to $\pm.00002$ Å; the same accuracy applies to the Hg 198 green line. Errors as great as .0001 Å are known to be very unlikely in the production of the other lines reported (Baird and Smith 1957; Engelhard 1959). The diversity of measurements which were made indicates strongly that the results are free from significant systematic errors of observation. In addition to the experiments described it may be added that the first two Kr 86 lines and first three Hg 198 lines in Table III as well as the 6057 line of Kr 86 have been used in this laboratory in a large number of precise length measurements whose results give no evidence of systematic error in the values reported.

In view of these considerations the values of Table III are presented with considerable confidence as being accurate to within the stated error limits.

REFERENCES

BAIRD, K. M. and SMITH, D. S. 1957. Can. J. Phys. **35**, 455.
BAIRD, K. M. 1958*a*. Comité intern. poids et mesures. Procès-verbaux, 2e série, B, **26**, M.111.
——— 1958*b*. J. phys., **19**, 390.
BARRELL, H. and PUTTOCK, M. J. 1947. Comptes rendus, 9e Conférence générale poids et mesures, 77.
BARRELL, H. 1951. Proc. Roy. Soc. A, **209**, 132.
CANDLER, C. 1951. Modern interferometers (Hilger & Watts, London), p. 55.

COMITÉ INTERN. POIDS ET MESURES. 1956. Procès-verbaux, 2e série, **XXV**, 98.
——— 1958*a*. Procès-verbaux, 2e série, B, **26**, M.15, M.173.
——— 1958*b*. Procès-verbaux des séances.
ENGELHARD, E. 1951. Symposium on Recent Developments and Technique in the Maintenance of Standards (National Physical Laboratory, Teddington).
——— 1958. Comité intern. poids et mesures. Procès-verbaux, 2e série, B, **26**, M.54.
——— 1959. Private communication.
HANES, G. R. 1959. To be published.
INTERNATIONAL ASTRONOMICAL UNION. 1958. Moscow Meeting, August 1958.
KESSLER, K. G. and MEGGERS, W. F. 1955. Optical Society American Meeting, October 1955, paper 27.
KOSTERS, W. and ENGELHARD, E. 1950. Comité intern. poids et mesures. 2e série, **XXII**, 139.
MASUI, T., TERRIEN, J., and HAMON, J. 1958. Comité intern. poids et mesures. Procès-verbaux, 2e série, B, **26**, 167.
MEGGERS, W. F. 1947. Comptes rendus, 9e Conférence générale poids et mesures, p. 75.
MEGGERS, W. F. and WESTFALL, F. O. 1950*a*. J. Research Natl. Bur. Standards, **44**, 447.
MEGGERS, W. F. and KESSLER, K. G. 1950*b*. J. Opt. Soc. Am. **40**, 737.
PERARD, M. 1950. Comité intern. poids et mesures. Procès-verbaux, 2e série, **22**, 27.
SMITH, D. S. 1957. Can. J. Technol. **34**, 521.
TERRIEN, J. 1958*a*. Comité intern. poids et mesures. Procès-verbaux, 2e série, B, **26**, M.135.
——— 1958*b*. Comité intern. poids et mesures. Procès-verbaux, 2e série, B, **26**, M.130.
——— 1958*c*. Comptes rend. acad. sci. **246**, 2362.
——— 1959. Private communication.
TOLANSKY, S. 1955. An introduction to interferometry (Oxford University Press), pp. 92, 137.

MODIFICATION OF PbS NOISE SPECTRA BY RADIATION[1]

R. L. WILLIAMS

ABSTRACT

The noise spectra of PbS photoconductive cells can be modified by optically excited carriers. Detailed wavelength studies at CO_2 temperatures have shown that g–r noise can be obtained using light of the 2.4-micron region, and the $1/f$ form with radiation of the 1.0-micron region. The effect is explained by assuming that minority carrier lifetimes in Kodak Ektron detectors are very short. The $1/f$ noise is only observed when optical carriers are produced very near the cell surface.

INTRODUCTION

Noise spectra of Kodak chemically deposited PbS photoconductive cells have been measured with excess incident radiation. The form of the noise spectra has been found to depend on the wavelength of the radiation.

EXPERIMENTAL TECHNIQUE

Wavelength studies were carried out at CO_2 temperatures using an Axler linear wedge filter. Wavelength bands 0.05 micron wide were selected between 1.0 and 2.4 microns. A typical set of measurements was made as follows. A series of noise spectra was taken with various levels of illumination falling on the cell, but using a fixed wavelength interval of the filter. A second set would then be taken in a similar fashion but using a different wavelength interval. The resistance ranges covered by the two sets of measurements were comparable.

A schematic diagram of the cell cryostat is given in Fig. 1. The measurements at CO_2 temperatures were performed with the cell chamber immersed in a mixture of dry ice and acetone. For most of the measurements air was trapped inside the system to assist in maintaining the cell at the temperature of the bath. Noise measurements were made between 10 c.p.s. and 16 kc.p.s. with a General Radio Wave analyzer. The signal was tapped off one stage before the meter circuit and passed through a Ballantine r.m.s. voltmeter. The signal from the mean-square output terminals of the Ballantine meter was recorded for at least 30 seconds for each measurement. The values obtained from the recorder, being proportional to the mean square of the noise voltage of the photoconductive cell, were corrected for the zero current noise by a simple subtraction.

The light beam used to produce resistance changes was modulated by a chopping disk with two narrow blades made of wire mesh. The response time of the cells, to this modulation, was recorded to determine the time constant corresponding to the various radiation conditions.

[1]Manuscript received January 6, 1959.
Contribution from the Canadian Armament Research and Development Establishment, Valcartier, Que.

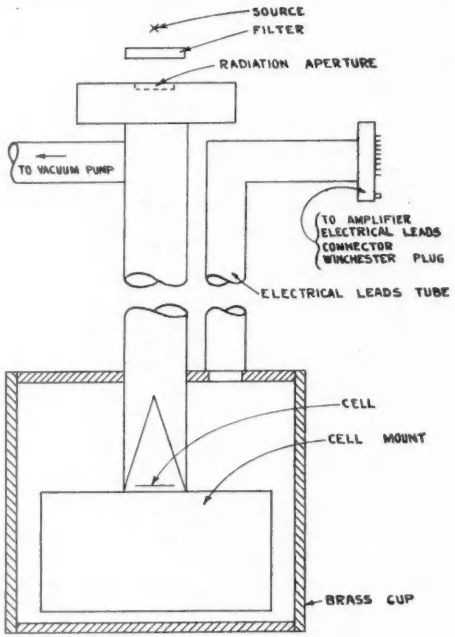

FIG. 1. Cell cryostat used in the investigation of the noise-wavelength dependence.

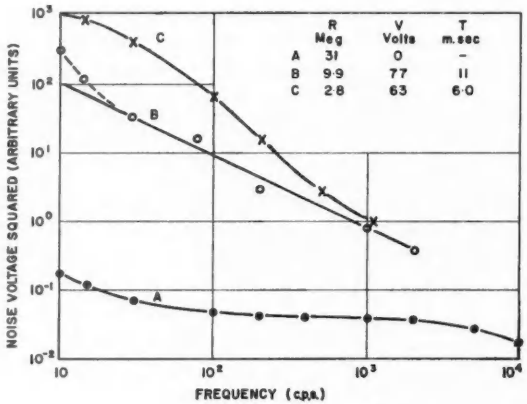

FIG. 2. Noise frequency change-over from the f^{-1} to the f^{-2} form (CO_2 temperatures).

EXPERIMENTAL RESULTS

Figure 2 is representative of the results that could be obtained with a cell operating at CO_2 temperatures. The cell resistance R_c in megohms, the cell voltage V_c in volts, and the cell time constant, in milliseconds, are recorded on the graphs. Curves B and C were obtained by changing the level of illumination to obtain arbitrary resistance values. The wavelength band in this case was between 1.75 and 1.80 microns. The curves shown are three of eight taken during this particular experiment. In general, the resistance was reduced by arbitrary amounts down to the minimum obtainable. When the same procedure was followed, using the wavelength region 1.00 to 1.05, only the $1/f$ form was obtained. By contrast, radiation in the 2.35 to 2.40 region produced domination of generation–recombination (g–r) noise when the resistance changed by only a factor of 2.

The results obtained with this cell can be expressed as follows. With sufficient radiation incident on the cell to maintain the resistance at approximately 2 megohms, a $1/f$ noise spectrum can be obtained by using wavelengths in the 1.0- to 1.5-micron region. Using wavelengths longer than 1.7 microns, the g–r form was always obtained. The wavelength at which the change from dominance by $1/f$ to g–r noise occurred was a function of the resistance of the cell. When the cell resistance was about 9 megohms, $1/f$ noise was dominant when the cell was irradiated with radiation in the 1.8-micron region, but a good g–r noise spectrum was obtained when the 2.4-micron region was used. The resistance of the cell with no external light source was 31 megohms.

The particular wavelength dependence mentioned above is typical of the cells studied, but other cells had in detail a different wavelength noise characteristic. At CO_2 temperatures some cells did not show such a wavelength dependence; however, such cells were completely dominated by $1/f$ noise at all temperatures and under all conditions investigated. By contrast, one cell required wavelengths of near 1 micron before $1/f$ noise appeared. A cell which had a room temperature spectrum which was partially of the g–r form usually showed the wavelength noise spectrum dependence.

Figure 3 illustrates the noise spectral change that could be observed at room temperature. With no excess radiation this cell exhibited no $1/f$ noise at 10 c.p.s., curve B.

At room temperature the intensity of radiation that could be obtained with the light source was too small to allow filtering of the radiation. A filament lamp operating at full voltage was used with apertures controlling the intensity. The operating temperature of the filament being near 3000° K ensures a predominance of short wavelength radiation (less than 1.5 microns). The spectrum change observed is shown by curve C. This type of spectrum change was usually complete when the cell resistance had changed by a factor of 3.

Fourteen cells were tested in this manner at room temperature. All cells under the radiation conditions discussed above were completely dominated by $1/f$ noise; three of these cells were dominated by $1/f$ noise without radiation.

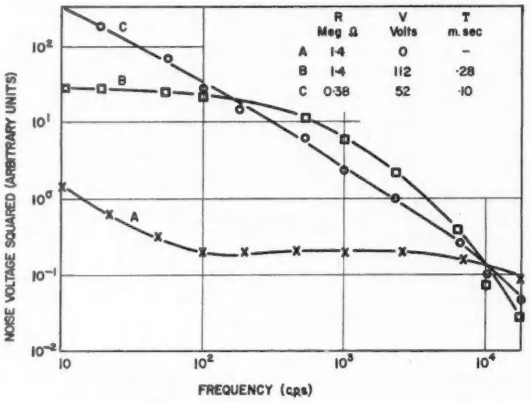

FIG. 3. Noise spectral changes affected at room temperature by increasing amounts of radiation from a tungsten lamp.

A general feature of the effect was that cells which had a very small $1/f$ component at room temperature required, at CO_2 temperatures, the shortest wavelengths to produce the $1/f$ noise, and vice versa.

Both a globular and a filament lamp were used for the CO_2 experiments to check that the radiation source was not producing the $1/f$ spectrum. Identical results were obtained with the two sources. The fact that g–r noise was observed using long wavelength light, from the same source whose short wavelengths produced $1/f$ noise, indicates that the spectrum could not arise from the radiation source. The cell contacts were shown not to be responsible for any of the effects, as identical results could be obtained with the contact area masked with black electrical tape.

The noise voltage squared dependence was checked and found to be $I^{1.8}$. Both the g–r and the $1/f$ noise components followed the same law. Discussing Fig. 2, it was pointed out that maintaining the cell resistance constant, which ensures the same voltage across, and current through, the cell, the spectrum could be changed. The effects cannot be associated with the particular current values used.

The dominance of the $1/f$ noise occurs because of an increase in magnitude of the $1/f$ noise component. This is demonstrated in Fig. 3. That the g–r noise component is below the $1/f$ component can be seen by using the formula for g–r noise as given by Petritz (1956). The validity of the noise formula has been established by Lummis and Petritz (1957). Using Wood's (1957) result that the mobility does not change under illumination, the ratio of the noise voltage squared for the condition of curve C, subscript 2, to that for the conditions of curve B, subscript 1, is

$$\frac{V_2^2}{V_1^2} = \left(\frac{V_{c_2}}{V_{c_1}} \frac{R_{C_1}+R_L}{R_{C_2}+R_L}\right)^2 \frac{R_{C_2}}{R_{C_1}} \frac{\tau_2}{\tau_1}.$$

In this expression V^2 is the mean-square noise voltage, V_c the bias voltage across the cell, R_L the load resistor, and τ the time constant. Using the values of the parameters given on Fig. 3 and the fact that R_L was equal to 1 megohm, the reduction of the g–r noise, as predicted by the above equation, is a factor of 16. Noise of the g–r form reduced by this factor might just be detectable, but is not apparent in the $1/f$ noise of curve C of Fig. 3.

A similar analysis, attempted on the noise spectra at CO_2 temperatures, was unsuccessful. Using the expression for g–r noise employed to obtain equation 1, the equation for the mean-squared noise voltage can be written in the form

$$V^2 = 4I^2 \left(\frac{R_c R_L}{R_c + R_L} \right)^2 \frac{R_c e \, \mu\alpha \Delta f}{1 + w^2 \tau^2}.$$

Here, e is the electronic charge, μ the mobility, α a geometrical factor, and Δf the bandwidth. This expression was fitted to g–r noise curves obtained from the same cell as used to obtain the data of Fig. 2, but using radiation in the 2.4-micron wavelength region. Values of $\mu\alpha$ were found to be a strong function of R_c at these temperatures, and the analysis was not continued.

INTERPRETATION

Noise of the $1/f$ form is believed to arise from trapping of carriers in slow surface states (Kingston 1956), which exist in or on the outside of a surface oxide layer (Lasser *et al.* 1956). Wang and Wallis (1957) have established that radiation can alter the surface potential of a semiconductor. Trapping effects in slow states, which are believed to give rise to $1/f$ noise (Kingston 1956), would certainly be affected by any change in potential at the surface. That the magnitude of the $1/f$ noise changes with radiation intensity, therefore, is not too surprising. The wavelength dependence of the noise must arise because of some additional feature, dependent upon the wavelength of the light employed.

Petritz *et al.* (1956) have suggested that the high sensitivity of PbS films may arise from the rapid trapping of the minority carriers into states which do not readily trap majority carriers, in this case, holes. Short minority carrier lifetimes prevent any appreciable diffusion of electrons. Under conditions of space charge neutrality the distribution of optically excited free holes is similar to that of the optically generated (trapped or free) minority carriers. The minority carrier lifetime in unsensitive films is of the order of 10^{-7} second (Petritz *et al.*) and in the sensitization process the minority carrier lifetime is believed to decrease to some small value. Assuming a value of 10^{-10} second and using Lummis and Petritz's (1957) result of 2 cm²/v-sec for the mobility of carriers, the room temperature diffusion length is .006 micron. As this is much shorter than the reciprocal of the absorption coefficient, the distribution of trapped and free carriers is approximately of the form $\exp -Ax$, where A is the absorption coefficient for radiation of wavelengths considered, and x is the distance from the surface.

The noise spectra changes were observed when the resistance of a cell had changed by a factor of 2 or 3. This indicates that the effects are important when the optically excited carriers are dominating the conduction process. Under the condition of short minority carrier lifetime mentioned above, the distribution of carrier approximates to $P_0 \exp -A_x$, where P_0 is the density of carriers per square centimeter at the surface. Neglecting mobility changes, a constant resistance requires that the integral of $P_0 \exp -A_x$ across the film be a constant. This implies that P_0 will be some function of A, i.e., if the film is thick compared to A^{-1}, P_0 is proportional to A. The surface potential must then be different for different wavelengths of light. P_0 is expected to be some function of A approximating to A^{-1}, as the films are of the order of 0.6 micron thick (Koch 1956), and the absorption coefficient is about 2.7×10^4 cm^{-1} at 1.8 microns (Avery 1954).

It is to be noted that the reciprocal of absorption coefficient of PbS for the radiation in the wavelength region used ($A \sim 2.7 \times 10^4$ cm^{-1}) is at least a factor of 10 larger than the room temperature Debye length. This indicates that the effects are not due to the position of excitation in the region of changing surface potential.

For an increase of the carrier density at the surface the probability of a transition to a slow surface state should increase. This is expected as the capture probability is normally proportional to the number of particles available for capture. A high probability of capture means that a larger percentage of the total number of carriers is involved in surface trapping and a larger $1/f$ noise component is expected. Lead sulphide has a larger absorption coefficient, the shorter the wavelength of light. Then on the basis of the above arguments, the shorter the wavelength the larger the $1/f$ component. Different surface conditions of different cells would give rise to a change, in detail, of the wavelength noise spectrum dependence observed. The different wavelength behavior, cell to cell, is expected on such grounds. For a particular cell, different resistances imply different carrier densities and different potential configurations at the film surface. Different wavelength noise spectrum relationships are then expected for the same cell but for different resistances.

The photons of short wavelength, as well as penetrating shorter distances into the film, are more energetic. If the difference in energy is considered as significant, the effects could result from excitation of some surface state which affects the surface trapping. Bray and Cunningham (1958) have found that rather narrow wavelength regions excite surface states on germanium. The effects, observed at liquid air temperatures, have been identified with slow surface states. In the present experiments the wavelengths required to produce a change of noise spectra was dependent on the level of radiation. This makes an explanation based on excitation of surface states unattractive, but it is appreciated that the first explanation suggested involves in some cases speculative values of physical parameters.

ACKNOWLEDGMENTS

The author wishes to acknowledge many helpful discussions with Dr. G. Giroux, Mr. J. Hampson, and Dr. G. T. Pullan.

REFERENCES

AVERY, D. G. 1954. Proc. Phys. Soc. B, **67**, 2.
BRAY, R. and CUNNINGHAM, R. W. 1958. International Conference on Semiconductors, Rochester.
KINGSTON, R. H. 1956. J. Appl. Phys. **27**, 101.
KINGSTON, R. H. and MCWHORTER, A. L. 1956. Phys. Rev. **103**, 334.
KOCH, G. 1956. Private communication.
LASSER, M., WYSOCKI, C., and BERNSTEIN, B. 1956. Semiconductor surface physics (University of Pennsylvania Press), p. 197.
LUMMIS, F. L. and PETRITZ, R. L. 1957. Phys. Rev. **105**, 502.
PETRITZ, R. L. 1956. Photoconductivity conference (John Wiley & Sons, Inc.), p. 49.
——— 1956. Phys. Rev. **104**, 502.
PETRITZ, R. L., LUMMIS, F. L., SORROWS, H. E., and WOOD, J. F. 1956. Semiconductor surface physics (University of Pennsylvania), p. 229.
WANG, S. and WALLIS, G. 1957. Phys. Rev. **107**, 949.
WOODS, J. F. 1957. Phys. Rev. **106**, 235.

PARAMAGNETIC RESONANCE LINE SHAPES[1]

PREM SWARUP[2]

ABSTRACT

A study of the line shape of the transitions of various concentrations of Cr^{+++} ion in potassium cobalticyanide and potassium aluminum alum single crystals has been made at 9300 Mc/s. The line shape is found to change gradually from Lorentzian to Gaussian with chromium concentration. Lorentzian shape of gadolinium ion in lanthanum ethyl sulphate and exchange narrowing in case of free radical and copper sulphate are reported. The line width and relative intensity of the transitions in a highly dilute cyanide salt at 4.2° K are plotted and it is found that the intensity followed the maximum of the matrix element squared for various transitions. The value of g is found to be 1.992. The actual concentration of Cr^{+++} in dilute salts is less than the concentration of the solution from which they are grown by more than a factor of 10 as the dilution is increased.

I. INTRODUCTION

The paramagnetic behavior of the triply ionized chromium in potassium chromicyanide has been studied as well as other ions of the transition groups in an attempt to determine the shape of the resonance lines as a function of the concentration of the paramagnetic ions and of the microwave power. It is well known that at microwave frequencies both storage and dissipation of the magnetic energy are involved when a wave is propagated through a paramagnetic sample immersed in a magnetic field. The magnetic properties of the medium are described in terms of a complex magnetic susceptibility:

$$\chi = \chi' - j\chi''$$

where the imaginary part χ'' is responsible for the absorption of the energy in the medium. The expressions for the two quantities χ' and χ'' are the same as those given by Kronig–Kramers in the case of electrical susceptibility. The r-f susceptibility, χ'', at a frequency ν is given by:

$$\chi''(\nu) = \pi\chi_0\nu_0 g(\nu)$$

where χ_0 is the static susceptibility, ν_0 is the resonance frequency, and $g(\nu)$ is the shape function which is normalized according to the relation $\int_0^\infty g(\nu)d\nu = 1$. The Bloch susceptibility expressions which hold well in the paramagnetic resonance are given by

$$\chi''(\nu) = \pi\chi_0\nu_0 \frac{2T_2}{1+4\pi^2T_2^2(\nu_0-\nu)^2}, \qquad (1)$$

$$\chi'(\nu) = \pi\chi_0\nu_0 T_2 \frac{4\pi T_2(\nu_0-\nu)}{1+4\pi^2T_2^2(\nu_0-\nu)^2}.$$

[1]Manuscript received April 6, 1959.
Contribution from Eaton Electronics Research Laboratory, McGill University, Montreal, Que.

[2]N.R.C. Postdoctorate Fellow, on leave of absence from the Institute of Applied Physics, University of Allahabad, India.

The Bloch equations in absence of any saturation give the line a Lorentzian shape as is well known in collision-broadened spectra. The broadening of the paramagnetic resonance line can be pictured as caused by neighboring spins limiting the lifetime of a given spin state by inducing transitions from it, which is mathematically parallel to the collision broadening of the spectral lines resulting in Lorentz shape function:

$$g(\nu) = \frac{2T_2}{1+4\pi^2 T_2^2(\nu_0-\nu)^2} \tag{2}$$

where T_2 is the 'transverse' or spin–spin relaxation time.

On the basis of the dipolar broadening of the magnetic resonance lines, Van Vleck (1948) derives expression for the moments of various orders of the shape functions $g(\nu)$. The $(2n)$th moment is defined as:

$$\langle(\Delta\nu)^{2n}\rangle_{\text{Av}} = \int_0^\infty g(\nu)(\Delta\nu)^{2n}\, d\nu. \tag{3}$$

An experimental check of his theoretical calculations to show that the nuclear resonance lines have essentially dipolar broadening, and that the lines have Gaussian shape, was successfully done by Pake and Purcell (1948) in the case of CaF_2. The ratio $\langle\Delta\nu^4\rangle_{\text{Av}}^{1/4}/\langle\Delta\nu^2\rangle_{\text{Av}}^{1/2}$, calculated theoretically as 1.25, was close to the experimental value of 1.24 ± 0.02.

Kittel and Abrahams (1953) have extended the calculations of Van Vleck to the magnetically dilute samples. If f is the probability that a lattice site of a nonparamagnetic crystal is occupied by a magnetic system, then the fourth moment of the shape function (assuming a simple cubic lattice with H_0 along (100) axis) is:

$$\begin{aligned}\langle\Delta\nu^4\rangle_{\text{Av}} &= 3[\langle\Delta\nu^2\rangle_{\text{Av}}]^2\{0.742+f^{-1}[0.098-0.021(S^2+S)^{-1}]\} \\ &= 3[\langle\Delta\nu^2\rangle_{\text{Av}}]^2 \qquad \text{for the Gaussian shape.}\end{aligned} \tag{4}$$

For $S = 1/2$, the shape is Gaussian for $f > 0.1$
and for $S = 3/2$, the shape is Gaussian for $f > 0.4$.

Broer (1943) first tried to evaluate the higher moments to determine the shape function. He used Heisenberg's theory of ferromagnetism in taking the shape function proportional to the Gauss function. The susceptibility would then have the form:

$$\chi''(\nu) = 2\pi\chi_0\nu_0 T_2 \exp[-4\pi T_2^2(\nu_0-\nu)^2].$$

Pure dipolar interaction between the spins, in the absence of exchange effects, crystalline fields, or quadrupole moment, gives resonance line a Gaussian shape. This is true both in the case of nuclear magnetic and electron paramagnetic resonance. If it is assumed that the only interaction between the different spins are dipolar and exchange coupling, the Hamiltonian functions can be expressed as:

$$\begin{aligned}\mathfrak{H} &= \text{Zeeman} + \text{exchange} + \text{dipolar energies} \\ &= Hg\beta\sum_j S_{zj} + \sum_{k>j}\tilde{A}_{jk}S_j \,.\, S_k + \sum_{k>j}\tilde{B}_{jk}[(S_j \,.\, S_k) - 3r_{jk}^{-2}(r_{jk} \,.\, S_j)(r_{jk} \,.\, S_k)].\end{aligned}$$

The constants $\tilde{A}_{jk} = -2J_{jk}$ and $\tilde{B}_k = g^2\beta^2/r^3_{jk}$, J_{jk} is the exchange integral, and r_{jk} the interatomic spacing. S_{zj} is the z component of the spin angular momentum vector of atom j. The presence of the exchange term ($\tilde{A}$) in the Hamiltonian increases the fourth moment relative to the square of second moment in the relation (4) resulting in the narrowing of the Gaussian line near the center and tapering gradually in the wings. The effect can be visualized by the fact that the exchange term $\tilde{A}$ commutes with S and, therefore, does not contribute to the second moment. $\mathcal{H}_{\text{dipolar}}$ and S do not commute and $\mathcal{H}_{\text{exchange}}$ does not commute with $\mathcal{H}_{\text{dipolar}}$, hence $\mathcal{H}_{\text{exchange}}$ contributes to the fourth moment. (Reference is made to the expressions of various moments given by Van Vleck (1957).) It has been observed in cases of undiluted copper salts and manganese salts (MacLean and Kor 1956) that the calculated line widths are much greater than those observed. This exchange contribution to the fourth moment is important only in the undiluted paramagnetic salts since the exchange integral decreases rapidly with the distance between the paramagnetic ions. At very high magnetic dilution, on the basis of dipolar interaction, a Lorentzian line shape is expected. The half width is expressed as $\Delta = 5.3\, f(g\beta\mu^2/ha^3)$ where the symbols have their usual meanings. The line width is linearly proportional to the concentration and the intensity is independent of the concentration.

II. THE LORENTZ AND GAUSSIAN SHAPES

The Lorentz and Gaussian expressions are:

$$\chi''(\nu) = \frac{P_0}{1+4\pi^2 T_2^2(\nu-\nu_0)^2}, \tag{5}$$

$$\chi''(\nu) = P_0 \exp\{-4\pi T_2^2(\nu-\nu_0)^2\}. \tag{6}$$

The spin–spin relaxation time T_2 is related to the width of the line between the half-maximum points by the relations: $\Delta\nu = 1/\pi T_2$ for Lorentzian and $\Delta\nu = \sqrt{\ln 2/\pi}\cdot 1/T_2$ for Gaussian lines. Substituting for T_2 in the relations 5 and 6, we get:

$$\chi''(\nu) = P_0 \Big/ \left[1+4\left(\frac{\nu-\nu_0}{\Delta\nu}\right)^2\right], \tag{7}$$

$$\chi''(\nu) = P_0 \exp\left[-4\ln 2\left(\frac{\nu-\nu_0}{\Delta\nu}\right)^2\right]. \tag{8}$$

The first derivatives of these are:

$$\frac{d\chi''(\nu)}{d\nu} = \left[\frac{d\chi''(\nu)}{d\nu}\right]_{\max} \cdot \frac{32\sqrt{3}}{9}\left(\frac{\nu-\nu_0}{\Delta\nu}\right)\left[1+4\left(\frac{\nu-\nu_0}{\Delta\nu}\right)^2\right]^{-2} \tag{9}$$

$$\frac{d\chi''(\nu)}{d\nu} = \left[\frac{d\chi''(\nu)}{d\nu}\right]_{\max} \cdot 3.869\left(\frac{\nu-\nu_0}{\Delta\nu}\right)\exp\left[-4\ln 2\left(\frac{\nu-\nu_0}{\Delta\nu}\right)^2\right] \tag{10}$$

having maximum values when $[(\nu-\nu_0)/\Delta\nu] = 1/(2\sqrt{3})$ in case for Lorentzian shape and when $[(\nu-\nu_0)/\Delta\nu] = 1/(2\sqrt{2\ln 2})$ in the Gaussian case. The

normalized graphs of the two derivatives, represented by 9 and 10, intersect at $[(\nu-\nu_0)/\Delta\nu] = 1$ when their magnitudes drop to quarter of their maximum values. Graph 1 shows the shapes of the absorption curves and their derivatives as represented by equations 7, 8 and 9, 10.

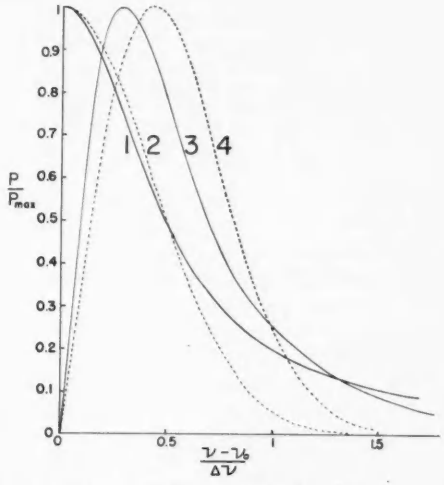

FIG. 1. Curves 1 and 2: Lorentzian and Gaussian line shapes of identical line widths. Curve 3: One side of the Lorentzian line derivative. Curve 4: One side of the Gaussian line derivative. The plot is between the normalized amplitude and the normalized frequency deviation from the resonance frequency.

III. EXPERIMENTAL TECHNIQUES

A conventional microwave paramagnetic-resonance spectrometer utilizing a magic T impedance bridge was used. A silver-plated cavity operating in TE_{102} mode was coupled to the end of a two-foot-long, stainless-steel, X-band waveguide. The whole assembly passed through a polystyrene head such that the cavity was centered between the poles of an electromagnet inside a double Dewar assembly. The cavity could be cooled to temperatures down to that of liquid helium. A 1000 c/s modulation on the magnetic field was kept below a peak to peak value of 0.5 oersted. The static magnetic field was swept at the rate of 2 oersteds/minute and was controlled by the driving motor of a Rectiriter recorder. The operating frequency was 9300 Mc/s. The sample volume was kept roughly to 0.15 cc. In the angular rotation experiments the crystal was hung at the end of a glass rod passing through the waveguide and the coupling iris. A graduated disk mounted on top of the rod indicated the orientation of the crystal. The microwave power entering the cavity was monitored. The Rectiriter recorded the differential absorption curve. A Sperry 2K39 Klystron giving out about 500 milliwatts of power was used in the saturation experiments.

The paramagnetic ion studied in detail is Cr^{+++} in $K_3Cr(CN)_6$ diluted by

the isomorphous $K_3Co(CN)_6$. It is a monoclinic crystal having its crystalline axis b perpendicular to the axes a and c, while $K_3Co(CN)_6$ is an orthorhombic crystal with $a \neq b \neq c$ and the three axes are perpendicular to each other. Although they differ slightly in their crystalline forms, they crystallize isomorphously. There are two magnetic complexes per unit cell which are oriented differently but their energy levels are identical when the magnetic field lies in either the (ac) or the (bc) planes of the crystal. The X-band transitions involving $M = \pm 1$ and $M = \pm 2$ (observed owing to a mixing of quantum states) at various angles of rotation are computed from the energy level diagrams. The four energy levels are derived from the spin Hamiltonian:

$$\mathcal{H} = g\beta\,(H_xS_x+H_yS_y+H_zS_z)+D(S_z^2-15/4)+E(S_x^2-S_y^2)$$

with $S = 3/2$, $D = 2.49$ kMc/s, $E = 0.33$ kMc/s, and $g = 1.992$. The energy levels can alternatively be determined by the methods of group theory and time inversion considerations as proposed by Koster and Statz (1959).

Potassium chromicyanide is diluted with the isomorphous potassium cobalticyanide in various proportions. The two salts were dissolved in distilled water in various proportions by weight and the crystals were grown by slow evaporation. The nominal concentration of Cr in the crystals as given by the concentration of the solution was found to be greatly different from the actual concentration. The concentration of Cr in the diluted samples was determined at Atomic Energy of Canada Ltd., Chalk River, by irradiation of the sample and counting the radioactivity. Table I lists the nominal and actual concentrations of the samples used in the experiment. It also lists the relative concentrations of the samples as determined by comparison of the paramagnetic intensity of absorption (total area of the derivative) of the $\langle -1/2 \rightarrow +1/2 \rangle$ transitions in $K_3CrCO(CN)_6$ with a known sample of diphenyl picryl hydrazyl. Care was taken in arranging the same orientation of the crystals.

TABLE I

Salt	Nominal concentration, % Cr	Actual concentrations	
		Chalk River results, %	Intensity comparison
$K_3Cr(CN)_6$	20	2.02	10.00
	10	0.65	5.58
	7		3.40
	5	0.43	.82
	1	0.02	.045
	0.5		.01
Cr^{+++} in $KAl(SO_4)_2.12H_2O$	4	.16	

IV. RESULTS AND DISCUSSION

The derivatives of the absorption obtained experimentally are plotted on the graphs with reference to the center of the derivative. The ratio $\{[d\chi''(\nu)]/d\nu\}/\{[d\chi''(\nu)]/d\nu\}_{max}$ was plotted along the axes of ordinates. The distance in oersteds on the recorder chart divided by the distance at which the amplitude drops to one quarter of its maximum value (at $(\nu-\nu_0)/\Delta\nu = 1$) representing $(H-H_0)/\Delta H$ was plotted along the abscissae.

Potassium Chromicyanide

Samples having various chromium concentrations have been examined. Graph 2 shows the experimental curves for the nominal concentrations of 0.5%, 1%, 5%, 7%, 10%, and 20% of chromium. It was observed that nominal 0.5% and 1% salts gave truly Lorentzian lines which broadened gradually to Gaussian at high concentrations. Table II tabulates the results.

TABLE II

Line shapes of Cr^{+++} transitions at 4.2° K

Transition	Actual dilution: 2% / Nominal dilution: 20%	0.6% / 10%	7%	0.4% / 5%	0.2% / 1%	0.5%
$-1/2 \rightarrow +1/2$	G	GL	GL	GL	L	L
$+1/2 \rightarrow +3/2$		GL	GL	GL	L	L
$-3/2 \rightarrow -1/2$		GL	GL	GL	L	L
$-1/2 \rightarrow +3/2$					L	L
$-3/2 \rightarrow +1/2$					L	L

NOTE: G: Gaussian, L: Lorentzian, and GL: between Gaussian and Lorentzian.

Potassium Chromium Alums

The shapes of the single resonance line corresponding to the $(-1/2 \rightarrow +1/2)$ transition in diluted potash chrome alums were studied. Undiluted chrome alums have been reported earlier to have Gaussian line shapes (Davis and Strandberg 1957). The crystals studied here had nominal Cr^{+++} concentrations of 4%, 10%, 20%, 50%, and 80%. Analysis of the 4% crystal gave the actual concentration of 0.16%, a factor of 25. Other crystals were not analyzed.

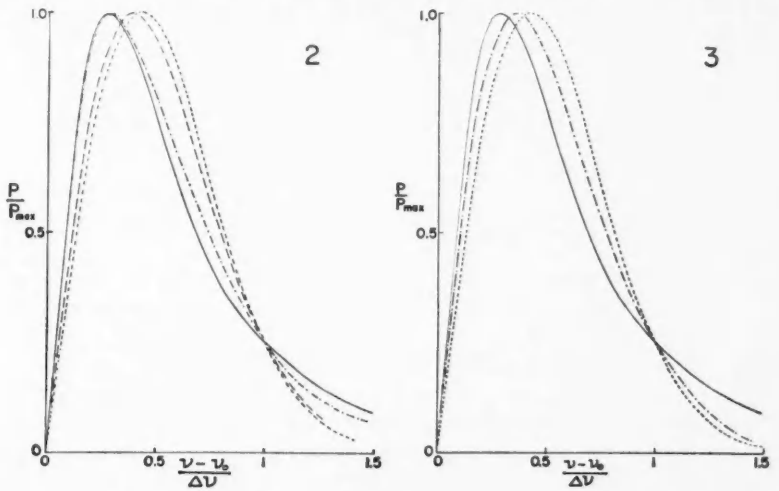

FIG. 2. Shapes of the differential absorption curves for different concentrations of Cr^{+++} in potassium cobalticyanide. The curves are represented by: nominal concentration 0.5% and 1% ——; 5% and 7% —·—·—; 10% — — —; and 20% – – –.

FIG. 3. Shapes of the differential absorption curves for different concentrations of Cr^{+++} in potassium aluminum sulphate. The curves are represented by: nominal concentration 10% by solid line, 20% by dot–dash line, and 80% by dotted line. The curve for 50% is closer to 80% and is not shown.

Graph 3 shows the shapes of the derivatives. Nominal 80% salt had a true Gaussian shape, 50% (not shown) was found to be close to 80% curve, 20% lies between the two shapes, and 10% is closer to the Lorentzian shape.

Gadolinium Ethyl Sulphate

A dilute sample of Gd^{+++} in lanthanum ethyl sulphate (about 1%) had shown Lorentzian line shape for all of its seven $\Delta M = \pm 1$ transitions and six $\Delta M = \pm 2$ transitions at liquid helium temperature. Graph 4 shows the Lorentzian line shape and the experimental points. The line width of $(-1/2 \rightarrow +1/2)$ transition was 20.8 oersteds.

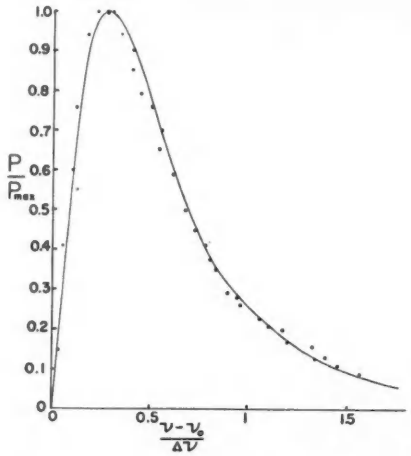

FIG. 4. Shape of the differential absorption curve for 1% gadolinium in lanthanum ethyl sulphate. The experimental points are shown by small circles on the true Lorentzian curve.

Exchange Narrowing

Two cases of exchange narrowing were studied. A powdered sample of free radical (diphenyl picryl hydrazyl) showed a line shape between Gaussian and Lorentzian at room temperature. The shape was not much changed at 4.2° K even though the line width had increased to nearly two and one-half times its room temperature value of 2 oersteds. A compact crystal of copper sulphate showed a narrow resonance line resembling Lorentzian.

Half Widths of Lines

The half widths ΔH (between half-maximum points) of the various transitions of the potassium chromicyanide crystal were measured at 4.2° K. The line widths remained practically constant for a particular transition on rotation of the crystal in the (*bc*) plane. The widths were measured with presumably no power saturation and no correction was made for the longitudinal relaxation time. The earlier reported r.m.s. widths of the undiluted crystal by Baker, Bleaney, and Bowers (1956) were 750 oersteds along *a* axis,

240 oersteds along b axis, and 700 oersteds along c axis. The magnetic field spectra of the resonance lines at different dilutions were plotted and the value of g tensor was determined by comparing the position of the resonance line with that of the resonance line of diphenyl picryl hydrazyl ($g = 2.0036$). The value was found to be $1.992 \pm .002$ in all the cases as compared with the value of $1.998 \pm .008$ in the undiluted crystal. The value of g was not found to vary throughout the temperature range (4.2° to 80° K). The relative peak intensities and the line widths of the five transitions observed in the nominal 0.5% sample at liquid helium temperature and at a crystal orientation of 90° to the direction of the magnetic field in the (bc) plane are shown in Fig. 5.

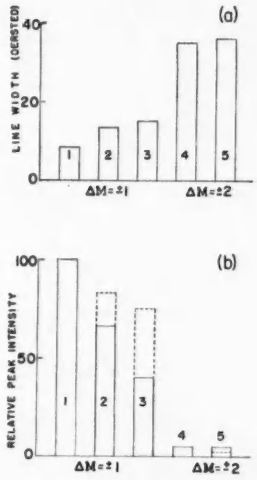

FIG. 5. Line widths and peak intensities, relative to $(-1/2 \rightarrow +1/2)$ transition, of the five transitions in 0.5% Cr^{+++} in potassium cobalticyanide crystal are shown in (a) and (b) respectively. The transitions are represented in order by $(-1/2 \rightarrow +1/2)$, $(-3/2 \rightarrow -1/2)$, $(+1/2 \rightarrow +3/2)$, $(-1/2 \rightarrow +3/2)$, and $(-3/2 \rightarrow +1/2)$. The dotted blocks in (b) represent the square of the matrix element relative to maximum for $(-1/2 \rightarrow +1/2)$.

Since the intensity measurements were made in the case of all transitions under similar conditions of the microwave power and temperature, the relative peak intensities could be compared to the maximum of the square of the perturbation matrix element of the magnetic moment of Cr^{+++} corresponding to the various transitions (Chang and Siegman 1958). The calculated matrix element square is shown by dotted blocks. The deviation of the experimentally observed intensities with the calculated one is marked in the $(3/2 \rightarrow -1/2)$ and $(-3/2 \rightarrow +1/2)$ transitions. The line width showed no variation on rotation in the (bc) plane. Great care had to be taken in setting the orientation of the crystal because a slight deviation from the (bc) plane separated the two spectra due to the two magnetic complexes per unit cell, and the line width might appear to have broadened.

Line Shape at the Onset of Saturation

The line shape of the nominal 0.5% Cr crystal $(-1/2 \rightarrow +3/2)$ transition had been studied at different power levels at the onset of saturation at 77° K. The shape remained Lorentzian although the width increased from its low power value. Holcomb (1958) had shown that in case of nuclear resonance, 'saturational' narrowing was observed and the shape changed from Gaussian to Lorentzian. Further work in this direction will be reported later.

V. CONCLUSIONS

The concentration of the paramagnetic impurity in the isomorphous diamagnetic crystal as compared with the concentration in the mother solution did not appear to follow a definite rule. Giordmaine, Alsop, Nash, and Townes (1958) have reported that in gadolinium magnesium nitrate actual concentrations were found to be less than the nominal values by somewhat more than a factor of 10. They found no such large differences in other materials examined such as copper ammonium sulphate. The present measurements in case of potassium chromicyanide indicated that at higher nominal concentrations, the factor (ratio of nominal to actual concentration) was 10 which increased to 50 at very low concentration. A sample containing a nominal concentration of 0.5% Cr had given a line width for the $(-1/2 \rightarrow +1/2)$ transition of 9 oersteds as compared with Townes' (1958) value of 12 oersteds. The same crystal had been successfully used as a Maser crystal in two setups in this laboratory operating at 10 cm and having same operating characteristics as reported elsewhere.

The shapes of the resonance lines of chromium salts were found to depend on the distribution of the paramagnetic ions in the isomorphous diamagnetic crystal lattice. The results could be explained on the basis of purely dipolar type of interaction between the spins.

ACKNOWLEDGMENTS

The author is indebted to Professor G. A. Woonton, Director, for affording all the laboratory facilities and for his constant encouragement and stimulating discussions. Thanks are due to Dr. G. V. Marr for his invaluable assistance, Professor G. W. Farnell and Professor E. J. Stansbury for discussing details of the operating Maser, and Professor L. Yaffe of the Chemistry Department for getting the crystals analyzed. The grants of the Defence Research Board and the National Research Council, which made the present research possible, are gratefully acknowledged.

REFERENCES

BAKER, J. M., BLEANEY, B., and BOWERS, K. D. 1956. Proc. Phys. Soc. B, **69**, 1205.
BROER, L. J. F. 1943. Physica, **10**, 801.
CHANG, W. S. and SIEGMAN, A. E. 1958. Stanford Electronics Laboratory Technical Report No. 156–1, May 16.
DAVIS, C. F. and STRANDBERG, M. W. P. 1957. Phys. Rev. **105**, 447.
GIORDMAINE, J. A., ALSOP, L. E., NASH, F. R., and TOWNES, C. H. 1958. Phys. Rev. **109**, 302.
HOLCOMB, D. F. 1958. Phys. Rev. **112**, 1599.

KITTEL, C. and ABRAHAMS, E. 1953. Phys. Rev. **90**, 238.
KOSTER, G. F. and STATZ, H. 1959. Phys. Rev. **113**, 445.
MACLEAN, C. and KOR, G. J. W. 1956. Appl. Sci. Research, B, **4**, 425.
PAKE, G. E. and PURCELL, E. M. 1948. Phys. Rev. **74**, 1184.
VAN VLECK, J. H. 1948. Phys. Rev. **74**, 1168.
——— 1957. Nuovo cimento, **6** (Suppl.), 993.

A SIMPLE GAMMA-RAY INSENSITIVE FAST-NEUTRON COUNTER[1]

G. M. Griffiths, P. P. Singh, Y. I. Ssu, and J. B. Warren

ABSTRACT

A gamma-ray insensitive fast-neutron counter is described which consists of a number of thin rectangular sheets of lucite coated with zinc sulphide and sandwiched together to form a rectangular block which is mounted on a photomultiplier. Pulse height spectra and absolute efficiency curves are presented for neutrons from 300 kev to 15 Mev.

INTRODUCTION

Chadwick in 1932 first identified fast neutrons by observation of the knock-on protons ejected from hydrogenous materials. Since that time many neutron counters have used the same neutron–proton interaction in either hydrogen-filled proportional counters (Coon and Nobles 1947), ionization chambers (Stafford 1948), or solid hydrogenous materials. Bell (1948) and Segel *et al.* (1954) employed organic phosphors successfully; however, these suffer from the fact that they are gamma-ray sensitive if the volume used is sufficiently large to give good neutron-detection efficiency. A thin layer of zinc sulphide powder placed on the face of a photomultiplier has been used to detect proton recoils from a layer of plastic resulting in a neutron counter with a very low gamma-ray sensitivity; however, the neutron efficiency is also small. Hornyak (1952) made a great improvement in detection efficiency while maintaining low gamma-ray sensitivity by using a molded button of lucite with zinc sulphide powder dispersed in it. As zinc sulphide is opaque to its own radiation the useful size of this device is limited. Since then several attempts have been made to improve the neutron-detection efficiency without increasing the gamma-ray sensitivity (Emmerich 1954; Brown and Hooper 1958). Recently a method, based on the fact that the ratio of the intensity of the slow light decay component to that of the fast component is different for protons and electrons in organic scintillators, has been used to discriminate between gamma rays and neutrons (Litherland *et al.* 1959; Owen 1958).

Below we describe the properties of a counter used in our laboratory for several years, which has an efficiency comparable to others we have seen reported, along with an excellent gamma-ray rejection ratio and simplicity of construction.

COUNTER CONSTRUCTION

The counter consists of a number of thin rectangular lucite sheets coated with zinc sulphide over their large faces and then sandwiched together to form a rectangular block which is mounted on an RCA 6342 photomultiplier. Pro-

[1]Manuscript received February 24, 1959.
Contribution from the Department of Physics, University of British Columbia, Vancouver, B.C.

tons knocked out of the lucite produce light in the thin zinc sulphide layers and the lucite plates conduct the light to the photomultiplier. To make the block, the lucite sheets were dipped in ethyl formate and while still wet a weighed quantity of zinc sulphide powder was sprinkled on evenly through a fine mesh nylon cloth. Then the plates were stuck together under pressure until dry. The block was then polished on a face perpendicular to the plane of the sheets and this face was mounted on the photomultiplier with Dow–Corning silicone oil. The other faces of the block were smoked with burning magnesium ribbon. The construction of a typical phosphor block is shown in Fig. 1.

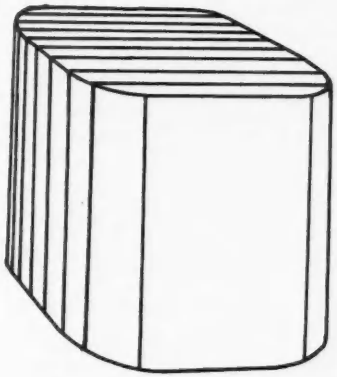

FIG. 1. The lucite – zinc sulphide sandwich block.

Both Patterson D and RCA 33-Z-20A zinc sulphide phosphors were tested. With a radium–beryllium neutron source the RCA phosphor gave about 30% more counts above a selected bias than the Patterson D phosphor and so was used for all further work. Tests to determine the optimum thickness of the zinc sulphide powder indicated that for thicknesses greater than 12 mg/cm^2 the gamma-ray sensitivity becomes appreciable and thicknesses less than 10 mg/cm^2 gave a satisfactory neutron response. Several lucite sheet thicknesses were tried and it was found that for radium–beryllium neutrons the efficiency decreased for thicknesses greater than 0.125 inch. The plate thickness determines a limit to the height of the block that can be usefully employed, since for a given height the light from the top of the block will not reach the photomultiplier as efficiently with thin plates as it would with thicker ones due to absorption in the zinc sulphide. Thus with increasing height a decreasing proportion of the light will get into the photomultiplier and after a certain height, which depends on the plate thickness, any additional height contributes very little light. However, greater plate thickness, although it means that the detector may be made longer, does not necessarily mean greater efficiency since for thicker plates more of the protons lose all their energy in the lucite. Protons stopped in lucite alone produce very small

pulses which are lost in the noise. A check on the transmission of light down the block was made by preparing a plastic sandwich with 0.125 inch thick plates 5 inches long mounted on a photomultiplier. A radium–beryllium source was placed 25 cm away to one side and the counting rate was observed, as a function of the length, which was altered by cutting sections from the end of the sandwich block. Little change in counting rate was observed until the length was reduced to 3 inches and the counting rate became roughly proportional to length for lengths less than 1.5 inches.

A rectangular block consisting of 1/8 inch square lucite rods packed together with zinc sulphide powder on all internal faces was made and tested. Its efficiency per unit volume for neutron detection was little if any better than that of the flat sheet assemblies and as it was more difficult to construct no further ones of this type have been made.

Tests were performed to find out whether the neutron-detection efficiency of the counter (using radium–beryllium neutrons) depended on the direction of neutron entrance (i.e. parallel or perpendicular to the lucite sheets). One might expect such an effect since the protons are scattered forward in the laboratory system, but within the errors of about 10% no effect was found either in the shape of the spectrum or in the number of counts obtained above a given bias.

Two blocks with the following characteristics were tested in some detail:

	Block I	Block II
Lucite thickness	1/32 inch	1/16 inch
Length	1 cm	2 cm
Cross section	4.2×4.2 cm	4.4×4.4 cm
No. of plates	50	28
ZnS thickness	7 mg/cm²	7 mg/cm²

The efficiency per unit volume for block I was 1.75 times that for block II. However, since its volume was less than half of that of block II it gave fewer counts for a given neutron flux. The results described below were obtained with block II.

COUNTER PERFORMANCE

(*a*) *Pulse Height Spectra*

The pulse height spectra and absolute efficiencies for the neutron counter were measured for neutrons of energies from 225 kev to 4.4 Mev using neutrons from the $T(p, n)He^3$ and $D(d, n)He^3$ reactions and for 17-Mev neutrons from the $T(d, n)He^4$ reaction. The differential pulse height spectra are shown in Figs. 2 and 3 along with spectra for photomultiplier noise and γ-rays of 1 Mev from Co^{60} and 6.14 Mev from the $F^{19}(p, \alpha, \gamma)O^{16}$ reaction. The pulse height scale is the same for all curves but the vertical scale is arbitrary and the curves are not normalized to each other.

(*b*) *Absolute Efficiency*

The absolute efficiencies were determined from knowledge of the neutron fluxes from the targets used. The tritium content of the tritium–zirconium

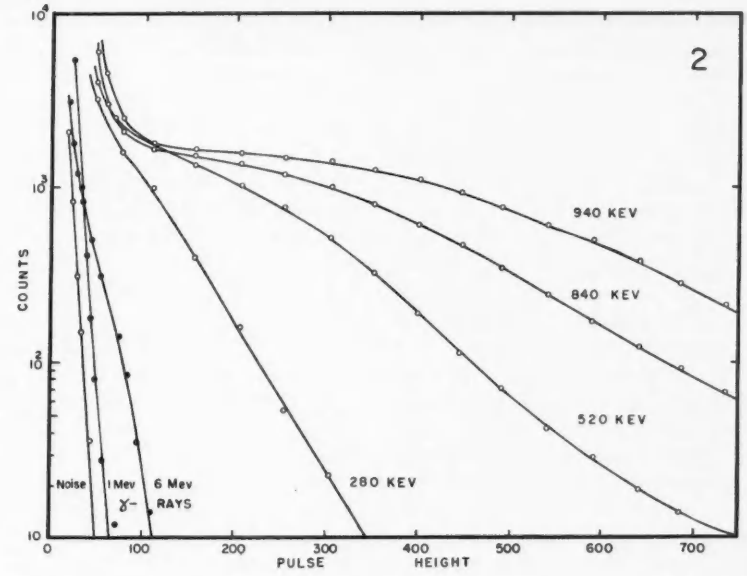

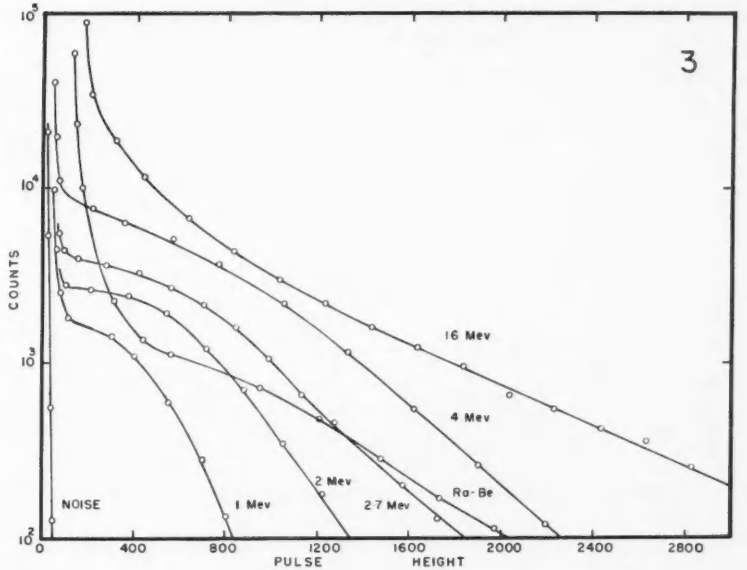

FIG. 2. Pulse height spectra for low-energy neutrons and for gamma rays. The curves are not normalized with respect to each other.

FIG. 3. Pulse height spectra for high-energy neutrons. The curves are not normalized with respect to each other.

target, kindly supplied by the Oak Ridge National Laboratory, was measured in terms of the absolute gamma-ray yield from the $T(p, \gamma)He^4$ reaction at 800 kev, using absolute differential cross-section data of Perry and Bame (1955) for this reaction and theoretical estimates of the scintillation counter efficiency. Low-energy neutrons from 280 kev to 940 kev were produced by the $T(p, n)He^3$ reaction and high-energy neutrons were produced by the $T(d, n)He^4$ reaction using the same target. Intermediate energy neutrons from 1.9 Mev to 4.2 Mev were produced by $D(d, n)He^3$ reactions using a heavy ice target of known thickness. The D_2O targets were made by condensing heavy water vapor from a constant volume dispenser onto a liquid air cooled gold plate. The dispenser–target system was calibrated by observing the shift in the 340-kev resonance of the $F^{19}(p, \alpha, \gamma)O^{16}$ reaction after a given pressure of vapor was deposited on a thin F^{19} target. From the measured energy loss of protons in passing through the ice layer and from the stopping power data given by Whaling (1958) the number of target deuterons per square centimeter was calculated. Neutron yields were obtained from cross-section data given by the review article of Fowler and Brolley (1956).

The neutron-detection efficiency for the counter is dependent on the neutron energy as shown in Fig. 4. Curve (*a*) shows the angular distribution of $D(d, n)He^3$ neutrons for 1.0-Mev incident deuterons as obtained by Hunter

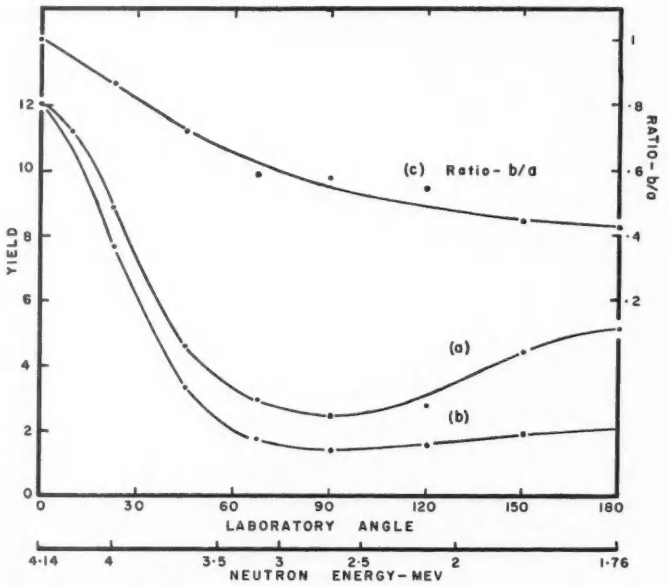

FIG. 4. The angular distribution of $D(d, n)He^3$ neutrons at 1.0 Mev. Curve (*a*): The distribution of Hunter and Richards (1949) obtained with a long counter. Curve (*b*): The distribution as seen by the lucite – zinc sulphide sandwich counter. Curve (*c*): The ratio of the curves (*b*) and (*a*), which are normalized to each other at zero degrees.

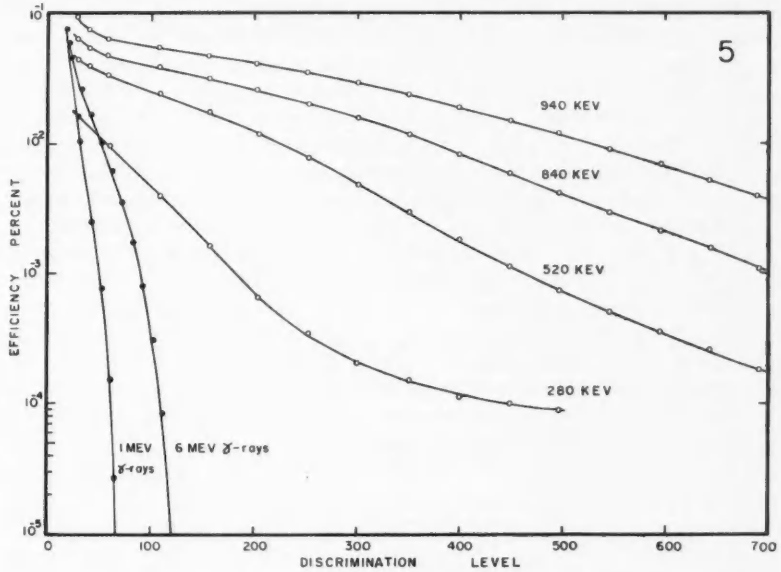

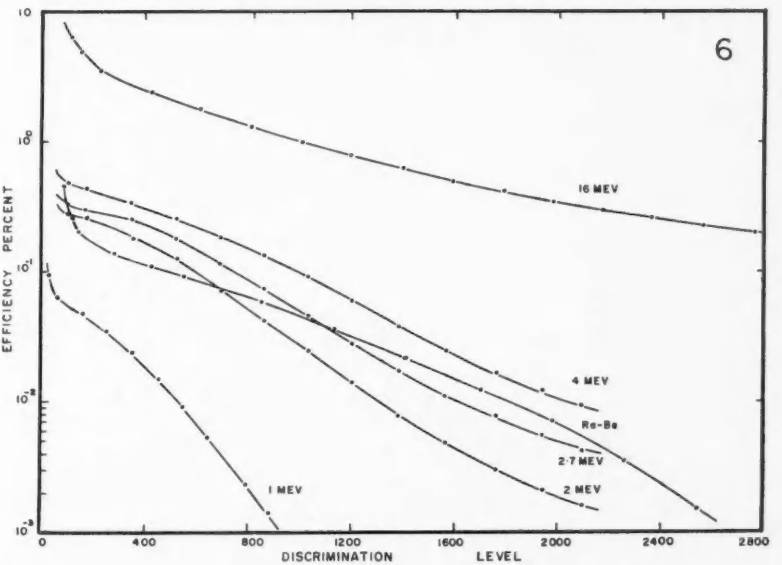

FIG. 5. Absolute efficiency vs. discrimination level for the low-energy neutrons. The ordinate for the gamma-ray curves should be multiplied by 10^{-2}.

FIG. 6. Absolute efficiency vs. discrimination level for the high-energy neutrons.

and Richards (1949) using a long counter and making small corrections for the change in efficiency with neutron energy as given by Hanson and McKibben (1947). Curve (*b*) shows the curve obtained with the present counter normalized to curve (*a*) at zero degrees. The ratio between the curves is shown by the upper line and indicates the decrease in efficiency for decreasing neutron energies. The absolute intrinsic efficiencies defined as the number of counts observed divided by the number of neutrons incident on the front face of the counter for various neutron energies as a function of discriminator bias level (integral bias curves) are shown in Figs. 5 and 6. The efficiency falls off rapidly for neutrons with energies less than 300 kev and is very small for thermal neutrons. It should be noted that the efficiency figures given here are smaller by a factor A, equal to the area of the front face of the counter, than those quoted by some authors who give the number of counts per unit neutron flux at the position of the counter. Figure 5 also shows on an expanded vertical scale the absolute efficiencies for Co^{60} and 6-Mev gamma rays. Note that for the gamma-ray curves the ordinates should be multiplied by 10^{-2}. The curves indicate that a bias may be chosen without serious loss of neutron counts to give gamma-ray efficiencies of 10^{-6} to 10^{-10} of the neutron efficiency at that bias.

As a crude first approximation one would expect the neutron-detection efficiency to be proportional to the neutron–proton scattering cross section, σ, and the mean range, R, of the scattered protons in the lucite, since for

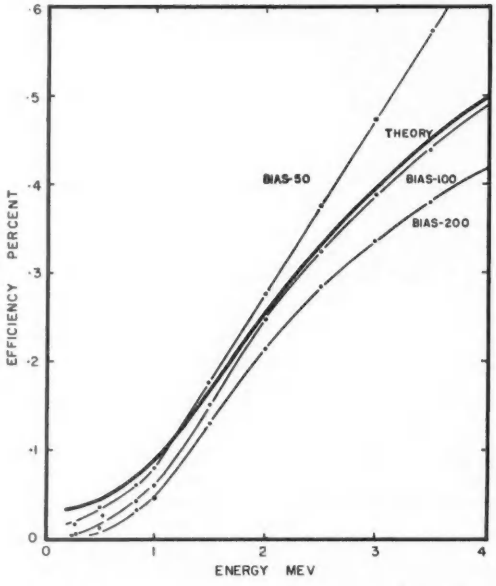

FIG. 7. Absolute efficiency vs. neutron energy for various biases. The thick curve shows a rough theoretical estimate of efficiency with energy on an arbitrary vertical scale.

all energies studied here the proton ranges are smaller than the thickness of the lucite plates. The validity of this assumption is indicated in Fig. 7, which shows experimental absolute efficiencies as a function of neutron energy for several discriminator levels and also shows a curve of the product $\sigma \cdot R$ as a function of neutron energy with arbitrary vertical normalization. The agreement in shape of the curves is quite good; the theoretical curve is rather flatter than the experimental ones suggesting that for lower-energy neutrons a larger proportion of the pulses are lost in the noise.

This counter has been used to detect the small yield of secondary neutrons produced by proton bombardment of heavy ice targets below the D(p, n) threshold in the presence of a much larger yield of 6-Mev γ-rays, and as a general monitor for fast neutrons.

ACKNOWLEDGMENT

One of us (P.P.S.) gratefully acknowledges the receipt of a National Research Council Studentship.

REFERENCES

BELL, P. R. 1948. Phys. Rev. **73**, 1405.
BROWN, B. and HOOPER, E. B., JR. 1958. Nucleonics, **16**, 96.
CHADWICK, J. 1932. Proc. Roy. Soc. A, **136**, 692.
COON, J. H. and NOBLES, R. A. 1947. Rev. Sci. Instr. **18**, 44.
EMMERICH, W. S. 1954. Rev. Sci. Instr. **25**, 69.
FOWLER, J. L. and BROLLEY, J. E. 1956. Revs. Modern Phys. **28**, 103.
HANSON, A. O. and MCKIBBEN, J. L. 1947. Phys. Rev. **72**, 673.
HORNYAK, W. F. 1952. Rev. Sci. Instr. **23**, 264.
HUNTER, G. T. and RICHARDS, H. T. 1949. Phys. Rev. **76**, 1445.
LITHERLAND, A. E., ALMQUIST, E., BATCHELOR, R., and GOVE, H. E. 1959. Phys. Rev. Letters, **2**, 104.
OWEN, R. B. 1958. Nucleonics, **16** (6), 54.
PERRY, J. E., JR. and BAME, S. J., JR. 1955. Phys. Rev. **99**, 1368.
SEGEL, R. E., SWARTZ, C. D., and OWEN, G. E. 1954. Rev. Sci. Instr. **25**, 689.
STAFFORD, G. H. 1948. Nature (London), **162**, 771.
WHALING, W. 1958. Handbuch der Physik, Vol. 34 (Springer-Verlag, Berlin), p. 193.

THE NEUTRON YIELD FROM HEAVY ICE TARGETS BOMBARDED WITH PROTONS BELOW THE $D(p, n)2p$ THRESHOLD[1]

P. P. Singh, G. M. Griffiths, Y. I. Ssu, and J. B. Warren

ABSTRACT

In connection with some experiments on the gamma-ray yield from the $D(p, \gamma)He^3$ reaction using heavy ice targets a considerable yield of neutrons was found even for proton bombarding energies well below the $D(p, n)2p$ threshold of 3.3 Mev. The yield, excitation function, and angular distribution of this neutron yield have been investigated both experimentally and by means of theoretical calculations. These studies confirm the suggestion that the neutrons are produced by a secondary reaction in which deuterons, scattered in the target by incident protons, collide with further target deuterons to produce $D(d, n)He^3$ reactions.

INTRODUCTION

The production of neutrons when heavy ice targets are bombarded with protons below the $D(p, n)2p$ threshold has been reported by Jennings *et al.* (1950), who suggested that the neutrons arise from deuterons, scattered by incident protons, colliding with other target deuterium atoms and producing $D(d, n)He^3$ reactions. In connection with some measurements on the gamma-ray yield from the $D(p, \gamma)He^3$ reaction this effect was found to contribute a considerable background (Griffiths and Warren 1955). Consequently we have made a detailed experimental and theoretical study of the effect.

EXPERIMENTAL

The gamma-ray insensitive neutron counter used in these experiments has been described previously (Griffiths *et al.* 1959). It consists of a block of lucite sheets with thin layers of zinc sulphide powder sandwiched between them, mounted on an RCA 6342 photomultiplier. A bias setting which made the 6-Mev gamma-ray sensitivity less than 10^{-9} of the neutron sensitivity was used. The absolute efficiency for neutron detection varied with neutron energy from 0.15% for 2-Mev neutrons to 0.3% for 4-Mev neutrons at this bias. The pulse height spectrum was analyzed with a 100-channel Computing Devices of Canada kicksorter.

The target chamber used is shown in Fig. 1. A gold-plated liquid air cooled copper plate formed the target backing. This could be turned to face an inlet hole through which heavy water vapor from the dispenser was admitted to the target chamber. For thin targets, the constant volume dispenser was evacuated, taps T_1 and T_2 were closed, and tap T_3 was opened to admit the required pressure of water vapor as measured by the oil manometer. Then tap T_3 was closed and T_1 was opened to admit the vapor slowly via the

[1]Manuscript received March 12, 1959.
Contribution from the Physics Department, University of British Columbia, Vancouver, B.C.

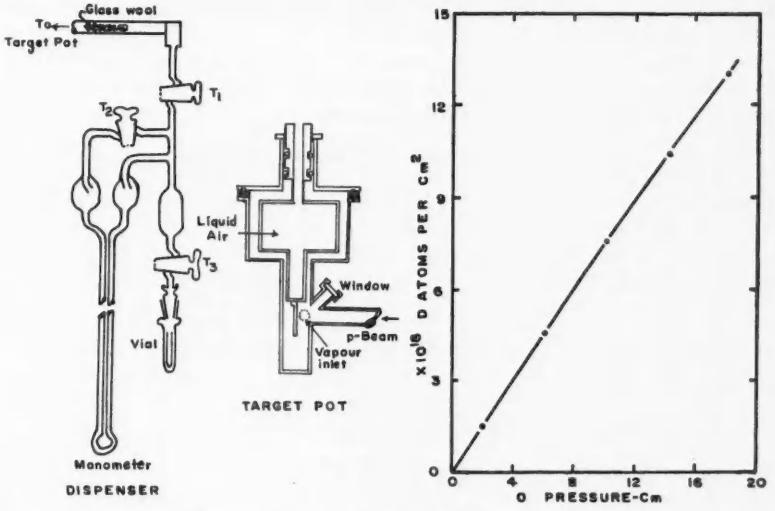

FIG. 1. Target chamber and heavy water vapor dispenser. The graph on the right shows the dispenser calibration in terms of target thickness versus dispenser pressure.

glass-wool diffuser to the target chamber. The target thickness as a function of dispenser pressure was calibrated by freezing the vapor on top of thin fluorine targets for various initial pressures in the dispenser and measuring the shift in the $F^{19}(p, \alpha, \gamma)O^{16}$ 340-kev resonance due to the energy loss of the protons in passing through the ice layers. From a knowledge of the stopping power of the protons in ice (Whaling 1958) the number of deuterium atoms per square centimeter on the target could then be calculated as a function of the manometer pressure (Fig. 1). When a thick target was required so that the incident protons would be stopped completely in the ice layer, taps T_1 and T_3 were opened for 2 minutes and then a measurement of the yield was made. The taps were opened for a further 2 minutes and a second yield measurement was made. When no increase in yield occurred for additional ice on the target, the target was judged to be "thick".

RESULTS

1. Thick Target Yield and Excitation Function

A thick heavy ice target was bombarded with protons of energies from 350 kev to 1.5 Mev and the neutron yield at zero degrees to the proton beam per millicoulomb of beam per steradian was obtained. Since the detection efficiency is a function of the neutron energy and since at any angle the neutron energies incident on the counter varied from approximately 2 Mev to 4 Mev, the mean neutron energy at 0° was estimated for each bombarding energy by assuming that on the average the deuterons were scattered at 45° to the proton beam direction and then by calculating the neutron energy in

the direction of the counter from the mechanics of the D(d, n)He^3 reaction. The experimental excitation function, shown in Fig. 2, has been corrected for the change in efficiency due to the change in mean neutron energy. The theoretical neutron yield as a function of proton energy calculated on the basis of the secondary process is also shown in Fig. 2.

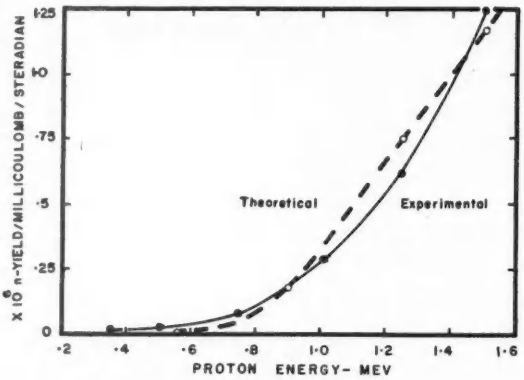

FIG. 2. The theoretical and experimental thick target excitation functions.

2. Thick Target Angular Distribution

With the counter subtending a solid angle of 0.15 steradian at the target the thick target neutron yield was measured for a proton energy of 1.5 Mev

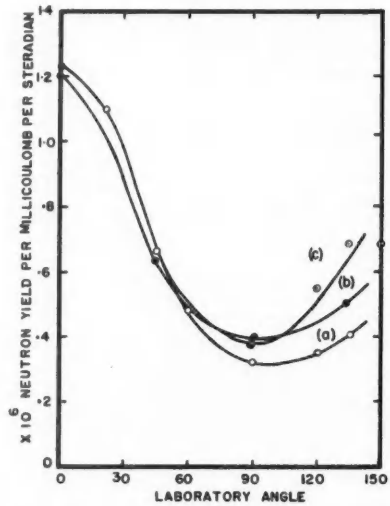

FIG. 3. The thick target angular distribution for 1.5-Mev incident protons. Curve (a), experimental results—uncorrected; curve (b), theoretical result; curve (c), experimental results—corrected for change in neutron-detection efficiency with mean neutron energy.

at seven different angles. The neutron yield observed at each is shown by the lower curve in Fig. 3. Since, for each counter position, neutrons from deuterons, scattered with various energies and travelling in various directions in the target, may reach the counter a rough estimate of the mean neutron energy and thence the mean detection efficiency for each counter position was made. The correction for efficiency change results in the upper curve of Fig. 3. The theoretical curve is also shown in the figure. The increase in neutron yield towards backward angles after a minimum at 90° results from the corresponding increase in the $D(d, n)He^3$ neutron yield at backward angles. In this case the effect is less pronounced than for a $D(d, n)He^3$ experiment since it is averaged over the scattered deuteron directions and energies in the target.

3. Pulse Height Spectrum

The pulse height spectrum from the fast-neutron counter produced by bombarding a thick heavy ice target with 1.5-Mev protons is shown in Fig. 4.

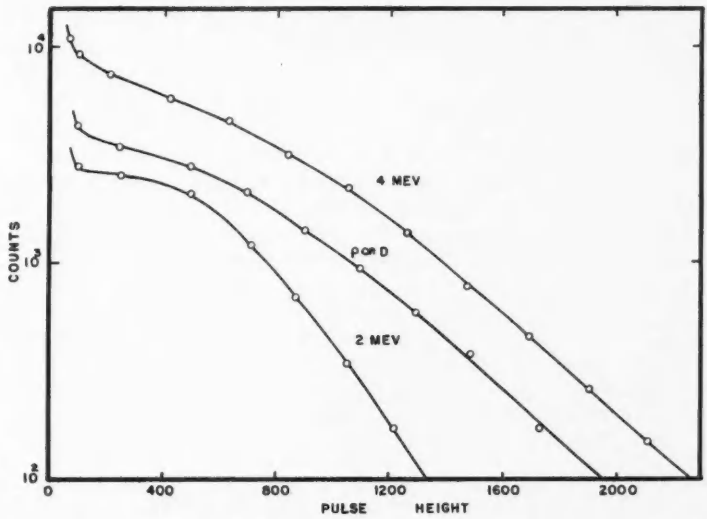

FIG. 4. The differential pulse height spectra from the neutron detector for 4-Mev and 2-Mev monoenergetic neutrons and for the neutrons from a heavy ice target bombarded with protons of 1.5-Mev energy.

For comparison the spectra produced by monoenergetic neutrons of 2-Mev and 4-Mev energy from the $D(d, n)He^3$ reaction are also shown. It is apparent that the neutrons from the ice target are comparable in energy to those from the $D(d, n)He^3$ reaction.

4. Thin Target Yield and Angular Distribution

A thin target containing 24×10^{18} deuterium atoms per square centimeter, approximately 70 kev thick for 1.5-Mev protons, was bombarded by 1.5-Mev protons and the neutron yield was measured as a function of angle. The

results are shown in Fig. 5. Since a large number of scattered deuterons escape from the back of the ice, it is not easy to make an estimate of the mean neutron-detection efficiency because it is difficult to estimate the neutron energy spectrum as a function of counter angle. Therefore no correction for

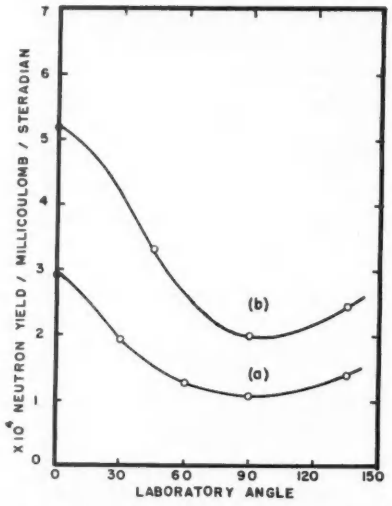

FIG. 5. The thin target yield and angular distribution function for 1.5-Mev protons. Curve (*a*), experimental results; curve (*b*), theoretical results.

the change of efficiency with neutron energy was applied to the curve. The theoretical curve is also shown. The two curves show good agreement in shape and the factor of about two between the absolute values may be partly accounted for by the fact that in the theory for the thin target it was assumed, for the sake of simplicity, that all the deuterons scattered in the ice layer started out at the front face of the layer which gives an overestimate of the neutron yield.

5. Effect of D_2O *Concentration*

If the neutron production from heavy ice targets is due to primary processes one would expect the neutron yield to depend linearly on the deuterium concentration in the target, whereas if the yield is due to secondary processes, as suggested here, one would expect the neutron yield to depend on the square of the deuterium concentration. This was checked by measuring the zero-degree neutron yield for 1.5-Mev protons using thick targets with various concentrations of heavy water in ordinary water. The results are shown in Fig. 6. The 6-Mev gamma-ray yield from the $D(p, \gamma)He^3$ reaction is directly proportional to the deuterium concentration as expected since it arises from a direct interaction of the incident protons with the target nuclei. However, it is clear that the neutron yield increases as the square of the

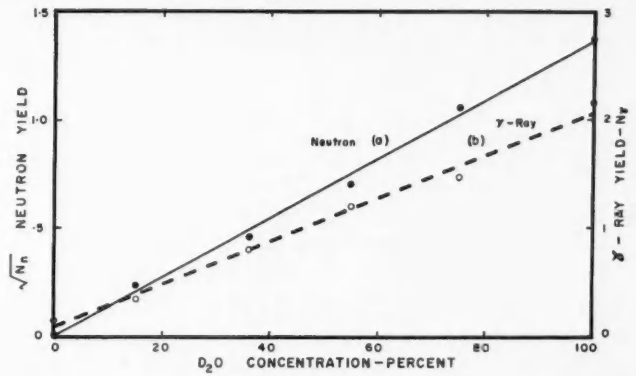

FIG. 6. The effect of D_2O concentration on the gamma-ray and neutron yields. The gamma-ray yield is plotted on a linear scale and the neutron yield is on a square-root scale.

concentration. This leaves no doubt about the secondary nature of the neutron production.

THEORETICAL ANALYSIS

Calculations have been made of the yield, excitation function, and angular distribution of neutrons from thick and thin targets of heavy ice bombarded with protons on the assumption that they are produced by scattered deuterons colliding with other deuterons in the target and producing $D(d, n)He^3$ reactions.

In the case of a thick target the calculations involved the following steps. The target was divided into six layers perpendicular to the proton beam direction as shown in Fig. 7(*a*), so that each layer has approximately one sixth of the incident proton energy of 1.5 Mev dissipated in it and in each layer the protons were considered to have a constant energy equal to the mean proton energy in the layer. The data of Sherr *et al.* (1947) and Taschek (1942) on proton–deuteron scattering were used to calculate the energy and the angular distribution of the deuterons from each layer. The scattered deuterons from each layer were divided into overlapping cones, Fig. 7(*b*), symmetrical about the proton beam direction, with angular limits for each cone such that the difference in the deuteron energies at the outside and the inside of the cone was equal for all cones. It was assumed that all deuterons entering a cone have an energy equal to the mean energy of the deuterons entering the cone. Further, assuming Rutherford scattering and using the analytical expression for the energy and angular dependence of the proton–deuteron scattering cross section the number of deuterons scattered into each cone was obtained by analytical integration between the angular limits of the cone. To allow for the fact that the scattering does not follow the Rutherford formula for all energies and angles due to some nuclear interaction, the results from the Rutherford formula were multiplied by the ratio of the measured cross section to the Rutherford cross section. This ratio was interpolated for

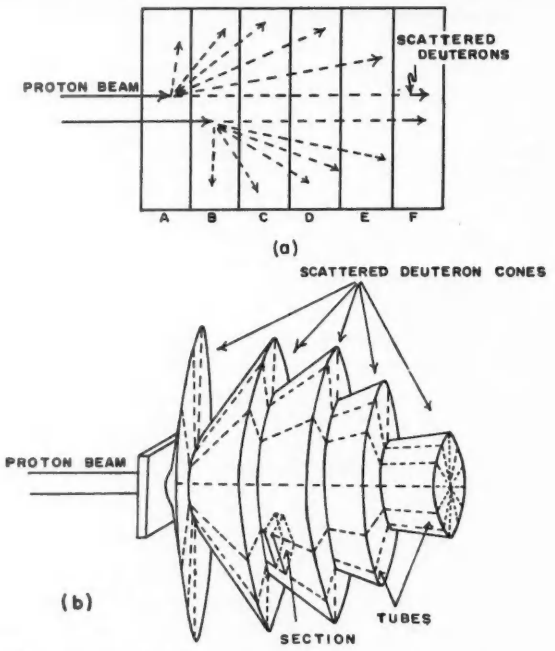

FIG. 7. The division of the thick target into layers, cones, tubes, and sections as used in the theoretical calculations.

the required energies from the results of Sherr *et al.* (1947) and Taschek (1942). Each cone was subdivided into 12 "tubes", Fig. 7(*b*), each tube containing 1/12 of the deuterons in the cone. All deuterons in each tube were assumed to travel down the center of the tube. For each tube the angle between this direction and the line joining the target to the detector was obtained geometrically. These angles were computed for the counter at 0°, 45°, 90°, and 135° with respect to the incident beam direction. Finally each tube was divided into "sections" along its length such that the energy loss of the deuterons in traversing each section was approximately equal to the difference between the deuteron energies at the outside and the inside of the particular cone. In all there were 672 sections. The stopping power data for heavy ice of Wenzel and Whaling (1952) was used to compute the thickness and hence the number of target deuterons in each section of the target. The yield and angular distribution of $D(d, n)He^3$ neutrons has been expressed by Hunter and Richards (1949) in terms of Legendre polynomials which were used to provide the relevant neutron yields from each section in the direction of the counter for four counter positions at 0°, 45°, 90°, and 135°. The total neutron yield from the thick target in the counter direction can be obtained by summing over all sections of each tube, over all tubes of each cone, over all cones of each layer, and over all layers.

Table I gives typical neutron yield data at 0° for each of the six layers with the energy of the protons in each layer.

TABLE I

Layer	Proton energy, kev	0° neutron yield per steradian per millicoulomb
A	1500 to 1322	3.25×10^{5}
B	1322 to 900	7.02×10^{5}
C	900 to 563	1.55×10^{5}
D	563 to 338	1.08×10^{4}
E	338 to 113	1.08×10^{4}
F	113 to 0	Neglected

From this table the thick target yield of neutrons as a function of energy can easily be obtained by adding the zero-degree contribution from the bottom of the table to the layer which has an incident proton energy equal to the particular energy at which the total yield is required. The theoretical results are plotted in Figs. 2, 3, and 5 along with the experimental results. In principle the calculations for the thin target yield and angular distribution function were the same as for the thick target calculations except that only one target layer was considered; however, since a large fraction of the higher-energy scattered deuterons escape from the thin target layer the yield from the low-energy scattered deuterons was considered in greater detail than for the thick target calculation.

The over-all agreement between theory and experiment leaves no doubt as to the secondary process responsible for the neutron production.

ACKNOWLEDGMENT

One of us (P.P.S.) wishes to thank the National Research Council of Canada for an award of a Studentship.

REFERENCES

GRIFFITHS, G. M. and WARREN, J. B. 1955. Proc. Phys. Soc. A, **68**, 781.
GRIFFITHS, G. M., SINGH, P. P., SSU, Y. I., and WARREN, J. B. 1959. Can. J. Phys. **37**, 858.
HUNTER, G. T. and RICHARDS, H. T. 1959. Phys. Rev. **76**, 1445.
JENNINGS, B., SUN, K. H., and LEITER, H. A. 1950. Phys. Rev. **80**, 109.
SHERR, R., BLAIR, J., KRATZ, H., BAILEY, C., and TASCHEK, R. 1947. Phys. Rev. **72**, 662.
TASCHEK, R. F. 1942. Phys. Rev. **61**, 13.
WENZEL, W. and WHALING, W. 1952. Phys. Rev. **87**, 499.
WHALING, W. 1958. Handbuch der Physik, Vol. 34 (Springer-Verlag, Berlin), p. 193.

MAGNETIC CONTROL ON THE VARIATIONS OF THE CRITICAL FREQUENCY OF THE F_2 LAYER OF THE IONOSPHERE[1]

R. G. RASTOGI[2]

ABSTRACT

The paper discusses the comparative influence of the true magnetic and smooth geomagnetic latitudes on the diurnal and latitudinal variations of the critical frequency of the F_2 layer (f_0F_2) at low latitudes. The diurnal variations of f_0F_2 are shown to differ considerably at stations having the same geomagnetic latitude, but the discrepancies disappear when the true magnetic latitude is taken into consideration. The latitudinal variation of noon values of f_0F_2 is also shown to present discrepancies for low latitude stations in the geomagnetic latitudes plot, but on true magnetic latitude plots the points fall regularly along a smooth curve.

Anomalous features in the diurnal and seasonal variations of the F_2 layer critical frequency were evident from the earliest ionospheric observations at Washington (Kirby, Berkner, and Stuart 1934) and Slough (Appleton and Naismith 1935). Longitudinal differences in f_0F_2 were first noted by Ranzi (1939), who showed that noon f_0F_2 were higher at Rome (41.8° N.) than at Washington (38.7° N.). Similar differences in f_0F_2 were noted between Washington (38.7° N.) and Tokyo (35.7° N.) by Maeda, Uyeda, and Shinkawa (1942), and it was realized that the Washington values fitted well with the values at the Asian stations if plotted according to geomagnetic rather than geographic latitude. It was found (National Bureau of Standards, U.S.A. 1945) that the stations at Guam, Kwajalein Atoll, Christmas Island, and Huancayo, which were widely separated in geographic latitude and longitude, experienced similar diurnal variations of f_0F_2. This resulted from the fact that these stations were at nearly equal geomagnetic latitude. Appleton (1946) was first to find considerable anomalies in the F_2 layer at the equator, and expressed the opinion that better conformity could be achieved if the stations were arranged in accordance with geomagnetic latitude. A belt of low values of f_0F_2 circling the earth and centered roughly on the magnetic equator was also discovered. The geomagnetic distortion of f_0F_2 was further studied by Liang (1947), Bailey (1948), Lung (1949), Maeda, K. (1954), and Maeda, H. (1955) and they all confirmed the geomagnetic latitude control of f_0F_2 distributions.

The importance of true magnetic inclination in F_2 variations has been stressed by Rawer (1951). An effort was made by Burkard (1954) to examine the relative importance of geomagnetic latitude and magnetic inclination in the distribution of noon f_0F_2, but no significant difference could be found. Recently Rastogi (1959), while studying the influence of solar activity on the

[1]Manuscript received April 13, 1959.
Contribution from the Division of Radio and Electrical Engineering, National Research Council, Ottawa, Canada.
Issued as N.R.C. No. 5231.
[2]National Research Council Postdoctorate Fellow.

geomagnetic control of the critical frequencies for the F_1 and F_2 layers, showed that the latitudinal distribution of f_0F_2 indicated less scatter when plotted against magnetic rather than geomagnetic latitudes. However, during a discussion of the geomagnetic influences on the F_2 layer at the recent U.R.S.I. Conference at Boulder, Martyn (1959) has expressed the view that it is better to plot f_0F_2 with respect to the smoothed geomagnetic equator rather than the actual magnetic equator. In this note it is intended to show that the latitudinal distribution of noon f_0F_2 in low and middle latitudes is controlled by the true magnetic latitude and not by the idealized geomagnetic latitude.

Magnetic latitude μ as referred to in this paper was derived from the magnetic inclination I of the station according to the relation

$$\tan \mu = 1/2 \tan I,$$

which is analogous to the relation between geomagnetic latitude and geomagnetic inclination.

In Fig. 1 are compared the seasonal variations of f_0F_2 during the low sunspot years 1952 to 1954 at pairs of ionospheric stations having approximately

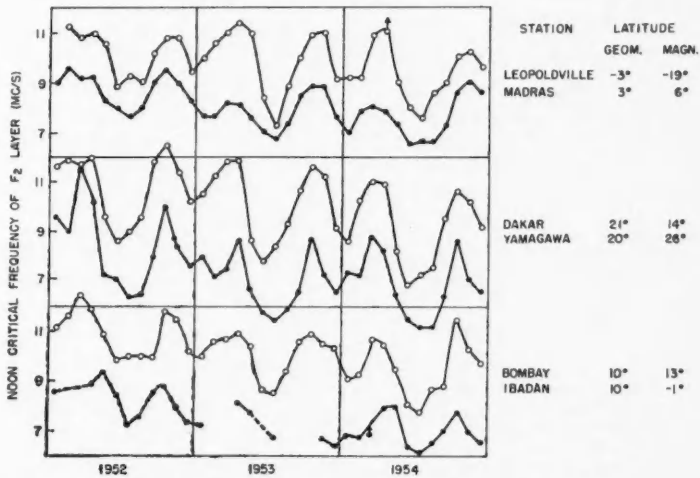

FIG. 1. Seasonal variations of the critical frequency of the F_2 layer during the years of low sunspot number (1952–1954) at pairs of ionospheric stations having same geomagnetic but different magnetic latitudes.

the same geomagnetic latitudes but different magnetic latitudes. The pairs of stations chosen and the corresponding latitudes are given below.

In Fig. 2 are shown the diurnal variations of f_0F_2 (averaged for the year 1954) at the pairs of stations Leopoldville–Madras and Bombay–Ibadan.

Comparing observations at Bombay and Ibadan (both having geomagnetic latitude, $\Phi = 10°$ N.), one finds that Bombay experienced much higher f_0F_2

Station	Latitude		
	Geographic, ϕ	Geomagnetic, Φ	Magnetic, μ
1. Leopoldville	4° S.	3° S.	19° S.
Madras	13° N.	3° N.	6° N.
2. Dakar	15° N.	21° N.	14° N.
Yamagawa	31° N.	20° N.	26° N.
3. Bombay	19° N.	10° N.	13° N.
Ibadan	8° N.	11° N.	1° S.

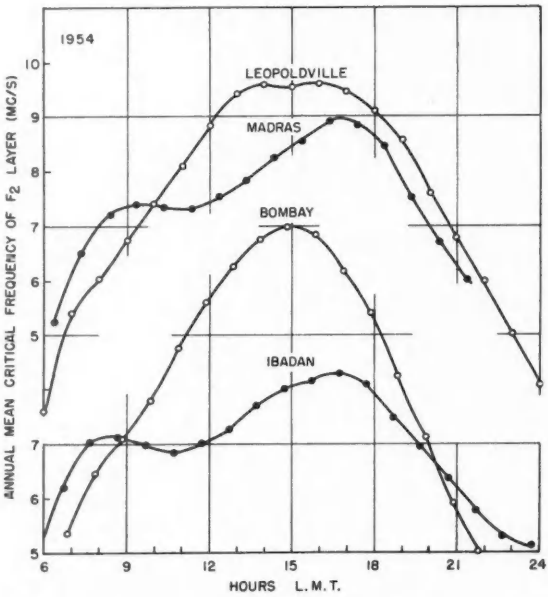

FIG. 2. Yearly average diurnal variations of the critical frequency of the F_2 layer at pairs of stations Leopoldville–Madras and Bombay–Ibadan. Note that the ordinate scales for the two pairs are shifted with each other.

than Ibadan. From a study of the ionosphere in the Asian Zone (Rastogi, unpublished) it was found that Bombay was very near the zone of f_0F_2 peak during these years, whereas the various ionospheric phenomena observed at Ibadan, specially the association of E_s with magnetic disturbances (Skinner and Wright 1957), justify listing Ibadan as an equatorial ionospheric station. Referring to Fig. 2 one finds that the diurnal variation of f_0F_2 at Ibadan had two maxima in the morning and evening hours, characteristic of any equatorial station. The diurnal variation of f_0F_2 at Bombay and Ibadan can be explained only in terms of the magnetic latitudes of these stations. The magnetic latitude of Bombay (13° N.) places it in the group of middle latitude stations and that of Ibadan (1° S.) justifies it as an equatorial station.

Comparing observations at Dakar ($\Phi = 21°$ N.) and Yamagawa ($\Phi = 20°$ N.) one finds that f_0F_2 at Dakar was much greater than at Yamagawa. The average values of f_0F_2 at Dakar were comparable with those at other stations, e.g. Ahmedabad, Formosa, Calcutta, or Bombay, occupying the peak region for f_0F_2. Yamagawa was well outside the anomalous belt at all times (Rastogi, unpublished). These features can be reconciled with the fact that the magnetic latitude of Yamagawa is 26° N. while that of Dakar is only 14° N.

In the top curve of Fig. 1 one notices that f_0F_2 values at Leopoldville were as high as at the middle latitude stations Bombay and Dakar. Further, the values of f_0F_2 at Leopoldville and Madras were much different, even though the geomagnetic latitudes of the two stations are the same. Referring to Fig. 2 one finds that diurnal variation of f_0F_2 at Madras had two maxima similar to that of Ibadan. The diurnal variation of f_0F_2 at Leopoldville showed only a single maximum, though the geomagnetic latitude of Leopoldville is only 3° S. The non-equatorial type of the diurnal variation and the high values of f_0F_2 at Leopoldville can be interpreted if one notices that the magnetic latitude of the station is 19° S., and then one expects f_0F_2 at Leopoldville to behave as at other middle latitude stations.

The latitudinal distribution of noon f_0F_2 during the low sunspot year of 1953–54 is now plotted against both geomagnetic and magnetic latitude for comparison. In Fig. 3 separate plots are given for three periods in the year: the northern solsticial months, May, June, July, and August 1953; the southern solsticial months November, December 1953 and January, February 1954; and the equinoctial months September, October 1953 and March, April 1954. The points corresponding to stations in three different zones, East, West and Intermediate, are plotted in different symbols.

A cursory glance of the figure shows that the points corresponding to low and middle latitude stations are much scattered in the geomagnetic latitude plots whereas these fall fairly along a smooth curve on magnetic latitude plots. The points most noticeably out of the smooth curve on geomagnetic plot correspond to Leopoldville, Lwiro, and Nairobi, Dakar, and Ibadan. The points for Leopoldville, Lwiro, and Nairobi represent the highest frequencies observed in the southern hemisphere but are very near to the geomagnetic equator. On the magnetic latitude plot these points are close to the region of peak f_0F_2. Similarly the point for Ibadan represents one of the lowest frequencies but on the geomagnetic latitude plot it lies at the region of northern f_0F_2 peak in any of the seasons. On the magnetic latitude plot the point corresponding to Ibadan occupies the region of minimum f_0F_2 and so low values of f_0F_2 at Ibadan are explained. Further, the point for Dakar lies far removed from the smooth curve on geomagnetic latitude plot. The points for stations Dakar ($\Phi = 20°$), Panama ($\Phi = 21°$), Mauii ($\Phi = 21°$), and Okinawa ($\Phi = 20°$) having about the same geomagnetic latitudes indicate the values of f_0F_2 differing by about 3 Mc/s. On the magnetic latitude plot all these points fall close to the smooth curve and the above discrepancies are removed.

These facts indicate that the latitude distribution of the noon values of

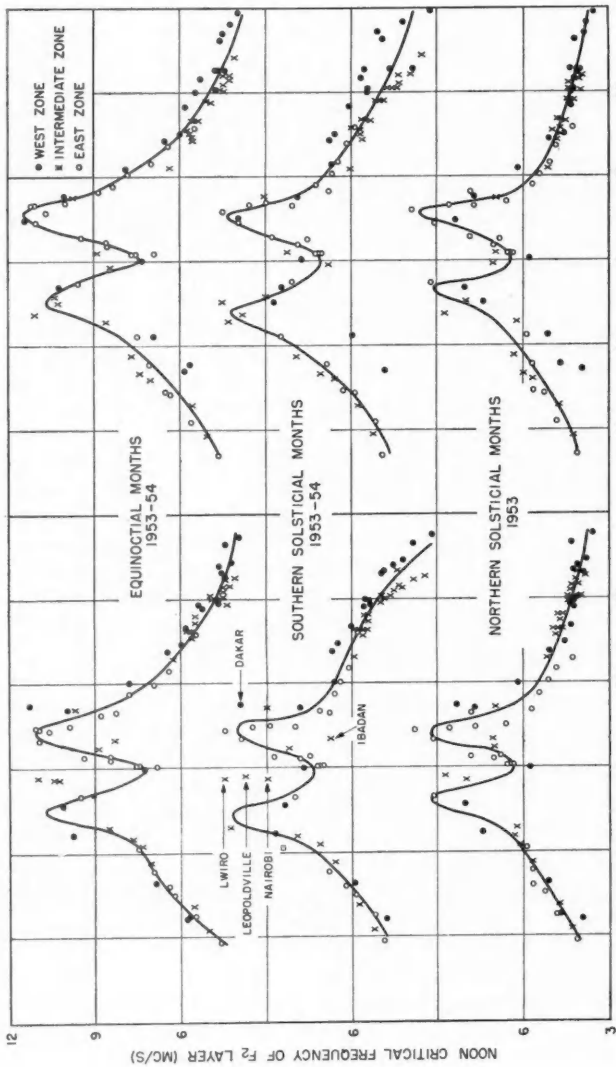

FIG. 3. The variations of the noon values of the critical frequency of the F_2 layer against the geomagnetic and magnetic latitudes, for the three seasons of a year of minimum sunspot number.

f_0F_2 within the anomalous equatorial belt may be controlled by the real magnetic latitude and not by the idealized geomagnetic latitude.

The latitudinal distribution of f_0F_2 at high northern latitudes does not show any comparative preference between geomagnetic and magnetic latitudes; the points are equally scattered on the two plots. Further, the points corresponding to the West Zone (North America) and Intermediate Zone (Europe) lie close to the smooth line in the summer months, but in the winter months these lie along two different smooth lines. In other words, stations in North America and Northern Europe having the same geomagnetic (or magnetic) latitude record the same f_0F_2 in summer, but during winter months f_0F_2 is greater at the American than at the European stations. It indicates that the factors predominantly controlling the F_2 ionizations at low latitudes may have comparatively less control at higher latitudes.

It may be noted that the points corresponding to southernmost stations of the West Zone lie fairly close to the smooth line in the geomagnetic latitude plot but are far from the line in the magnitude latitude plot. This may indicate a comparatively greater control of the geomagnetic than the magnetic latitude in the South American Zone. The abnormal features of the F_2 layer at the South American stations have been discussed by Rastogi in a separate paper. The low values of f_0F_2 at these stations are suggested due to the abnormal distribution of magnetic dip lines in that region.

ACKNOWLEDGMENTS

The author is thankful to Dr. B. Bonnet and Dr. N. J. Skinner for supplying him with the ionospheric data at the stations Lwiro and Ibadan respectively. The author would also like to express his appreciation to Dr. P. M. Millman for helpful discussions and suggestions.

REFERENCES

Appleton, E. V. 1946. Nature **157**, 691.
Appleton, E. V. and Naismith, R. 1935. Proc. Roy. Soc. A, **150**, 685.
Bailey, D. K. 1948. Terrestrial Magnetism and Atmospheric Elec. **53**, 41.
Burkard, O. 1954. Z. Geophys. **20**, 75.
Kirby, S. S., Berkner, L. V., and Stuart, D. M. 1934. Proc. Inst. Radio Engrs. **22**, 481.
Liang, P. H. 1947. Nature **160**, 642.
Lung, H. L. 1949. J. Geophys. Research, **54**, 177.
Maeda, K., Uyeda, H., and Shinkawa, H. 1942. Rept. Phys. Inst. Rad. Waves No. 2.
Maeda, K. 1954. Rept. Ionosphere Research Japan, **8**, 155.
Maeda, H. 1955. Rept. Ionosphere Research Japan, **9**, 59.
Martyn, D. F. 1958. Report of U.S.A. National Committee on International Scientific Radio Union Conference at Boulder.
National Bureau of Standards, U.S.A. 1945. I.R.P.L. Bulletin, F.6.
Ranzi, I. 1939. Ricerca sci. **10**, 926.
Rastogi, R. G. 1959. J. Atmospheric and Terrest. Phys. **14**, 31.
——— Unpublished.
Rawer, K. 1951. Proc. Second Meeting 1950. Mixed Comm. Ionosphere, 140.
Skinner, M. J. and Wright, R. W. 1957. Proc. Phys. Soc. (London) B, **70**, 833.

THE C–X SYSTEM OF N_2^+ [1]

P. K. CARROLL[2]

ABSTRACT

The $C\,^2\Sigma_u^+$–$X\,^2\Sigma_g^+$ system of N_2^+ has been investigated under high resolution in the region 1650–2000 Å. Fifteen bands of the system have been analyzed and accurate rotational constants and other data for the $C\,^2\Sigma_u^+$ state have been derived. Anomalies in the rotational and vibrational structure are discussed. Some evidence in favor of a predissociation between the levels $v = 2$ and $v = 3$ of the $C\,^2\Sigma_u^+$ state is presented.

I. INTRODUCTION

The $C \rightarrow X$ bands of N_2^+ form a fairly extensive system which stretches from about 1370 Å to 2070 Å. The system was discovered by Hopfield (1930) and later extended by Watson and Koontz (1934), who made a vibrational analysis and identified the lower state as the ground state of N_2^+. Setlow (1948) revised the vibrational scheme of Watson and Koontz and the correctness of the new analysis was verified by Miescher and Baer (1953) by means of the isotope effect. Setlow also made rotational analyses of a number of the bands and reported a marked anomaly in the B_v–v curve for the upper state, $C\,^2\Sigma_u^+$, at low v values. Wilkinson (1956), using much higher resolution, studied a number of bands arising from the levels $v' = 3$ and 4.

The system presents a number of features of interest. Apart from the anomalously large B values reported by Setlow for the lower vibrational levels in the upper state, there appears to be an irregularity in the vibrational structure as well. Furthermore, the intensity of the system is particularly sensitive to excitation conditions. In discharges through helium which contains a trace of nitrogen, the bands for $v' \geqslant 3$ appear very readily with great intensity. In discharges through pure nitrogen, however, the bands are difficult to excite and lower vibrational levels in the upper state are favored. It was originally believed that the enhancement of levels with $v' \geqslant 3$ in the helium discharge was due to collisions of the second kind between He^+ and nitrogen molecules in the ground state. Douglas (1952), however, suggested that an inverse predissociation could be responsible for the observed intensity distribution.

The work described below was undertaken with the following objects in view:

(1) To obtain accurate data on the rotational and vibrational structure of the $C\,^2\Sigma_u^+$ state. In Setlow's work the resolution used was insufficient to separate the P and R branches and this leads to uncertainty and inaccuracy in the analyses while Wilkinson has studied the levels $v = 3$ and 4 only. In

[1]Manuscript received April 8, 1959.
Contribution from the Division of Physics, National Research Council, Ottawa, Canada. Issued as N.R.C. No. 5242.

[2]Physics Department, University College, Dublin. National Research Council Postdoctorate Fellow 1953–55.

the present work attention was particularly focused on the bands with $v' < 3$ as these are difficult to excite and have been very inadequately studied. Extensive data for the lower state are available in the studies of Douglas (1952) and previous workers on the near ultraviolet bands of N_2^+.

(2) To prove or disprove the presence of irregularities in the vibrational and rotational structure, with particular reference to the bands of low v' values.

(3) To elucidate, if possible, the process by which selective excitation occurs in helium discharges. In particular a predissociation limit between the levels $v = 2$ and $v = 3$ of the $C\,^2\Sigma_u^+$ state was sought as this would confirm the Douglas theory of inverse predissociation at $v' = 3$.

II. EXPERIMENTAL

Three different sources were used in the experiments. The first source employed was a hollow cathode discharge tube with a cylindrical anode and a slot-shaped water-cooled aluminum cathode. When helium mixed with a trace of nitrogen was passed through this source, the bands with $v' \geqslant 3$ were excited with great intensity. Discharges were also run in this tube using pure nitrogen at low pressure. It was hoped that in this case the excitation of the $C\,^2\Sigma_u^+$ state would be due to electronic collisions so that a more normal intensity distribution than that obtained in the helium discharge would result. Bands of the system with $v' = 0$, 1, and 2 were in fact observed with this source, but the Lyman–Birge–Hopfield bands of N_2 also appeared with considerable intensity and partially masked the N_2^+ bands. In an attempt to get higher excitation a hollow cathode of the type described by Naudé and Hugo (1953) was employed. In this tube a thin-walled iron cathode is mounted in the center of a large glass bulb and by varying the current through the tube the temperature of the cathode can be controlled. It was found that as the temperature of the cathode rose, the pressure necessary to maintain the discharge decreased, while the degree of excitation of the nitrogen increased. The condition most favorable for the excitation of N_2^+ spectra was reached at the stage when the cathode was just beginning to glow. At lower temperatures, bands of neutral nitrogen were enhanced whereas, if the cathode became red hot and if the pressure decreased, the discharge became white and omitted the spectrum of atomic nitrogen. The third source investigated was a mildly condensed discharge through pure nitrogen at low pressure. This source gave spectra rather similar to that given by the hot cathode discharge described above, i.e., the $C \rightarrow X$ bands appeared in moderate strength while the spectrum of neutral nitrogen molecule was largely absent.

The spectra were investigated in the third and fourth orders of the 3-meter vacuum spectrograph in the National Research Council of Canada. The optical arrangement described by Herzberg (1956) was used to eliminate the lower unwanted orders. Wavelengths were measured in the usual way against second-order iron arc lines. Comparisons made between different plates suggest that within a given set of measurements the wave numbers of lines are correct to about 0.08 cm^{-1}. Between one set of measurements and another, however, approximately constant differences of as much as 0.20 cm^{-1} have

been observed so that in absolute magnitude the wave numbers of lines may be in error by this amount. On the best plates, lines of equal intensity separated by more than 0.30 cm^{-1} were clearly resolved, indicating a resolving power of about 170,000. Lines as close together as about 0.18 cm^{-1}, although not fully resolved, could be identified as two distinct features and were measured as such.

III. RESULTS

In all, the fine structure of 15 bands was studied. These bands were, in order of decreasing wavelength: 3–10, 4–11, 5–12, 6–13, 0–6, 1–7, 2–8, 3–9, 4–10, 5–11, 6–12, 1–6, 2–7, 3–5, and 0–2. The analyses of the bands are given in Table I.

Table I includes data on four of the bands studied by Wilkinson (1956). Apart from the general desirability of having a set of homogeneous measurements on a band system, there are other reasons for including the new measurements of these bands. In the first place, over the region of the 3–10 and 4–11 bands, the new measurements differ from Wilkinson's by an amount varying from about 0.60 cm^{-1} at 50,500 cm^{-1} to 1.10 cm^{-1} at 50,200 cm^{-1}; the present measurements are believed to be correct to within the limits mentioned above. Furthermore, Wilkinson's analysis of the 4–10 band seems to be incorrect. Finally the resolution in the present work appears to be about twice

TABLE I

Wave numbers of the lines in the $C\,^2\Sigma - X\,^2\Sigma$ bands of N_2^+ (cm^{-1})

	0–2 band		0–6 band		1–6 band		1–7 band		2–7 band		2–8 band	
N	*R*(*N*)	*P*(*N*)	*R*(*N*)	*P*(*N*)	*R*(*N*)	*P*(*N*)	*R*(*N*)	*P*(*N*)	*R*(*N*)	*P*(*N*)	*R*(*N*)	*P*(*N*)
0									54093.93			
1										54087.31	52154.47	52145.68
2	60232.12	60217.10	51993.70	51978.50		54029.44			98.12	83.19	56.48	41.49
3	32.81	11.73		73.69		24.72	52068.04		99.61	78.36	57.93	36.84
4	32.81	05.75	95.57	68.34	54046.61	19.40	69.94	52043.63	54100.24	73.22	58.67	31.72
5	32.12	60199.02	95.57	62.29	46.61	13.67	70.93	37.79	00.48	67.46	59.17	26.10
6	30.71	91.56	95.00	55.74	46.01	06.86	70.93	31.52	00.24	61.01	59.17	19.94
7	28.38	83.36	93.90	48.58	44.75	53999.64	69.94	24.86	54099.15	54.05	58.67	13.37
8	25.55	74.25	92.15	40.84	43.14	91.93	68.50	17.21	97.66	46.61	57.22	06.21
9	21.83	64.40	90.01	32.56	40.73	83.52	66.54	09.09	95.65	38.40	55.52	52098.40
10	17.39	54.03	87.07	23.62	37.93	74.63	64.04	00.66	92.92	29.84	53.38	90.17
11	12.16	42.78	83.58	14.14	34.51	64.97	60.94	51991.48	89.81	20.68	50.59	81.47
12	06.22	30.76	79.38	04.07	30.45	54.89	57.39	81.86	85.97	10.90	47.32	72.16
13	60199.50	18.12	74.77	51893.36	25.47	44.12	53.31	71.59	81.69	00.74	43.52	62.46
14	92.05	04.68	69.77	82.13	20.30	32.84	48.46	60.97	76.82	53989.77	39.17	52.09
15	84.01	60090.41		70.31	14.40	21.06	43.25	49.64	71.27	78.21	34.37	41.30
16	75.20	75.45	57.74	57.94	08.01	08.41	37.34	37.84	65.50	66.32	29.14	29.92
17	65.57	59.87		44.96	00.74	53895.48	30.89	25.31	58.93	53.81	23.20	18.04
18	55.20	43.51	43.21	31.63	53993.21	81.74	23.87	12.51	51.79	40.87	16.84	05.82
19	44.04	26.36			85.03	67.51	16.53	51899.08	44.24	27.30	09.99	51992.95
20	32.30	08.63	26.14		76.19	52.69	08.57	85.10	35.92	13.00	02.52	79.56
21	19.79	59990.15			66.67	37.45	00.08	70.49	26.88	53898.15	52094.46	65.66
22	06.40	70.75			56.97	21.51	51991.00	55.52	18.00*	82.80	86.41*	51.19
23	60092.60				46.33	04.92		39.94	08.01	66.64	77.35	36.21
24		29.97			35.21	53787.80		23.74	53997.79	50.82*	67.84	21.11*
25					23.55	70.13		06.99	86.40	33.79	57.71	05.03
26					11.02	51.80			75.13	16.33	47.52	51888.66
27					53898.15	32.80			62.69	53798.29		71.73
28					84.83	13.53			50.45	79.75		54.31
29					71.47	53693.62			37.33	60.70		36.43
30					57.65	73.40			23.55	41.10		18.00
31					43.79					20.79		
32										53699.70		

*Perturbed.

TABLE I (*Concluded*)

	3–5 band		3–9 band		3–10 band	
N	$R(N)$	$P(N)$	$R(N)$	$P(N)$	$R(N)$	$P(N)$
2		60072.66		52238.79	50382.04	50366.96
3				34.42	83.79	62.61
4	60088.74	61.89		29.44	84.78	57.83
5	88.43	55.57		24.06	85.44	52.67
6	87.46	48.64		17.91	85.66	46.75
7	85.81	40.97	52256.25	11.45	85.44	40.52
8	83.65	32.72	55.30	04.52	84.78	34.00
9	80.83	23.86	53.97	52197.01	83.79	26.85
10	77.23	14.33	51.97	89.02	82.31	19.35
11	72.84	04.25	49.56	80.75	80.30	11.53
12	68.04	59993.27	46.63	71.80	77.87	03.05
13	62.42	81.69	43.14	62.38	74.90	50294.17
14	56.33	69.59	39.27	52.46	71.63	84.89
15	49.45	56.76	34.78	42.08	67.79	75.11
16	41.96	43.27	29.92†	31.23	63.66	64.91
					63.45*	
17	33.80	29.16	24.57†	19.84	58.93	54.29
	33.57*				58.60*	
18	25.10	14.35	18.74	08.15	53.85	43.20
				07.85*		42.96*
19	15.57	59899.05	12.33	52095.82	48.20	31.69
		98.78*		95.48*		31.32*
20	05.48	83.05	05.47	82.98	42.20	19.74
21	59994.73	66.34	52198.08	69.67	35.75	07.31
22	83.28	48.98	90.28	55.90	28.82	50194.44
23	71.33	30.98	81.94	41.64	21.45	81.15
24	58.55	12.30	73.20	26.92	13.77	67.42
					13.58	
25	45.43	59793.12	63.92	11.76	05.61	53.29
					05.43	
26	31.36	73.34	54.17	51996.15	50297.20	38.79
					96.78	38.61
27	16.65	52.68	44.07	79.85	87.86	23.73
					87.66	23.54
28	01.58	31.64	33.28	63.53	78.34	08.35
				63.26	78.13	08.17
29	59885.70	09.83	22.09	46.38	68.48	50092.58
				46.18	68.22	92.31
30	69.22	59687.40	10.64	28.91	58.08	76.28
			10.43	28.63	57.87	76.03
31		64.39	52098.56	10.93		59.61
			98.35	10.69		59.38
32	34.41	40.58	86.05	51892.49		42.46
			85.82	92.27		42.20
33		16.47	73.06	73.56		24.69
				73.25		
34		59591.46	59.62	54.32		06.90
			59.20	53.98		06.70
35			45.61	34.37		
			45.40	33.89		
36			31.44	14.13		
			30.95	13.82		
37				51793.45		
				92.97		
38				71.93		

	4–1 band		4–11 band		5–11 band		5–12 band		6–12 band		6–13 band	
N	$R(N)$	$P(N)$	$R(N)$	$P(N)$	$R(N)$	$P(N)$	$R(N)$	$P(N)$	$R(N)$	$P(N)$	$R(N)$	$P(N)$
0					52462.41		50661.55					
1	52355.61	52346.81		50509.82	65.02		64.04	50655.16				50803.15
2	57.70	42.80		06.03	66.91	52452.27	66.08	51.44				50799.48
3	59.27	38.41		01.79	68.55	47.91	68.04	47.24		52560.18		95.30
4	60.33	33.55		50497.14	70.00	43.18	69.15	42.67	52581.74	55.42		90.97
5	60.90	28.18	50524.86	92.03	70.75	38.01	70.25	37.66	82.54	50.38		86.08
6	61.12	22.45	25.27	86.53	70.75	32.35	70.89	32.22	83.03	44.80		80.86
7	60.90	16.19	25.27	80.58	70.75	26.27	70.89	26.50	83.03	38.92	50819.09	75.15
8	60.00	09.44	24.86	74.21	70.00	19.73	70.62	20.40	82.54	32.58	19.09	69.26
9	58.84	02.23	24.07	67.43	69.08	12.83	69.95	13.72	81.74	25.80	18.61	62.88
10	57.07	52294.67	22.72	60.15	67.53	05.38	68.84	06.69	80.40	18.68	17.75	56.16
11	55.14	86.50	21.02	52.48	65.62	52397.54	67.30	50599.33	78.73	11.06	16.57	49.03
12	52.26	77.83	18.84	44.43	63.19	89.17	65.45	91.57	76.51	03.03	14.92	41.53
13	49.15	68.76	16.28	35.90	60.36	80.51	63.19	83.38	73.98	52494.64	12.93	33.67
14	45.52	59.28	13.24	26.94	57.04	71.36	60.53	74.80	70.92	85.73	10.57	25.46
15	41.49	49.50	09.82	17.57	53.36	61.68	57.46	65.86	67.54	76.46	07.89	16.82
16	36.97	38.82	06.03	07.80	49.20	51.63	54.11	56.54	63.73	66.90	04.70	07.89
17	31.90	27.85	01.79	50397.61	44.57		50.10	46.74	59.50		01.20	50698.49
18	26.53	16.48	50497.14	87.04	39.52	30.22	45.91	36.57	54.81	46.28	50797.33	88.76
19	20.51		92.03	75.96	34.09	18.84	41.25	26.03	49.70	35.27	93.04	78.65
20	14.22	52192.36	86.53	64.51	28.18		36.20	15.18	44.16	23.96	88.44	68.06
21	07.30	79.60	80.58	52.67	21.94	52294.78	30.79	03.99	38.36	12.21	83.54	57.14
22	00.12	66.40	74.21	40.52	15.07	82.23	24.96	50492.04	32.07	00.09	78.21	45.96
23	52292.30	52.70	67.43	27.73	07.77	69.24	18.77	79.96	24.80*	52387.72	71.94*	34.27
24	84.00	38.61	60.15	14.59	00.09		12.02	67.48	18.09‡		66.38‡	
25		23.97	52.48		52392.08	41.81	05.18	54.71	10.58‡		59.93‡	
26		08.95	44.43		83.71	27.20	50597.90	41.38			53.13‡	
27		52093.30			74.65			27.75			45.86‡	
28								13.78			38.50‡	
29								50399.54			30.60‡	
30											22.31‡	

*Perturbed.
†Perturbation not detected due to blending of P and R lines.
‡Probable continuation of R branch. Identification somewhat doubtful due to presence of perturbation.

that attained by Wilkinson. As a result of this, not only is there less blending of lines but there is also a partial resolution of the spin fine structure at higher N values of the 3–9 and 3–10 bands and in these bands, a small perturbation can be detected (see below).

Transitions from the levels $v' \geqslant 3$ were analyzed from plates taken with the helium–nitrogen discharge. A typical spectrogram taken with this source is reproduced in Fig. 1(*a*). On this and on similar spectrograms, transitions from the levels $v' = 2$ and 1 are extremely weak. Curiously enough, however, transitions from $v' = 0$ occur with moderate strength and it was in fact from plates taken with the helium–nitrogen source that the 0–2 and 0–6 bands were measured. The effect is illustrated in Fig. 2, which shows the 0–2 band appearing with an intensity comparable to that of the adjacent 3–5 band while the 1–3 and 2–4 bands are completely absent. Presumably this intensity distribution is due to the fact that the 3–5 band, which has a small transition probability according to the Franck–Condon principle, is enhanced by the excitation conditions while the 0–2 band, although not favored by the excitation conditions, has a large transition probability.

A comparison of Fig. 1 and Fig. 2 illustrates another interesting feature of the system. Whereas at longer wavelengths, for the $\Delta v = -8$, -7, -6, and -5 sequences, the vibrational structure of the system degrades in the wrong direction, i.e., in the sense opposite to the rotational structure, at shorter wavelengths, as for instance for the $\Delta v = -2$ sequence shown in Fig. 2, the vibrational structure and rotational structure degrade in the same direction. At the intermediate stage, particularly in the $\Delta v = -3$ sequence, the heads of the bands almost coincide resulting in a crowded and complex structure.

Apart from the 0–6 and 0–2 bands the other transitions for $v' < 3$ were analyzed from plates taken with the hollow cathode discharge through pure N_2. A typical spectrogram obtained from this source is reproduced in Fig. 1(*b*), which shows the 1–7 and 2–8 bands.

IV. MOLECULAR CONSTANTS

The band origins and rotational constants were derived by the usual graphical methods and the results are shown in Table II. The bands were chosen in such a way that each vibrational level in the upper state from $v = 0$ to $v = 6$ was studied at least twice. In this way the correctness of the analyses could be checked and more accurate B values obtained. Table III gives the mean values of B for the upper state from $v = 0$ to $v = 6$. Here it should be pointed out that the accuracy and the extent of the data vary from band to band. In preparing Table III, therefore, extra weight was given to B values which were considered more reliable. Figure 4 shows a plot of B against v for the $C\,^2\Sigma_u^+$ state based on the data in Table III. It is seen that over the whole range of v investigated, the curve is non-linear with the departure from linearity being most pronounced at low v values. It is of interest to note that the dependence of B on v is quite different from that given by Setlow (1948), according to whom the B values increase rapidly with decreasing v reaching the value 1.62 cm^{-1} for $v = 0$.

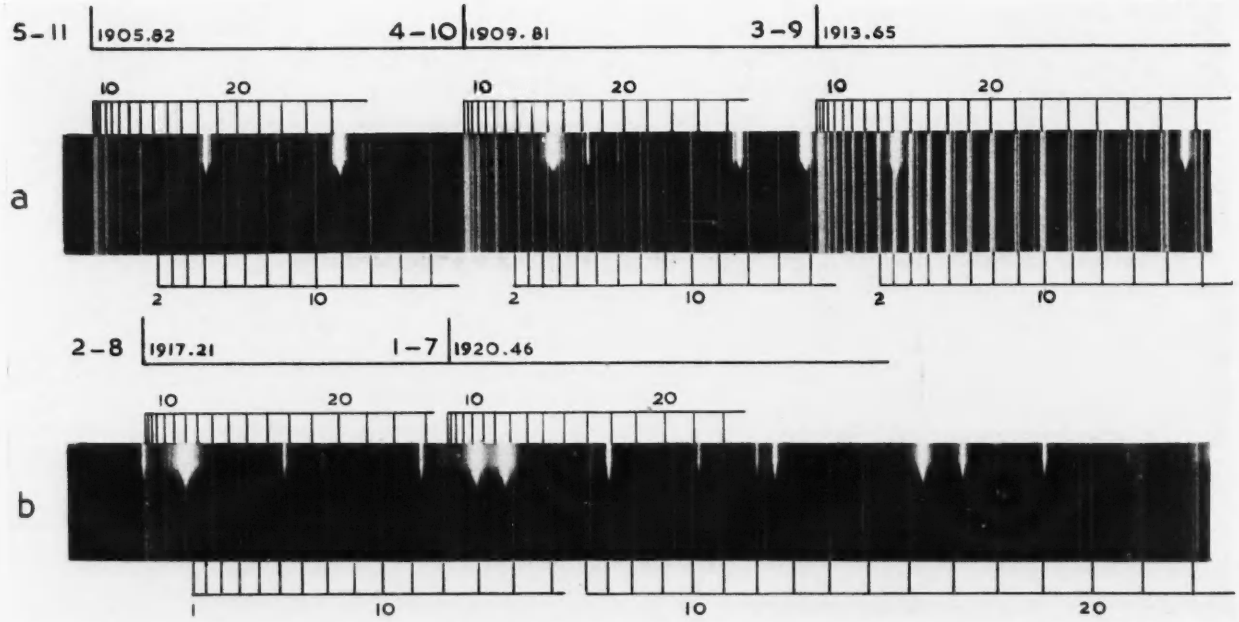

FIG. 1. (*a*) The 5–11 band, 4–10 band, and part of the 3–9 band as observed using a hollow cathode discharge through helium containing a trace of N_2.
(*b*) The 2–8 and 1–7 bands observed in the hot hollow cathode source using pure N_2.
Here and in Fig. 2, the *R* and *P* branches are indicated by the leading lines above and below the spectrogram respectively.

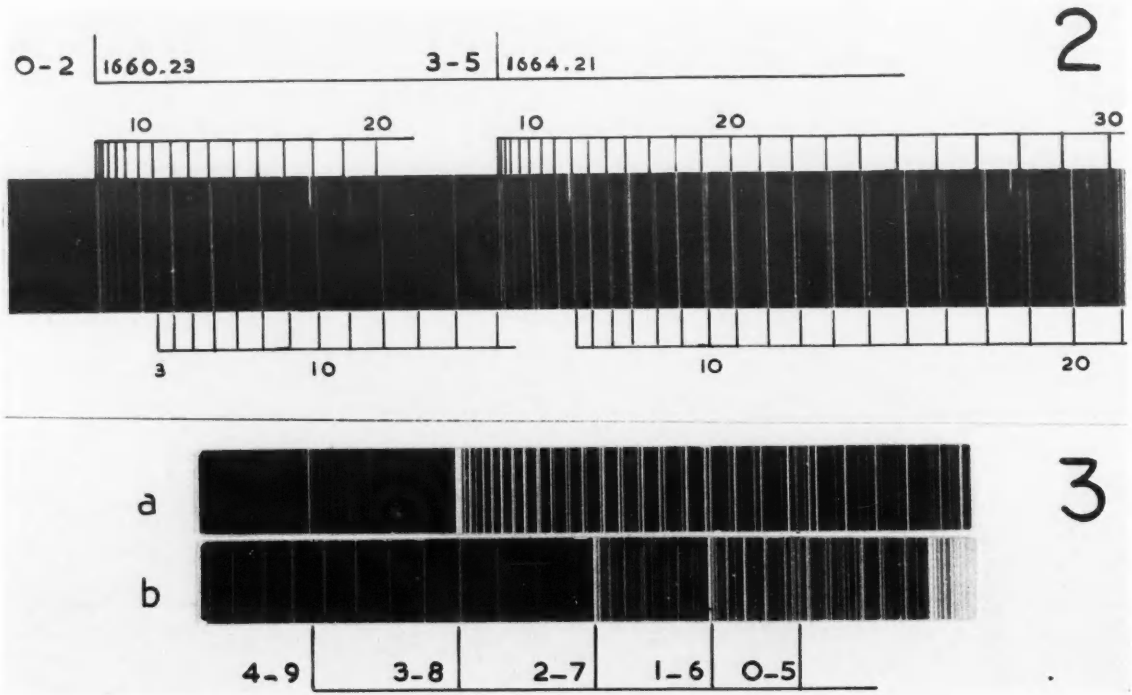

FIG. 2. The 0–2 and 3–5 bands of the $C \rightarrow X$ system. Source as in Fig. 1(*a*).

FIG. 3. The $\Delta v = -5$ sequence of the $C \rightarrow X$ system as observed (*a*) with the helium–nitrogen source and (*b*) with the cold hollow cathode discharge through pure N_2. The strong structure to the right of the 2–7 band in (*b*) is part of the 2–8 band of the Lyman–Birge–Hopfield system.

TABLE II

Band constants (cm^{-1})

v'–v''	B'	B''	ν_0
3–10	1.496_7	1.723_9	50374.1_8
4–11	1.490_3	1.703_8	50513.4_2
5–12	1.479_8	1.681_5	50658.5_0
6–13	1.468_8	1.658_2	50806.3_2
0–6	1.511	1.806	51986.3_0
1–7	1.512_2	1.788_1	52061.2_6
2–8	1.504_3	1.765_7	52148.9_9
3–9	1.497_2	1.745_2	52246.2_2
4–10	1.489_1	1.724_1	52350.1_6
5–11	1.481_1	1.704_5	52459.5_2
6–12	1.470_3	1.683_3	52571.4_8
1–6	1.508_8	1.805_4	54037.3_6
2–7	1.502_7	1.785_7	54090.9_1
3–5	1.497_0	1.825_2	60080.2_9
0–2	1.509	1.883	60225.0_0

Average $D' = 4.0\times10^{-6}$
Average $D'' = 6.1\times10^{-6}$

TABLE III

Data for state $C\,^2\Sigma$

v	0	1	2	3	4	5	6
B	1.509_8	1.509_6	1.503_5	1.4970	1.489_8	1.480_4	1.470_0
$\Delta G(v+\frac{1}{2})$	2051.1	2029.7	2004.3	1976.0	1946.1	1913.0	

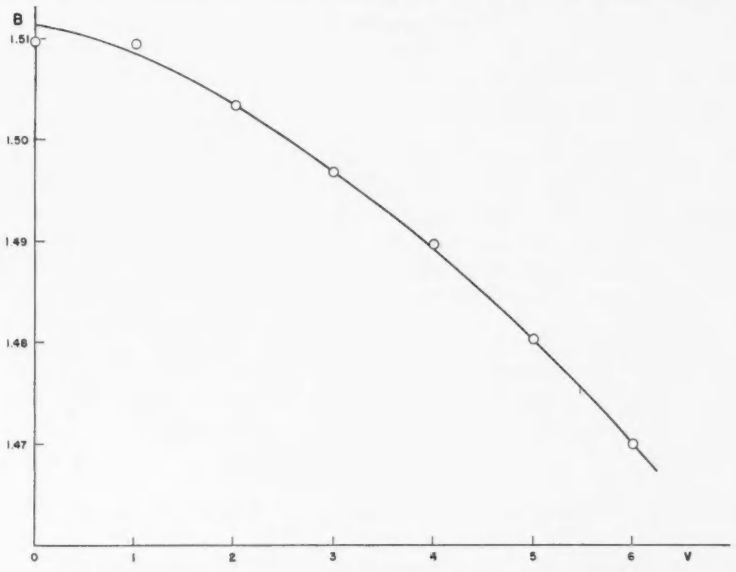

FIG. 4. The variation of B with v in the $C\,^2\Sigma$ state. The shape of the curve for $v < 2$ is somewhat uncertain. Clearly the curve could be made to pass through the point B_1, in which case B_0 would be considerably removed from its extrapolated position. Unfortunately B_1 is not known with sufficient accuracy to determine the course of the curve definitely.

Table III also gives the vibrational intervals in the $C\,^2\Sigma$ state. These have been obtained from the band origins and are believed to be correct to about 0.30 cm^{-1}. As in the case of the B values, the dependence of $\Delta G(v+\frac{1}{2})$ on v is non-linear over the whole range investigated. A graph of $\Delta G(v+\frac{1}{2})$ against v gives a curve which is qualitatively very similar to the B_v versus v curve. In this case the curvature is again most pronounced at low v values. Because of this, it is not possible to represent the vibrational levels in the $C\,^2\Sigma$ state by the orthodox vibrational formula. Furthermore, it is not possible to determine an accurate value of ν_e. However, one can derive the approximate value 64,628 cm^{-1} which should not be in error by more than ± 2 cm^{-1}. An accurate value of ν_{00} can of course be obtained by combining the present results with the known data for the ground state of N_2^+. The value obtained is

$$\nu_{00} = 64{,}542.0 \text{ cm}^{-1}.$$

V. ROTATIONAL PERTURBATIONS

Three small but definite perturbations are observed in the rotational structure of the bands. The most obvious of these occurs in the level $v = 3$ of the $C\,^2\Sigma$ state. It has been mentioned that only at higher N values (> 24) is it possible to detect a partial resolution of the doublet structure of the P and R branches. Nevertheless in the 3–10 band the $R(16)$ and $P(18)$ lines obviously consist of two incompletely resolved components while $R(17)$ and $P(19)$ each consist of two distinct lines. The effect is also observed in the P branch of the 3–9 band; it is not detected in the R branch due to the blending of lines. It is present in the 3–5 band also but here the effect is less noticeable due to the decrease in resolution at the shorter wavelengths.

It is obvious that the appearance of spin structure is due to an increase in the splitting of the levels $N = 17$ and $N = 18$ in $v = 3$ of the $C\,^2\Sigma$ state. The average value of the observed splitting is 0.21 cm^{-1} for the lines arising from $N = 17$ and 0.31 cm^{-1} for the lines from $N = 18$. The higher-frequency members of the doublets fit smoothly into their appropriate P and R series; clearly therefore only one component of the spin doubling in the state $C\,^2\Sigma_u^+$ is affected. One would normally attribute such a perturbation to a $^2\Pi_u$ state. Only one such state is known for N_2^+, namely the upper state, $A\,^2\Pi_u$, of the Meinel infrared bands. This state, however, very probably converges to the limit $N(^4S)+N^+(^3P)$ at 70,358 cm^{-1} and if this is so, it cannot be responsible for the perturbation in $C\,^2\Sigma$ which is observed at 71,084 cm^{-1}. Furthermore, according to Mulliken (private communication), no other $^2\Pi_u$ state is expected theoretically in this energy region. However, the configuration

$$KK(\sigma_g 2s)^2(\sigma_u 2s)(\pi_u 2p)(\sigma_g 2p)(\pi_g 2p),$$

which produces the $C\,^2\Sigma_u^+$ state, also gives rise to a $^2\Sigma_u^-$ state and this may well be responsible for the observed perturbation. A consideration of the selection rules shows that in this case only one spin component of the $C\,^2\Sigma$ state will be affected.

A second perturbation is observed in the level $v = 2$ at $N = 23$. It is found that the $P(24)$ and $R(22)$ lines in the 2–7 and 2–8 bands are displaced to higher

energies by about 0.30 cm^{-1}. The perturbation may also effect transitions from higher N levels, but the effect is smaller and its detection less certain. In contrast to the perturbation in $v = 3$, no spin splitting is observed in the present case so that both spin components of the upper state must be equally displaced. A similar perturbation is found at $N = 24$ in the level $v = 6$. Again both spin components are affected and in this case the level is shifted to lower energies by about 0.40 cm^{-1}. These perturbations could be due to the states $^4\Sigma_u^-$ or $^2\Delta_u$ (case b) which arise from the same electron configuration as $C\,^2\Sigma_u^+$ and which should lie at about the same energy. It is also possible that the perturbation in $v = 2$ is due to some high levels in the $B\,^2\Sigma$ state.

VI. VIBRATIONAL STRUCTURE OF THE $C\,^2\Sigma$ STATE

The band measurements given by Watson and Koontz (1934) and Tanaka (1953) cannot all be represented by a vibrational formula of the usual kind. In particular if one uses a formula which represents the higher levels of the $C\,^2\Sigma$ state satisfactorily, it leads to considerable error for the levels $v = 0$, 1, and 2. Setlow (1948) believed that rotational perturbations were produced in these lower levels by a $^2\Pi$ state and that this effect, combined with the limited accuracy of the available measurements, could account for the observed anomaly. As stated in Section IV, however, the data based on band origins leave no doubt that the $\Delta G(v+\frac{1}{2})$ versus v curve is abnormally shaped. The curve shows that the vibrational intervals at lower v values are smaller than predicted by an extrapolation of the intervals at higher v values. If we consider this effect as being due to a perturbation, it would correspond to an upward shift of the lower levels from their original unperturbed positions. The shift falls off rapidly, but smoothly, with increasing v; there is no indication of a discontinuity at $v = 3$ as mentioned by some of the earlier workers.

The variation of B with v, described above and shown in Fig. 4, can be correlated directly with the anomalous vibrational structure. It is particularly interesting to note that the B versus v and $\Delta G(v+\frac{1}{2})$ versus v curves follow the same pattern, such that where the vibrational intervals are abnormally small the B values are also abnormally small. This is a feature of vibrational perturbations and occurs for example in the upper state of the AgH bands (see Bengtsson and Olsson 1931; Gerö and Schmid 1943) and in the $B\,^2\Sigma$ state of N_2^+ (Douglas 1952).

Douglas (1952) has interpreted the unusual shape of the ΔG curve for the $B\,^2\Sigma$ state in terms of an interaction between the potential curves for the $B\,^2\Sigma$ and $C\,^2\Sigma$ states. He suggested that the interaction was such that a repulsion takes place between the two curves leading to a decrease in the equilibrium internuclear distance for the $C\,^2\Sigma$ state. At the time this appeared to be supported by the large B_0 value given by Setlow (1948). We know now that in fact the B_0 value is abnormally small. But this does not invalidate Douglas's suggestion. It may well be that the repulsion between $B\,^2\Sigma$ and $C\,^2\Sigma$ is such that upward displacement of the lower part of the $C\,^2\Sigma$ state is much more pronounced than any lateral displacement of the potential minimum. This could lead to anomalies in the vibrational and rotational structure of the kind described above.

VII. PREDISSOCIATION

When the system is observed in helium–nitrogen discharges, the level $v' = 3$ is excited with great intensity. Higher vibrational levels are also excited, but to an extent that falls off fairly rapidly with increasing v'. Bands with $v' < 3$ are absent or weak. It was suggested by Watson and Koontz (1934) that this curious intensity distribution was due to resonance excitation of N_2^+ in collisions between ionized helium atoms and nitrogen molecules in the ground state. There are, however, objections to this theory. In the first place Tanaka (1953) has pointed out that in this process maximum excitation should occur at $v' = 4$ and not at $v' = 3$ as observed. In the second place it is difficult to see how levels as high as $v' = 9$ and 10 can be excited as they lie considerably above the ionization potential of helium.

Douglas (1952) has proposed that the intensity distribution in the helium discharge should be attributed to an inverse predissociation from a state arising at the dissociation limit $N(^4S)+N^+(^3P)$. In this process, energy considerations show that the level $v = 3$ should be preferentially excited. The extra energy required to excite the higher vibrational levels could be supplied by the relative kinetic energy of the ^4S atom and ^3P ion as they approach along the potential curve of the repulsive state. The process of inverse predissociation would be expected to be important in discharges such as the helium–nitrogen discharge where it is very likely that a large number of nitrogen atoms and atomic ions is present. On the other hand, as pointed out by Douglas, if the C state is excited directly by electron collisions and if the density of atoms and atomic ions is small, one would expect a decrease in the intensity of the bands due to predissociation to be observed at $v' = 3$. It was hoped that in present work the spectra taken with the hollow cathode discharge through pure nitrogen would provide some definite evidence on this point. In particular a breaking off in the rotational structure of bands from the level $v' = 2$ was sought as this would settle the question decisively. However, the branches in the 2–7 and 2–8 bands appeared to behave in a normal way without any sudden breaking off or drop in intensity. This of course does not mean that predissociation is absent because it could well occur above the point at which the branches fade in the normal way. The highest rotational level observed was $N = 31$, which is about 517 cm^{-1} below $N = 0$ of $v' = 3$ and it is quite possible for predissociation to occur above this point. In fact, from the appearance of the vibrational structure of the bands, it is highly likely that this is the case. Thus Fig. 3 shows, side by side, spectra of the $\Delta v = -5$ sequence taken with the helium–nitrogen discharge and the cold, hollow cathode discharge through pure nitrogen. In the latter case it is clearly seen that bands with $v' = 2$, 1, and 0 are well developed while only a faint trace of bands with $v' > 2$ can be detected. It is very difficult to interpret this behavior in any way other than in terms of a predissociation.

It is evident that the predissociation must be a weak one. The fact that the bands with $v' \geqslant 3$ appear strongly in the helium discharge suggests that the lifetime with respect to predissociation must be at least of the same order as the lifetime with respect to radiation. Further evidence that the predissociation

is weak is provided by the fact that in direct electronic excitation the bands with $v' \geqslant 3$ still appear, although very feebly.

The configuration $N(^4S)+N^+(^3P)$ gives rise to 12 states of species Σ_g^+, Σ_u^+, Π_g, and Π_u each of which can occur as doublets, quartets, and sextets. Of these $^2\Sigma_u^+$ and $^2\Sigma_g^+$ are undoubtedly the upper and lower states respectively of the first negative bands, while the $^2\Pi_u$ state is very probably the upper state of the Meinel bands. Bearing in mind that g states cannot predissociate u states and that predissociation of a doublet state by a sextet state would be much more strongly forbidden than by a quartet state, we are led to the conclusion that the predissociating state is probably $^4\Sigma_u^+$ or $^4\Pi_u$. According to Mulliken (private communication) the $^4\Sigma_u^+$ state should be stable and lie 1 to 2 volts below the $C\,^2\Sigma$ state. We therefore conclude that the state responsible for the predissociation is very probably $^4\Pi_u$. Thus it is seen theoretically that a predissociation of state $C\,^2\Sigma$ must be a forbidden one—which is at least consistent with the experimental observation that it is weak.

I am very grateful to Dr. G. Herzberg and Dr. A. E. Douglas for their valuable advice and suggestions in the course of this problem, and to Professor R. S. Mulliken for providing important information on the electronic structure of N_2^+. I am also indebted to Professor T. E. Nevin for his interest in the work and for reading the manuscript and to Sister Cabrini for her assistance in the measurement and analysis of several of the bands. Finally I should like to thank Mr. J. Shoosmith for his expert help in photographing the spectra.

REFERENCES

BENGTSSON, E. and OLSSON, E. 1931. Z. Physik, **72**, 163.
DOUGLAS, A. E. 1952. Can. J. Phys. **30**, 302.
GERŐ, L. and SCHMID, R. 1943. Z. Physik, **121**, 459.
HERZBERG, G. 1956. Proc. Roy. Soc. A, **234**, 516.
HOPFIELD, J. J. 1930. Phys. Rev. **36**, 789.
MIESCHER, R. and BAER, P. 1953. Helv. Phys. Acta, **26**, 91.
NAUDÉ, S. M. and HUGO, T. J. 1953. Can. J. Phys. **31**, 1106.
SETLOW, R. B. 1948. Phys. Rev. **74**, 153.
TANAKA, Y. 1953. J. Chem. Phys. **21**, 1402.
WATSON, W. W. and KOONTZ, P. G. 1934. Phys. Rev. **46**, 32.
WILKINSON, P. G. 1956. Can. J. Phys. **34**, 250.

NOTES

ON MAINTAINING AN OBJECT AT A UNIFORM TEMPERATURE

C. M. Carmichael and A. D. Misener

INTRODUCTION

When it is desirable to maintain an object at a constant temperature and without temperature gradients in the object itself, one common practice is to suspend it in a uniformly heated enclosure. If high precision is required, particularly with respect to the absence of temperature gradients in the object, considerable attention must be paid to the uniformity of the temperature of the enclosure as well as its constancy. We have undertaken to test experimentally what external conditions are necessary to maintain a temperature uniform to within 0.003° C over metal objects of reasonable size.

Interest in this problem was aroused by the work of Thompson (1956) in developing a new pendulum apparatus for determining the relative acceleration of gravity. By placing his penduli in a thick-walled, insulated, and heated metal case he could maintain their average temperature constant to the required ±0.01° C, but there was a gradient of 0.05° C along their length and their average temperature was about 0.08° C below the average of the case as read by 20 thermistors placed symmetrically over its inner surface.

Two types of experiment were performed. In the first type the objective was to produce as uniform a temperature in the suspended bodies as possible using ordinary laboratory techniques. In the second type, constant temperature gradients were produced on the enclosure and the resultant gradients on the suspended objects were measured. Since no enclosure can have an absolutely uniform temperature all over its surface, it is hoped that these latter results will be of some value in estimating the gradients likely to exist on enclosed specimens where direct measurement is impracticable.

APPARATUS AND PROCEDURE

The chamber used consisted of an 18-in. length of 6-in. diameter steel tubing of $\frac{1}{4}$-in. wall thickness onto which were bolted flat steel end plates using 0 rings for vacuum seals. The outer surface was wrapped with 28-gauge copper wire spaced so that adjacent wires were about $\frac{3}{8}$ inch apart and divided into six separate heating coils each covering about one-sixth of the surface. Insulation for the chamber consisted of a layer of fiber glass 1 in. thick surrounded by 6 inches of foamed polystyrene which was strong enough to act as the supporting base.

Heat was supplied to the system by passing direct current through the heating coils under the control of a relay operated by an a-c. bridge circuit. One arm of the bridge consisted of a thermistor, fastened to the outside of the

steel chamber, which threw the bridge off balance as its temperature changed from any predetermined value in the range 20° C to 100° C. The phasing of the circuit was such that a change in temperature of the control thermistor of plus or minus 0.001° C would turn the heating current off and on respectively. Because of the time lag in the heat flow through the chamber walls the temperature of the inner surface showed a fluctuation of ±0.005° C periodic with the heating cycle.

It was found that while any point on the inner surface remained constant to the nearest 0.01° C it was not possible to prevent differences in temperature of about 0.1° C over the surface. This was not uniform enough, so a second container was placed inside the chamber to act as the uniform temperature enclosure. Of the several enclosures tried the most successful was a 12-in. long copper cylinder, 4 in. in diameter, and having a $\frac{1}{8}$-in. wall thickness. This was supported on cork feet in the center of the steel chamber. Inside the enclosure objects with various shapes and conductivities were suspended on nylon threads. Best results were obtained with an object consisting of a cylindrical bar of aluminum 9 in. long and $1\frac{1}{2}$ in. in diameter (Fig. 1).

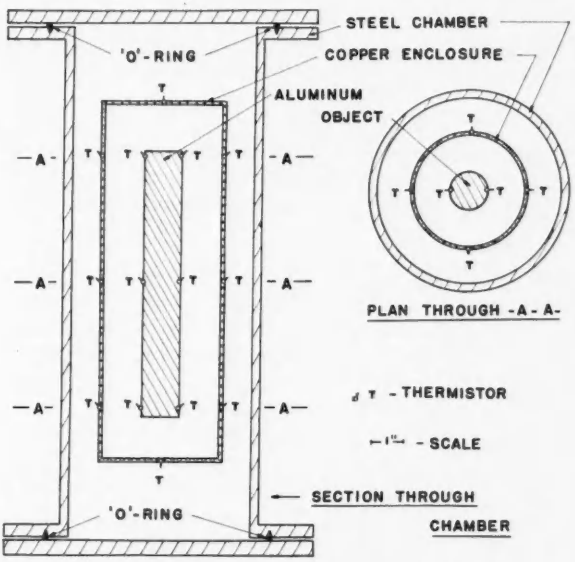

FIG. 1. Diagram of chamber, enclosure, and object showing location of thermistors.

Temperatures were measured using 20 Veco 32A38 bead thermistors, 14 on the enclosure and 6 on the object. These were calibrated against each other for several ranges of about 1° C using a Beckman thermometer which could be read to the nearest 0.001° C. For calibration the thermometer, with the thermistors taped around the bulb in a single layer, was placed in a small

mercury bath which was in turn immersed in a water bath. The resistances of the thermistors were measured with an H.W. Sullivan Ltd. Wheatstone bridge with which the resistance could be measured to the nearest 0.1 ohm. This corresponds to reading the temperature, for the thermistors used, to $\pm 0.001°$ C. In practice it was found that the time necessary to balance the bridge for this precision was too long so that measurements of temperature were not reproducible to better than about 0.002° C. Best thermal contact between thermistor and metal was obtained by drilling small holes in the wall of the enclosure and object and inserting the thermistors in these along with a drop of mercury.

Measurements were made with a range of air pressures in the system. It was found that for ordinary pressures the effects of convection made it difficult to adjust the power supplied to the individual heating coils so as to produce the uniform temperature condition, particularly when using odd-shaped objects. Thus for most of the work the pressure was maintained at 0.01 to 0.02 mm of Hg.

The general measurement procedure was to read the resistance of each of the 20 thermistors at hourly or half-hourly intervals each day during a period of 1 week or more for each series of measurements. After any adjustment of power to the heating coils or relocation of the thermistors the system was left for 1 day or longer before readings were taken.

RESULTS

In investigating the equilibrium temperature over the surface of an object in relation to the temperature over the surface of the enclosure in which it was suspended, two types of measurements were made.

Uniform Temperature

With careful adjustment of the power supplied to the individual heating coils the temperatures over the copper enclosure showed a standard deviation of about 0.003° C, which was about one and one-half times the reading error. Under these conditions the temperatures over the suspended object showed a standard deviation of about 0.002° C or about the same as the reading error. The temperature of either enclosure or object did not, however, remain constant. There was a random drift of about 0.002° C per hour with the object showing a time lag of several hours. Thus over a period of days the control circuit used could not maintain the temperature of the object constant to better than 0.01° C. Because of this drift it was difficult to compare the equilibrium temperature of the object with that of the enclosure to the limit of temperature-measuring accuracy. The nearest to an equilibrium condition was reached when the random drift was small and roughly periodic about a constant temperature over a period of several hours so that the temperature of both the enclosure and the object showed a similar periodic change. Under these conditions the object reached the same temperature as the enclosure. For example, in the same region of the temperature scale as Thompson worked, during a period of 4 hours the average of 56 readings of the 14 thermistors on

the enclosure was 41.1328° C with a standard deviation of 0.0033° C and for the same period the average of the 24 readings of the 6 thermistors on the aluminum object was 41.1332° C with a standard deviation of 0.0025° C.

Temperature Gradients

The second set of measurements, where a temperature gradient was set up along the length of chamber, enclosure, and object, were more valuable in determining the usefulness of this type of apparatus for holding an object at a constant and uniform temperature. The power supplied to the heating coils on the chamber was adjusted so as to produce temperature gradients, from top to bottom of the chamber, of up to 2° C, both with the top hotter than the bottom and vice versa. There was no appreciable difference between the measurements for the top hotter than the bottom and those for the top colder than the bottom for pressures of the order of 0.01 mm Hg, indicating heat transfer was mainly by radiation and conduction. For the dimensions and materials used in the apparatus there was a roughly 10-fold reduction in temperature gradient from chamber to enclosure to object as indicated in Table I.

TABLE I

Temperature differences over outer chamber, inner enclosure, and suspended object

Location of thermistors	Temperature (°C) at:			Temperature differences between top and bottom, °C
	Top	Middle	Bottom	
Outer steel chamber	39.8	41.0	41.9	2.1
Inner copper enclosure	40.68	40.86	41.01	0.33
Suspended aluminum cylinder	40.859	40.864	40.870	0.011

THOMPSON, L. 1956. Ph.D. Thesis, University of Western Ontario, London, Ontario.

RECEIVED MARCH 31, 1959.
DEPARTMENT OF PHYSICS,
UNIVERSITY OF WESTERN ONTARIO,
LONDON, ONTARIO.

NEGATIVE AND OSCILLATORY LONGITUDINAL MAGNETORESISTANCE

R. BARRIE

The purpose of this note is to report the result of numerical calculations of the longitudinal magnetoresistance of semiconductors and semimetals, for the case in which the scattering of the electrons is due to the acoustic modes of the lattice vibrations and the magnetic field is so large that the quantization of the electron orbits is important. The conductivity, σ, in the presence

of the magnetic field, H, is related to that in zero field, σ_0, by the expression (Barrie 1957; Argyres 1958)

$$\sigma/\sigma_0 = -3\{\ln(1+e^{\eta_0})\}^{-1}\int_{H'/2}^{\infty} g(x,H')\frac{\partial}{\partial x}f(x-\eta_H)\,dx \tag{1}$$

where

$$g(x,H') = \sum_n \{x-(n+\tfrac{1}{2})H'\}^{1/2}\Big[\sum_n \{x-(n+\tfrac{1}{2})H'\}^{-1/2}\Big]^{-1}$$

and

$$f(x-\eta_H) = (e^{x-\eta_H}+1)^{-1}.$$

In this equation, $x = \epsilon/kT$, $H' = \hbar eH/kTm^*c$, $\eta_0 = \zeta_0/kT$, and $\eta_H = \zeta_H/kT$; ζ_0 and ζ_H are the Fermi energies in the absence and presence, respectively, of the magnetic field; $\epsilon = (n+\frac{1}{2})(\hbar eH/m^*c)+\epsilon'$ is the electron energy, with n the oscillator quantum number associated with the transverse motion of the electrons and ϵ' the translational energy in the direction of the fields. The sums over the non-negative integer n are from zero to that maximum value of n which leaves $\{x-(n+\frac{1}{2})H'\}$ positive. For the assumptions involved in the derivation of (1), the reader is referred to the papers quoted above. The function $g(x, H')$ suffers discontinuities, so no assumptions concerning the step-function nature of $f(x-\eta_H)$ were made.

In addition to (1), a relation is needed between η_H and η_0. If the assumption is made that the number of electrons in the band is not altered by the magnetic field, then

$$F_{\frac{1}{2}}(\eta_0) = (H'/2)\sum_{n=0}^{\infty} F_{-\frac{1}{2}}\{\eta_H-(n+\tfrac{1}{2})H'\} \tag{2}$$

where

$$F_k(\eta) = \int_0^{\infty} x^k(e^{x-\eta}+1)\,dx\,.$$

The general nature of the dependence of η_H/η_0 and of the magnetoresistive ratio $\Delta\rho/\rho_0$ $(=(\sigma_0/\sigma)-1)$ on H' as η_0 is increased is illustrated in Figs. 1, 2, and 3.

If there are unfilled levels below the band being considered, the magnetic field can, through its alteration of the energy-level distribution, change the number of electrons in the band. Equation (2) would then have to be suitably modified. For semimetals, (2) will be valid, but for semiconductors it is not. The value 40 for η_0 would represent a rather extreme case of a semimetal and the value -20, a rather extreme case of a semiconductor. If the alteration of the levels in the lower band is less marked than in the upper, the suitable modification of (2) will lead to an increase in $\Delta\rho/\rho_0$. This would, for example, be the case in an intrinsic semiconductor in which the hole effective mass is much greater than the electron effective mass.

In comparisons of theory and experiment, it is often assumed that the

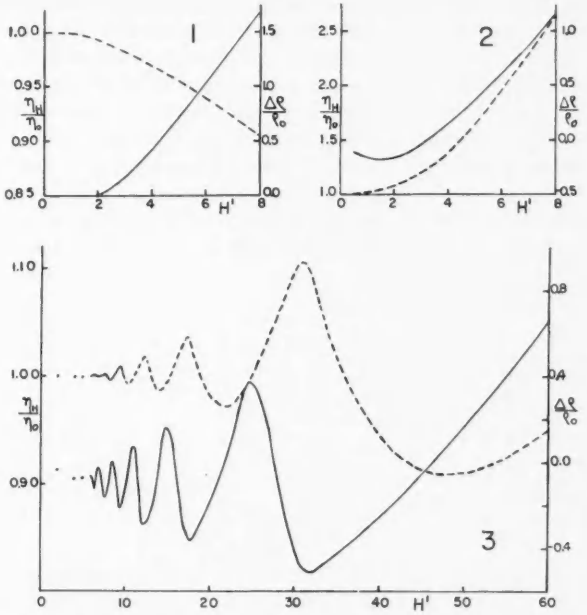

FIGS. 1–3. Plot of η_H/η_0 and $\Delta\rho/\rho_0$ as functions of H'. – – – η_H/η_0; ——— $\Delta\rho/\rho_0$.
FIG. 1. $\eta_0 = -20$. FIG. 2. $\eta_0 = 0.92$. No calculations were made for $H' < 0.5$. FIG. 3. $\eta_0 = 40$. The isolated points are for $H' = 2$, 4, and 5. No curve is drawn through these points as the oscillations became very rapid.

oscillations can be approximated by an analytic function, e.g. Broom's use of the theory of Davydov and Pomeranchuk for impurity scattering (Broom 1958). This approximation is made in the theory when $H' \ll \eta_H$ (Argyres), a condition not always satisfied in the experiments on semimetals. For the problem discussed here, the oscillations are represented analytically by $-\cos\{2(\pi\eta_H/H') - (\pi/4)\}$. The numerical analysis was undertaken to check this approximation. If the reciprocals of the reduced fields H' at which $\Delta\rho/\rho_0$ is a minimum are plotted against the appropriate series of integers, a straight line should be obtained, whose slope is $1/\eta_H$ and whose intercept on the number axis is $-1/8$. When this graph is drawn for $\eta_0 = 40$ (the minimum at $H' = 32$ being that for the integer unity) a straight line is obtained of slope $1/40$. The intercept on the number axis, however, is $-1/4$. The analytic approximation thus indicates the correct period of the oscillations, but the wrong phase.

The most interesting result of the calculations is the appearance of a negative $\Delta\rho/\rho_0$. This is in general agreement with experiments on indium arsenide (Sladek 1958). In this material, $\Delta\rho/\rho_0$ oscillates between positive and negative values. To obtain better agreement, the calculated mean value of $\Delta\rho/\rho_0$ during one oscillation would have to be increased. This could perhaps

be achieved by one of two modifications required in the theory. First, the effect of energy-level broadening was neglected in the derivation of (1). This would remove the discontinuities in $g(x, H')$ and thereby tend to smear out the oscillations. It might also raise the mean value of $\Delta\rho/\rho_0$. Secondly, the scattering of the electrons in indium arsenide, at the temperatures involved in the experiment, is due to ionized impurities; the equation corresponding to (1) would have to be derived for this type of scattering.

The author would like to thank Miss P. E. Grossmith for carrying out most of the numerical work. He would also like to thank the National Research Council of Canada for the award of a grant during the tenure of which the work was performed.

ARGYRES, P. N. 1958. J. Phys. Chem. Solids, **4**, 19.
BARRIE, R. 1957. Proc. Phys. Soc. B, **70**, 1008.
BROOM, R. F. 1958. Proc. Phys. Soc. **71**, 470.
SLADEK, R. J. 1958. Phys. Rev. **110**, 817.

RECEIVED FEBRUARY 2, 1959.
DEPARTMENT OF PHYSICS,
THE UNIVERSITY OF BRITISH COLUMBIA,
VANCOUVER, BRITISH COLUMBIA.

SUGGESTED MODIFICATIONS TO A METHOD FOR THE DETERMINATION OF THE ABSOLUTE AMPERE*

M. ROMANOWSKI AND R. BAILEY

While the absolute unit of electrical resistance is determined by several different methods, the unit of current is determined exclusively by means of current balances (coaxial coils or torque dynamometer types). Silsbee (1949), after having examined the results obtained from various current balances, commented as follows: "There is an evident need for the development of some radically different method for measuring current in absolute amperes that will not be subject to the same type of systematic error."

Only one such method is known to exist. It is based on the fact that we can express the magnetic induction B, produced in a high-quality magnet, by means of two equations from which the induction vector is eliminated, thus obtaining a relation between current and quantities which can be expressed in terms of mechanical units.

The first of these equations, $F = BlI$, expresses the force F resulting from the action of the field of magnetic induction B on a conductor of length l carrying a current I (Fig. 1). The second equation, $BK = MI$, is deduced from the relationship of the e.m.f. induced in a search coil† rotating between

*Issued as N.R.C. No. 5233.
†The inductive constant K of this coil has to be determined beforehand, by an independent operation, in terms of the value of a computable self-inductor.

the poles of the magnet, and the e.m.f. induced in the secondary of an inductor of known value M. The primary of this inductor is energized with the same current I and this current is reversed synchronously with the 180° flip of the search coil. The two e.m.f.'s are compared with a ballistic galvanometer.

This method has been used by Dupouy and Jouaust in 1935. In 1936, Briggs suggested that its precision might be increased by substituting a balance equipped with a freely suspended rectangular coil in place of the Cotton-type balance used by Dupouy and Jouaust.

The difficulties associated with the reversals of current, in addition to those already existing in the remaining parts of the experiment, have prevented

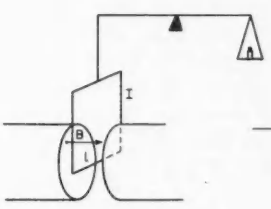

FIG. 1.

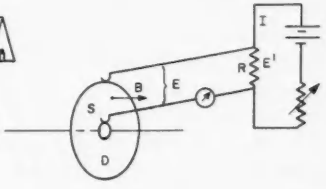

FIG. 2.

this method from becoming a serious rival to the current balance. In the course of a re-examination of the problem we came to the conclusion that the reversals of current and the difficulties associated with the calibration of the mutual inductor M (in terms of a computed standard) can be avoided by using a homopolar generator instead of a search coil. In fact, this substitution transforms the method into a completely direct-current one.

The values of the e.m.f. E (Fig. 2), generated between the rim and the center of a conductive disk D (thin metal platings on glass) rotating in a magnetic flux Φ, is expressed by $E = \Phi n$ where n is the number of revolutions per second. This electromotive force can be balanced by the drop of potential E' across a resistor R (measured in terms of absolute ohm) through which flows the current I. When $E = E'$, the relation becomes $\Phi n = BSn = RI$, S being the area of the disk.

With a good magnet it is relatively easy to obtain a field of a density of 0.5 Weber/m^2. In a disk of 7-cm radius the flux Φ will be equal to 7.5×10^{-3} Weber. Using $n = 80$ r.p.m. the induced e.m.f. E will be of the order of 10 mv. This corresponds to a drop of potential E' created by a current $I = 0.1$ A in 0.1 Ω.

The equation $BSn = RI$, combined with $F = BlI$, gives I^2 in terms of S, n, R, and l.

In an actual experiment the position of the brush at the axis of the disk cannot be known with sufficient accuracy; this contact can be replaced by another brush contact on a second disk of much smaller diameter. The resulting loss of flux will be small.

An alternative technique would be to use a radius sector rotating in a

conducting ring. It may be necessary to try both experimentally before taking the final decision.

By using two disks which rotate in opposite directions it is possible to create more degrees of freedom for analyzing secondary phenomena. The e.m.f. E may be opposed to the e.m.f. created by another homopolar generator of computable characteristics. This procedure, although probably very difficult, should not, a priori, be excluded. The technique of computed generators has been demonstrated from the work done on the Lorenz apparatus (Smith 1914).

The problems connected with creating a stable and reproducible field with the required homogeneity over the surface of the disk are difficult but not insurmountable with modern techniques based on the use of proton resonance.

We may summarize by observing that the Briggs freely suspended coil is capable of yielding a high accuracy in the operation of the "weighing" of the current. If, in addition, we substitute the homopolar generator for the flip-coil technique, we should obtain a higher accuracy for the second operation by eliminating the necessity for a well-known mutual inductance of high value and the problems related to the reversals of current.

These two operations appear to constitute a method of sufficient accuracy to warrant an experimental trial. This would provide an independent check of the present classical balance technique for determining the absolute ampere.

Briggs, G. H. 1936. J. Sci. Instr. **13**, 127.
Dupouy, G. and Jouaust, R. 1935. J. phys. **6** (7), 123.
Silsbee, F. B. 1949. National Bureau of Standards Circular 475, p. 29.
Smith, F. E. 1914. Phil. Trans. Roy. Soc. A, **214**, 27. (National Physical Laboratory Collect. Research (1938), Vol. 11, paper 13, p. 209; Vol. **24**, p. 277.)

Received April 21, 1959.
Division of Applied Physics,
National Research Council,
Ottawa, Canada.

THE PHYSICAL SOCIETY

MEMBERSHIP of the Society is open to all who are interested in Physics.

FELLOWS pay an Entrance Fee of £1 1*s*. ($3.15) and an Annual Subscription of £2 2*s*. ($6.00).

STUDENTS: A candidate for Studentship must be between the ages of 18 and 26, and pays an Annual Subscription of 5*s*. ($0.75).

MEETINGS: Fellows and Students may attend all Meetings of the Society including the annual Exhibition of Scientific Instruments and Apparatus.

PUBLICATIONS include the *Proceedings of the Physical Society*, published monthly, and *Reports on Progress in Physics*, published annually. Volume XXI, 1958, is now available (price £3 3*s*. ($9.45)). Members are entitled to receive any of the Publications at a reduced rate.

Further information can be obtained from:

THE PHYSICAL SOCIETY
1, LOWTHER GARDENS, PRINCE CONSORT ROAD
LONDON, S.W.7, ENGLAND

NOTES TO CONTRIBUTORS

Canadian Journal of Physics

MANUSCRIPTS

General.—Manuscripts, in English or French, should be typewritten, double spaced, on paper 8½×11 in. **The original and one copy are to be submitted.** Tables and captions for the figures should be placed at the end of the manuscript. Every sheet of the manuscript should be numbered. Style, arrangement, spelling, and abbreviations should conform to the usage of recent numbers of this journal. Greek letters or unusual signs should be written plainly or explained by marginal notes. Characters to be set in boldface type should be indicated by a wavy line below each character. Superscripts and subscripts must be legible and carefully placed. Manuscripts and illustrations should be carefully checked before they are submitted. Authors will be charged for unnecessary deviations from the usual format and for changes made in the proof that are considered excessive or unnecessary.

Abstract.—An abstract of not more than about 200 words, indicating the scope of the work and the principal findings, is required, except in Notes.

References.—References should be listed **alphabetically by authors' names,** unnumbered, and typed after the text. The form of the citations should be that used in current issues of this journal; in references to papers in periodicals, titles should not be given and only initial page numbers are required. The names of periodicals should be abbreviated in the form given in the most recent *List of Periodicals Abstracted by Chemical Abstracts.* All citations should be checked with the original articles and each one referred to in the text by the authors' names and the year.

Tables.—Tables should be numbered in roman numerals and each table referred to in the text. Titles should always be given but should be brief; column headings should be brief and descriptive matter in the tables confined to a minimum. Vertical rules should not be used. Numerous small tables should be avoided.

ILLUSTRATIONS

General.—All figures (including each figure of the plates) should be numbered consecutively from 1 up, in arabic numerals, and each figure referred to in the text. The author's name, title of the paper, and figure number should be written in the lower left corner of the sheets on which the illustrations appear. Captions should not be written on the illustrations.

Line drawings.—Drawings should be carefully made with India ink on white drawing paper, blue tracing linen, or co-ordinate paper ruled in blue only; any co-ordinate lines that are to appear in the reproduction should be ruled in black ink. Paper ruled in green, yellow, or red should not be used. All lines must be of sufficient thickness to reproduce well. Decimal points, periods, and stippled dots must be solid black circles large enough to be reduced if necessary. Letters and numerals should be neatly made, preferably with a stencil (**do NOT use typewriting**) and be of such size that the smallest lettering will be not less than 1 mm high when the figure is reduced to a suitable size. Many drawings are made too large; originals should not be more than 2 or 3 times the size of the desired reproduction. Whenever possible two or more drawings should be grouped to reduce the number of cuts required. In such groups of drawings, or in large drawings, full use of the space available should be made; the ratio of height to width should conform to that of a journal page (4¾×7½ in.), but allowance must be made for the captions. **The original drawings and one set of clear copies (e.g. small photographs) are to be submitted.**

Photographs.—Prints should be made on glossy paper, with strong contrasts. They should be trimmed so that essential features only are shown and mounted carefully, with rubber cement, on white cardboard, with no space between those arranged in groups. In mounting, full use of the space available should be made. **Photographs are to be submitted in duplicate;** if they are to be reproduced in groups one set should be mounted, the duplicate set unmounted.

REPRINTS

A total of 50 reprints of each paper, without covers, are supplied free. Additional reprints, with or without covers, may be purchased at the time of publication.

Charges for reprints are based on the number of printed pages, which may be calculated approximately by multiplying by 0.6 the number of manuscript pages (double-spaced typewritten sheets, 8½×11 in.) and including the space occupied by illustrations. Prices and instructions for ordering reprints are sent out with the galley proof.

Contents

T. B. A. Senior—The scattering of electromagnetic waves by a corrugated sheet 787

M. J. Laubitz—Thermal conductivity of powders - - - - - - - - 798

R. W. Parsons and L. Katz—The photodisintegration of tantalum - - - 809

T. A. Eastwood and J. C. Roy—The occurrence of $(n, 3n)$ reactions in a nuclear reactor - 815

J. C. Roy—Evidence for neutrons with an energy of 20.3 Mev in the NRX reactor - 827

K. M. Baird and D. S. Smith—Kr 86 and Hg 198 wavelength standards - - 832

R. L. Williams—Modification of PbS noise spectra by radiation - - - - - 841

Prem Swarup—Paramagnetic resonance line shapes - - - - - - - - 848

G. M. Griffiths, P. P. Singh, Y. I. Ssu, and J. B. Warren—A simple gamma-ray insensitive fast-neutron counter - - - - - - - - - - - - - 858

P. P. Singh, G. M. Griffiths, Y. I. Ssu, and J. B. Warren—The neutron yield from heavy ice targets bombarded with protons below the $D(p, n)2p$ threshold - 866

R. G. Rastogi—Magnetic control on the variations of critical frequency of the F_2 layer of the ionosphere - - - - - - - - - - - - - - - - 874

P. K. Carroll—The C–X system of N_2^+ - - - - - - - - - - - - - - 880

Notes

C. M. Carmichael and A. D. Misener—On maintaining an object at a uniform temperature - 890

R. Barrie—Negative and oscillatory longitudinal magnetoresistance - - 893

M. Romanowski and R. Bailey—Suggested modifications to a method for the determination of the absolute ampere - - - - - - - - - - 896

Printed in Canada *by* University of Toronto Press